

Investigations on physico-chemical aspects of lead-based alloys for nuclear applications

Inauguraldissertation
der Philosophisch-naturwissenschaftlichen Fakultät
der Universität Bern

vorgelegt von

Stephan Heinitz

von Deutschland

Leiter der Arbeit

Prof. Dr. A. Türler

Departement für Chemie und Biochemie der Universität Bern
Labor für Radio- und Umweltchemie

Originaldokument gespeichert auf dem Webserver der Universitätsbibliothek Bern



Dieses Werk ist unter einem Creative Commons Namensnennung-Keine kommerzielle Nutzung-Keine Bearbeitung 2.5 Schweiz Lizenzvertrag lizenziert. Um die Lizenz anzusehen, gehen Sie bitte zu <http://creativecommons.org/licenses/by-nc-nd/2.5/ch/> oder schicken Sie einen Brief an Creative Commons, 171 Second Street, Suite 300, San Francisco, California 94105, USA.

Urheberrechtlicher Hinweis

Dieses Dokument steht unter einer Lizenz der Creative Commons
Namensnennung-Keine kommerzielle Nutzung-Keine Bearbeitung 2.5 Schweiz.
<http://creativecommons.org/licenses/by-nc-nd/2.5/ch/>

Sie dürfen:



dieses Werk vervielfältigen, verbreiten und öffentlich zugänglich machen

Zu den folgenden Bedingungen:



Namensnennung. Sie müssen den Namen des Autors/Rechteinhabers in der von ihm festgelegten Weise nennen (wodurch aber nicht der Eindruck entstehen darf, Sie oder die Nutzung des Werkes durch Sie würden entlohnt).



Keine kommerzielle Nutzung. Dieses Werk darf nicht für kommerzielle Zwecke verwendet werden.



Keine Bearbeitung. Dieses Werk darf nicht bearbeitet oder in anderer Weise verändert werden.

Im Falle einer Verbreitung müssen Sie anderen die Lizenzbedingungen, unter welche dieses Werk fällt, mitteilen.

Jede der vorgenannten Bedingungen kann aufgehoben werden, sofern Sie die Einwilligung des Rechteinhabers dazu erhalten.

Diese Lizenz lässt die Urheberpersönlichkeitsrechte nach Schweizer Recht unberührt.

Eine ausführliche Fassung des Lizenzvertrags befindet sich unter
<http://creativecommons.org/licenses/by-nc-nd/2.5/ch/legalcode.de>

Investigations on physico-chemical aspects of lead-based alloys for nuclear applications

Inauguraldissertation
der Philosophisch-naturwissenschaftlichen Fakultät
der Universität Bern

vorgelegt von

Stephan Heinitz

von Deutschland

Leiter der Arbeit

Prof. Dr. A. Türler

Departement für Chemie und Biochemie der Universität Bern
Labor für Radio- und Umweltchemie

Von der Philosophisch-naturwissenschaftlichen Fakultät angenommen

Bern, den 28.06.2013

Der Dekan
Prof. Dr. S. Decurtins

Manie and amalgam did I make,
Weening to fixe them to great availe,
And thereto Sulphure did I take,
Tartar, egges, whites, and oyle of the snayle,
But ever of my purpose did I faile,
For what for the more, and what for the las,
Evermore something wanting there was.

George Ripley, *The Compound of Alchymy*, 1591



An alchemist at work in his laboratory, from a woodcut by Hans Weiditz, ca. 1520

Table of contents

Foreword	7
I General overview	11
I.1 History.....	11
I.2 Spallation neutron sources and transmutation	11
I.3 Accelerator driven systems - MYRRHA.....	12
I.4 The spallation process.....	13
I.5 Target material requirements.....	15
I.6 Liquid metals in nuclear applications	15
I.6.1 Lead-bismuth eutectic	17
I.6.2 Liquid metal chemistry.....	19
I.6.3 The polonium problem.....	20
I.7 Motivation	21
II Stability of construction materials in lead-gold eutectic.....	23
II.1 Introduction	23
II.2 Lead-gold eutectic	24
II.2.1 Properties of lead-gold eutectic.....	24
II.2.2 Simulation of nuclear properties.....	25
II.2.3 Solution of elements in LGE.....	28
II.2.4 Solubility of steel elements in molten Pb alloys.....	30
II.3 Experimental.....	33
II.3.1 Preparation of LGE.....	33
II.3.2 The experimental loop.....	34
II.3.3 ICP-OES measurements.....	35
II.4 Results.....	36
II.5 Discussion	40
II.6 Summary	43
III Extraction of radionuclides from liquid metals.....	45
III.1 Introduction.....	45
III.1.1 Polonium separation from liquid meals	45
III.1.2 Properties of molten hydroxides.....	46
III.1.3 Literature overview on alkaline extraction of polonium from liquid metals.....	47
III.1.3.1 Extraction of impurities from molten Pb metal.....	47
III.1.3.2 Extraction of impurities from molten Bi metal.....	49
III.1.3.3 Extraction of impurities from molten LBE.....	49
III.1.3.3.1 Extraction of polonium from molten LBE	49
III.1.3.3.2 Extraction of various nuclear reaction products from molten LBE	52
III.1.4 Objective of this work	52
III.2 Experimental.....	54
III.2.1 Sample preparation	54
III.2.1.1 LBE samples containing polonium.....	54
III.2.1.2 Samples containing a mixture of spallation products.....	54
III.2.1.3 Preparation of the hydroxide mixture	55
III.2.2 The extraction device	55
III.2.3 Modifications on the extraction device	56
III.2.4 Experimental procedure	57
III.2.4.1 LBE samples containing polonium.....	57
III.2.4.2 Samples containing a mixture of spallation products.....	58
III.2.5 Analysis techniques.....	59
III.2.5.1 Liquid scintillation counting	59
III.2.5.2 Measurements using γ spectrometry	59

III.3	Results	60
III.3.1	Extraction of polonium from liquid LBE	60
III.3.2	Experiments with extraction of spallation products	65
III.3.2.1	Extraction of radionuclides from irradiated Bi	66
III.3.2.2	Extraction of radionuclides from irradiated LBE	67
III.3.2.3	Extraction of radionuclides from irradiated Pb	68
III.4	Discussion	70
III.4.1	Results on polonium extraction from LBE	70
III.4.2	Extraction of spallation products	73
III.5	Summary	77
IV	Mobility of polonium in solid Pb, Bi and LBE	79
IV.1	Introduction	79
IV.1.1	Diffusion theory	79
IV.1.2	The laws of Fick	81
IV.1.3	Segregation effects in metals	82
IV.1.3.1	The behaviour of polonium in various metals	83
IV.1.3.2	Investigations on polonium in lead	84
IV.1.3.3	Investigations on polonium in bismuth	85
IV.1.3.4	Investigations on polonium in LBE	85
IV.2	Experimental	87
IV.2.1	Impurities in LBE	87
IV.2.2	Sample preparation	87
IV.2.2.1	Preparation of cylindrical metallic samples	87
IV.2.2.2	Sample preparation for diffusion studies	89
IV.2.2.3	Sample preparation for segregation studies	89
IV.2.3	Analysis techniques	89
IV.2.3.1	Microtome sectioning of the samples	90
IV.2.3.2	Liquid scintillation counting	90
IV.2.3.3	α spectrometry	91
IV.2.4	Theoretical considerations	92
IV.2.5	Data analysis	94
IV.2.5.1	Diffusion of a thin substance film into a semi-infinite medium	94
IV.2.5.2	The simplified segregation model of Lea and Seah	95
IV.3	Results and discussion	97
IV.3.1	Diffusion studies	97
IV.3.2	Segregation studies	101
IV.3.2.1	α spectrometry results	101
IV.3.2.2	Results from microtome sectioning	103
IV.3.2.3	Additional measurements and problems	106
IV.4	Summary	109
V	Final conclusions and outlook	110
	References	112
	Appendix	120
	Acknowledgements	128

Foreword

During the course of my stay at the Paul Scherrer Institute, Switzerland, I had the opportunity to get known to many interesting aspects of physics and chemistry important for nuclear applications. For the period of my PhD, I was able to work in a very interesting field of science involving liquid metals, exotic elements and radioactivity. Many challenging problems had to be solved and I am very thankful to the scientific aid I received from my colleagues at work.

This manuscript should summarize the scientific outcome of investigations on various topics performed between 2009 and 2012. It will be divided into four main parts, each dealing with its own specific problem devoted towards physics, chemistry and radiochemistry of lead-based alloys. In order to ease the understanding for the reader, each part will have an introduction on its own to explain the specific problems. After a general overview in the first part, which should guide the reader towards the topic related to liquid metals in nuclear systems, the second part of this manuscript will describe investigations dealing with liquid metal corrosion. The third part will mostly focus on chemical problems concerning the extraction of radionuclides from liquid metals. Investigations related to physical phenomena of diffusion and segregation in solidified metals will be presented in the forth part of this thesis.

The whole work will be largely focused on polonium, and the current study should give more insight into the physical and chemical behaviour of this radioactive element in a complex liquid metal based nuclear system. Working with this element taught me many interesting aspects and methods in radiochemistry involving sputtering, radiography and spectroscopy.

Certainly, it is not possible to deal with every minute facet of each topic and I regret for not having implemented all into this manuscript. However, with this PhD thesis, I hope to have provided a valuable source of information for future studies and I would be glad to have mined a tiny but precious piece of hard-rocked granite of science.

I General overview

I.1 History

The discovery of radioactivity by H. Becquerel more than one century ago [1] has significantly influenced the development of mankind. Several technologic advancements were made towards the peaceful use of energy originating from a radioactive nucleus. With the discovery of neutron-induced fission by O. Hahn and F. Strassmann in 1938 [2], nuclear power generation had become the most important application within the last 50 years and nowadays represents an important factor of economical vitality for most industrialized countries. As of beginning of 2013, 435 nuclear power plant units are operational in 31 countries, and 68 new units are under construction, most of them in Asia [3].

After accidents at the Chernobyl reactor in 1986 and the Fukushima Dai-ichi power plant in 2011, nuclear power became drastically less accepted to the society, resulting in major resistance against nuclear power in the public [4]. Nuclear technology undoubtedly represents the centre of present-day discussions concerning future safe, ecological and economical energy generation. Many unanswered questions persist concerning repository strategies for long-lived, highly radioactive waste that is generated in the currently operating nuclear power plants all over the world. Much effort is therefore put into research and development towards new technologies to cope with this burden [5].

One promising strategy was already discussed since the 90ies of the last century. Radioactive nuclear waste may be converted into less hazardous forms by a process called transmutation [6]. Already in 1917, with the successful transformation of nitrogen to oxygen, it was shown by E. Rutherford [7] that transmutation of elements can indeed occur, but only if highly energetic particles are available. These particles are needed in order to penetrate into the nucleus of an atom and to modify its internal structure in such a way that it changes its chemical identity, i.e. its atomic number. In principle, the transmutation of any element into another is practically possible if the flux and energy of incoming particles (neutrons, protons, α -particles etc.) is high enough. It was suggested to use this idea for the transmutation of nuclear waste originating from nuclear fission [8]. Hazardous, long-lived radioactive isotopes could be converted into isotopes with much smaller half-life under the action of an intense particle flux. Ironically, facilities capable to deliver such high particle fluxes at that time were only nuclear fission reactors.

With the development of powerful proton accelerators, this circumstance is significantly changing since the last 20 years [9]. New facilities that provide comparable neutron fluxes but omit the use of fissile material are evolving in scientific research centres. Based on a process called spallation, such facilities rely on a beam of protons originating from a particle accelerator.

I.2 Spallation neutron sources and transmutation

Spallation sources generate neutrons by a collision reaction between a particle beam and a target material [10]. Similar to research reactors, the generated neutrons can then be used for various scientific applications such as material investigations, particle physics, isotope production and chemical analysis [11]. Spallation neutron sources thus represent appropriate substitutes for research reactors based on nuclear fission that have possibly less safety issues and thus could lead to a higher acceptance in the public.

As a spallation facility requires high-energy protons available only in a proton accelerator, only few research centres do have access to such devices. The SINQ spallation neutron source at PSI, Switzerland [12], ISIS at Rutherford Appleton Laboratory in the UK [13] as well as the SNS in Oakridge, USA [14] and J-Parc, Tokai-Mura, Japan [15], are pioneering facilities with respect to the development of the spallation technology. SINQ uses a Cockcroft Walton generator and in following stages two cyclotrons to produce an intense beam of 600 MeV protons hitting a solid Pb target. At ISIS, neutrons are created with a pulsed 160 kW proton beam hitting a water-cooled W target. At SNS

and J-Parc, which are facilities that became operational within the past 10 years, linear accelerators coupled with a synchrotron to supply the proton beam. In both facilities, beam energies in the order of 1 GeV are used. In these two facilities, a liquid metal (Hg) target is employed for neutron production, representing a favourable technology for the design of high power spallation units. Furthermore, in Europe the European Spallation Source (ESS) [16] is planned to be built in Lund, Sweden, representing the next generation of high power spallation facilities to be built in the near future.

Concerning the transmutation of nuclear waste, such spallation neutron sources can be combined with a subcritical reactor core containing long-lived hazardous nuclides. These nuclides involve, on one hand, minor actinides such as Pu, Am, Cm isotopes and ^{235}U fission products on the other [17]. In a first step, these nuclides are chemically separated from spent nuclear fuel, which then may be reprocessed and reused. The second step involves transmutation of the separated fraction of hazardous nuclides, where fission products are “burned” by neutron capture and actinides by undergoing fission. In the scientific community, the whole process is referred as partitioning and transmutation (P&T) of nuclear waste representing the basis for an innovative fuel cycle [5].

For an efficient fission of minor actinides, high energetic, fast neutrons are required. Having a moderated neutron spectrum, conventional light water reactors cannot be used to transmute actinides. For this purpose, reactors with a fast neutron spectrum are much more efficient. Due to physical aspects relevant for reactor safety (delayed neutron fraction, void reactivity) it is not possible to develop fast critical reactors with a high fraction of minor actinides in the fuel. This problem may be overcome by using in a subcritical reactor core driven by a spallation neutron source [8].

Such a hybrid system is currently foreseen as a promising nuclear facility capable to perform efficient transmutation of long-lived radiotoxic waste. In such a system, a reactor coolant is needed that doesn't moderate the neutrons generated within the spallation source and within the reactor core. Liquid metals such as Na, Pb or its eutectic with Bi fulfil this requirement [10]. Since these materials are also suited well for the use as target material in high power spallation systems, it seems obvious to employ liquid metal coolant and target technology into such a hybrid system.

1.3 Accelerator driven systems - MYRRHA

In contrary to conventional nuclear fission reactors, Accelerator Driven Systems (ADS) are nuclear fission reactors with a subcritical core [10]. An external neutron source is needed to sustain the nuclear chain reaction, thus eliminating the major problem of reactor core meltdown. Similar to a spallation neutron source, an external proton beam hits a heavy metal target producing a cascade of neutrons emitted by spallation reactions. In case of emergency, the proton beam will be cut off, stopping the neutron production in the core, thus shutting down the reactor. The promising goal of ADS systems is the possibility to use minor actinides as fission fuel in the reactor core [8, 18], at the same time transmuting them to less hazardous material.

Up to now, several scientific research projects have been launched to gather data on the physics of transmutation [19-21]. The ADS project called MYRRHA was launched 1997 at the SCK-CEN research centre in Mol, Belgium and is thought to demonstrate the feasibility of ADS reactor systems [22]. Thought to be ready for service by 2025, this experimental test facility shall prove the possibility of transmuting highly radioactive waste. In support to MYRRHA, the GUINEVERE project (Generator of Uninterrupted Intense Neutrons at the lead Venus Reactor) was devoted towards design and feasibility studies on an ADS demonstration reactor. Within this project, neutrons were generated by the reaction $T(d,n)^4\text{He}$ inside a subcritical zero power experimental reactor via a 250 keV deuteron accelerator [23]. The aim was to perform criticality and reactivity studies with varying reactor core designs and different operation modes of the accelerator. The GUINEVERE project has shown the feasibility of the ADS principle and delivered first promising results [24] that will be implemented into MYRRHA design.

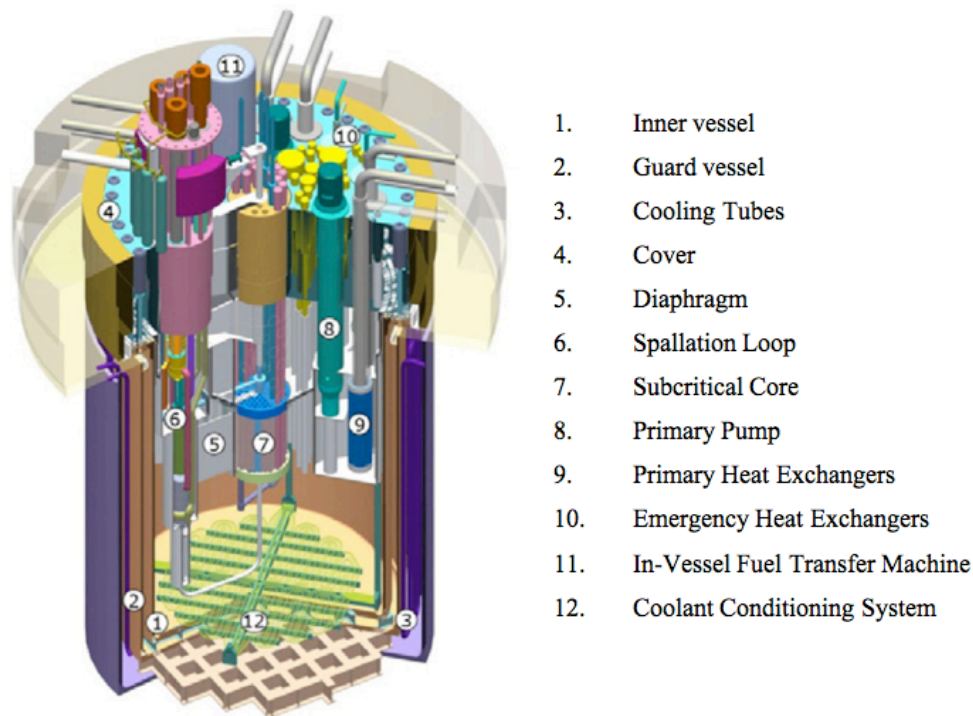


Figure 1: The conceptual design of the MYRRHA reactor [25]

The MYRRHA reactor itself is currently planned to use approx. 4000 tons of liquid metal coolant that have to be continuously pumped through the reactor core. A mixture of Pb and Bi is foreseen as spallation and coolant material. A preliminary layout of the reactor is given in Figure 1. Main design parameters of the reactor core and its components were given in [26]. Although it is also planned to be used for material investigations and isotope production, the main goal of MYRRHA is to show the feasibility of an ADS transmutation plant. In order to understand the behaviour of such complex facility, substantial effort has to be invested into basic research on this new reactor design and the development of suitable equipment in order to keep the facility in a stable and controllable status.

To give the reader a simplified overview on the processes and problems occurring in spallation facilities in general, the following sections will be devoted towards physical and chemical aspects of the topic.

1.4 The spallation process

The spallation process is induced by a beam of charged particles, in most cases protons originating from a particle accelerator that is guided towards a dense material acting as target. Spallation can be described as a two-stage process [11]. At first, the accelerated particle beam induces numerous collisions with nucleons of the target atoms releasing high-energy particles by the intra-nuclear cascade. As a result, the target atoms become highly excited and subsequently undergo several follow-up de-excitation reactions. During this second stage, they lose energy by evaporation of nucleons into the surrounding where mainly light particles low in energy are emitted. If the excess energy of the target atoms is high enough, they additionally may undergo fission. A schematic view on the processes occurring during spallation is depicted in Figure 2.

The number of neutrons emitted per incident proton, or neutron yield, depends on the target material itself and on the energy of the incident protons. An approximate relationship is given by equation (1):

$$yield = 0.1(A + 20)(E - 0.12), \quad (1)$$

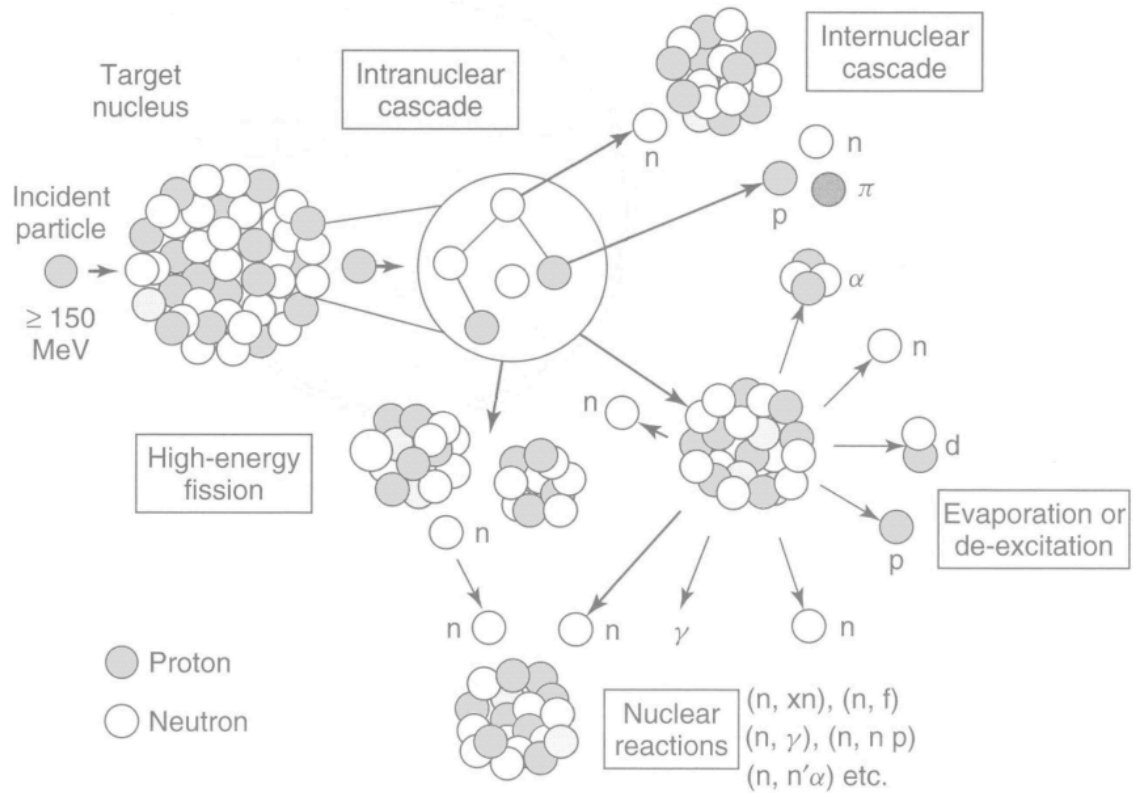


Figure 2: Schematic view on possible pathways of the spallation reaction; picture taken from [10]

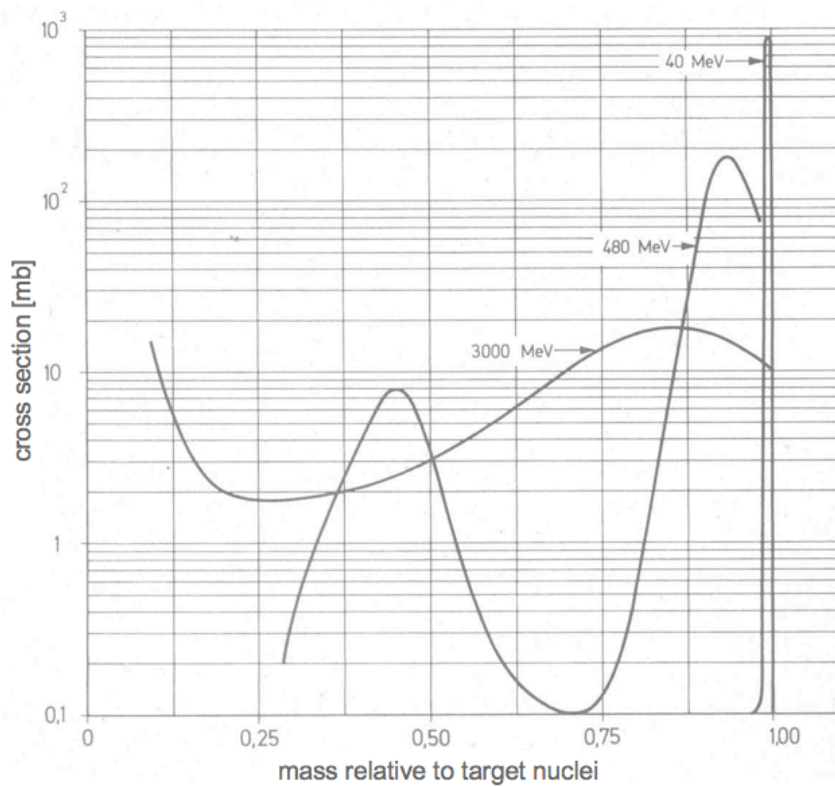


Figure 3: Mass dispersion of spallation products as function of beam energy; figure taken from [11], based on data from [28]

where A represents the atomic number of the target material and E the energy of the incident protons in GeV [27]. As can be easily seen, increasing the beam energy E and choosing a target material that consists of elements with a high atomic number results in a higher neutron yield. On one hand, the more energy is transferred to an atom, the more nucleons will spall off or evaporate. On the other hand, the higher the atomic number of the target material, the higher is the fraction of neutrons in the nucleus. This implies that for an efficient spallation reaction, highly energetic particle beams should be used in combination with targets made from a heavy element with a high neutron number.

As a consequence of the variety of nuclear reactions constituting the spallation process, a large number of different nuclear reaction products are formed, called the residual nuclei. These residual nuclei represent a diverse mixture of evaporation and fission products with a certain distribution of atomic mass. For a target material with an atomic number Z , nuclides of all elements with atomic numbers from 1 to $Z + 1$ will be formed. Depending on the energy of the incident particles, the amount of evaporation or fission products will vary. A graphical representation of this functional relationship is given in Figure 3.

1.5 Target material requirements

Apart from a high proton number, the target material has to meet several other different requirements to be suitable for use in a spallation facility. It should not absorb generated neutrons and be resistant to the irradiation by the beam. Moreover, it must withstand the thermal stresses induced by the charged beam. For this reason, it should have high thermal and electrical conductivity [9]. Finally, a high melting point and chemical inertness are favourable if solid materials are to be used. Usually, stacks of W, Ta or U bricks are used as target, and beam energies in the MeV to GeV range are used.

The scientific community is currently aiming toward higher neutron fluxes, which implies the development of more powerful particle accelerators delivering higher beam energies and currents [10]. For spallation target engineers, the heat dissipation problem becomes more and more severe with the resulting increase of heat loads. Even up to date it is a challenging task to establish reliable cooling for a solid metallic target if continuously hit by a 1 mA beam of 1 GeV protons, corresponding to a heat load of 1 MW [29]. As a consequence, water or He is used to cool the target during operation, which additionally complicates target operation and design. Another approach is the implementation of mechanical equipment to keep the target in a constant movement, e.g. rotation, to distribute the heat load. This solution, however, is a considerable engineering challenge, because the moving target has to be kept in vacuum. In such a system, tightness of bearings and sealings must be assured to minimize any leakage of radioactivity and to guarantee a reliable operation of the facility.

Another problem consists of irradiation damage induced within the target material by the high power particle beam, which could lead to mechanical failure of the target. Although not a scientifically justified scale, the dpa-value (displacements per atom) is commonly used as a measure of radiation damage. It is calculated on the basis of the total energy transferred to the material divided by the mean energy required to displace one atom from its lattice site in the particular material. The dpa number has proved as a useful reference to characterize the amount of radiation a material had been exposed to, and to characterize changes of its properties under the influence of irradiation [9]. The material damages caused by irradiation limit the lifetime of the spallation target, implying an exchange of the target if the predicted lifetime or dpa-value is reached. The problem of structural damage and heat load caused by irradiation can be partly mitigated by using a liquid heavy metal target.

1.6 Liquid metals in nuclear applications

Liquid metals have been studied since the early development of fission energy in the early 1950s as reactor core coolants mainly in the US and Russia [30, 31]. Several test facilities were built for investigating their use for peaceful energy production [17]. Liquid metal cooled reactors were also developed in Russia for submarine military purposes [32].

Nowadays, liquid metals play an important role in the development of many future nuclear technologies. Among these are fusion energy blanket applications, high power neutron spallation sources and, more recently, accelerator-driven systems proposed for high-level radioactive waste transmutation [33]. Additionally, liquid metals are foreseen for the development of new nuclear reactor designs. Currently being developed by a broad research community, the lead fast reactor (LFR) and the sodium fast reactor (SFR) should serve as a liquid metal cooled experimental nuclear facility to demonstrate the feasibility of such reactor systems [34]. The final goal of this research is the construction of the European Lead-cooled System (ELSY), an industrial scale 1500 MWth reactor for electricity generation designed to utilize Pb as reactor coolant [35]. Some companies are developing small-scale reactors cooled by Pb-Bi with thermal output powers below 100 MWt [15]. Based on a modular design, these reactors should be easily transportable and installable at any remote place where reliable energy supply is needed.

Spallation facilities that currently are being developed are aiming towards higher neutron yields and higher beam power. As already stated in the preceding chapter, this requires new cooling solutions and a frequent exchange of targets, if solid targets are used. This makes the use of solid targets unattractive. For spallation sources with beam powers exceeding the megawatt range, liquid metal targets can offer several advantages over solid targets. Facilities operating with liquid metals may achieve comparable neutron fluxes while having better heat dissipation performance. Additionally, liquid metal targets do not suffer from irradiation damage [9]. However, their use requires active pumping systems and the construction of large and complex liquid metal loops where irradiation damage still occurs. Therefore, the exchange frequency of such a target is determined more by the lifetime of their components, especially the proton beam window [36].

Apart from a low melting point, these liquid metals should meet the requirement of a high atomic number. Apart from Hg, which is the only metal that is liquid at room temperature, also Tl, Pb and Bi meet this condition. The last three named metals have melting points below 350 °C, which is still relatively high for applications in nuclear industry considering steel corrosion induced by the flowing metal [37]. An overview on some physical properties of these metals is given in Table 1.

The use of Tl is generally ruled out because of its high toxicity. Elemental Bi was used in the past during the US research program on liquid metal-fuelled reactors [38]. Experience with Pb cooling exists in Russian experimental test reactors [17]. However, both metals need auxiliary heating systems in order to keep them liquid within the facility. In case of solidification, pumping or convection of the metal may come to halt, resulting in complete failure of the system. Thus, precautions have to be taken for these metals in order to avoid temperature drops below the melting point of the metallic fluid.

Table 1: Some physical properties of Pb, Bi, Hg and Tl

element	melting point [K]	boiling point [K]	density at 20°C [g/cm ³]	atomic number <i>A</i>	toxicity
Hg	234	630	13.55	200.6	high
Tl	577	1733	11.85	204.4	very high
Pb	601	2016	11.35	207.2	moderate
Bi	544	1806	9.75	209	low

Certainly Hg, as the only metal liquid at room temperature, has significant advantages over Pb and Bi concerning the operation temperature. Facilities operating with Hg may avoid the use of heating equipment, thus facilitating access to pumps or pipes during repair works. Hg does also not oxidize at ambient conditions, which is important for keeping loops and equipment free of oxide contamination during refill operations.

These factors have largely influenced the decision in favour to Hg for some spallation neutron sources in the past. Thus, two spallation sources operating with Hg were recently built – the Spallation Neutron Source SNS at Oak Ridge National Laboratory [39] and the Japanese Spallation Neutron Source JSNS at the Japan Atomic Energy Research Institute JAERI [40]. The latter is currently out of service

because of substantial damage suffered by the earthquake in March 2011. Hg was also considered as a possible target material for the European Spallation Source ESS until recently, but has been dropped for the favour of a rotating W target [41].

However, the liquid state of Hg at ambient temperature, apart from causing the above-mentioned advantages easing facility operation, also is the origin of major problems of the Hg technology. Typically, radioactive material has to be solid before it can be disposed after shutdown of the facility. However, up to now, there is no proven technology for solidification and storage of large amounts of radioactive Hg [42]. Moreover, the high vapour pressure of Hg requires stringent safety precautions in order to avoid any spreading of its toxic vapours. The volatility and toxicity of Hg are reasons why the European Union and the United Nations are currently putting effort into imposing measures to ban Hg from industrial usage, reflecting the shift away from what is a highly toxic material to more acceptable substitutes.

The use of liquid Pb as target material and cooling medium has several crucial disadvantages for the operation of a nuclear facility. Firstly, within a liquid metal loop many measurement and control devices have to assure reliable operation for controlling flow velocity, temperature, pressure etc. Such instruments have a maximum operation temperature, which often lies below the melting point of Pb. Bearings, valves, stopcocks and other equipment needed to run a liquid metal loop often fail at temperatures exceeding 400 °C. It is a big engineering challenge to keep a large liquid Pb loop operational. Heating and more complex temperature controls are added complications to facility system and operations. Up to now, experience with liquid Pb in nuclear facilities is available in Russia within their lead cooled fast reactor program [17]. At the Helmholtz-Zentrum Dresden-Rossendorf a Pb-cooled neutron time-of-flight facility nELBE is operational, where experience in cooling with molten Pb does exist [43].

In order to overcome the problems arising from the disadvantageous properties of Hg and Pb, it has been considered to use low melting and high boiling heavy metal alloys as liquid coolants. Mixtures of low-melting elements often exhibit significantly lower melting temperatures than their constituents. An overview on the possible alloys of Pb with Sn, In, Cd, Bi and others is given in the reference book of R. Lyon [30].

For example, a eutectic mixture of Pb, Bi and Cd is called Wood's metal and exhibits a melting point below 75 °C [44]. Several other alloys of Bi and Pb with nonferrous metals (e.g. Sb, Sn and In) were prepared in the past and applied as low melting casting metals and solders [30]. However, only Pb and Bi are of major interest as cooling and spallation target materials for next generation nuclear systems, because they have the highest nucleon quantity, resulting in better neutron yields. Additionally, the neutron absorption cross-section for these metals is lowest. Their excellent self-shielding of hazardous radiation is yet another reason that makes their use favourable.

1.6.1 Lead-bismuth eutectic

Lead-bismuth eutectic (LBE) is a silver-grey ductile solid alloy, consisting of 45.5 wt% Pb and 55.5 wt% Bi. In presence of oxygen it acquires a dark grey surface due to Pb oxidation. The binary Bi-Pb phase diagram is shown below in Figure 4.

Naturally occurring Pb is a mixture of four stable Pb isotopes, which have different abundances and nuclear physical properties. Bi is an isotopically pure element with only one isotope, ^{209}Bi . The eutectic mixture of both metals exhibits a clearly lower melting point (398 K) making it more suitable for cooling applications. Many properties of LBE such as heat capacity, surface tension, viscosity and density are comparable to those of the pure elements. An extensive overview on properties of Pb, Bi and their eutectic alloy may be found in [30, 37, 46].

Apart from the lower melting point compared to the constituting elements, LBE shows a negligible volume change upon melting at normal atmospheric pressure [37]. Similarly to Pb and Bi, LBE, has a significantly lower vapour pressure than Hg [30]. The high surface tension makes LBE to drip off from nearly every non-metal surface, making handling and waste treatment rather easy. As dissolution

rates in liquid Bi typically exceed those in liquid Pb, liquid LBE usually attacks unprotected steels more aggressively than liquid Pb coolant [47]. Lower operating temperatures that can be used for LBE-based facilities however counteract the increased corrosion effect induced by the presence of Bi, thus reducing engineering challenges and increasing the lifetime of structure materials [9].

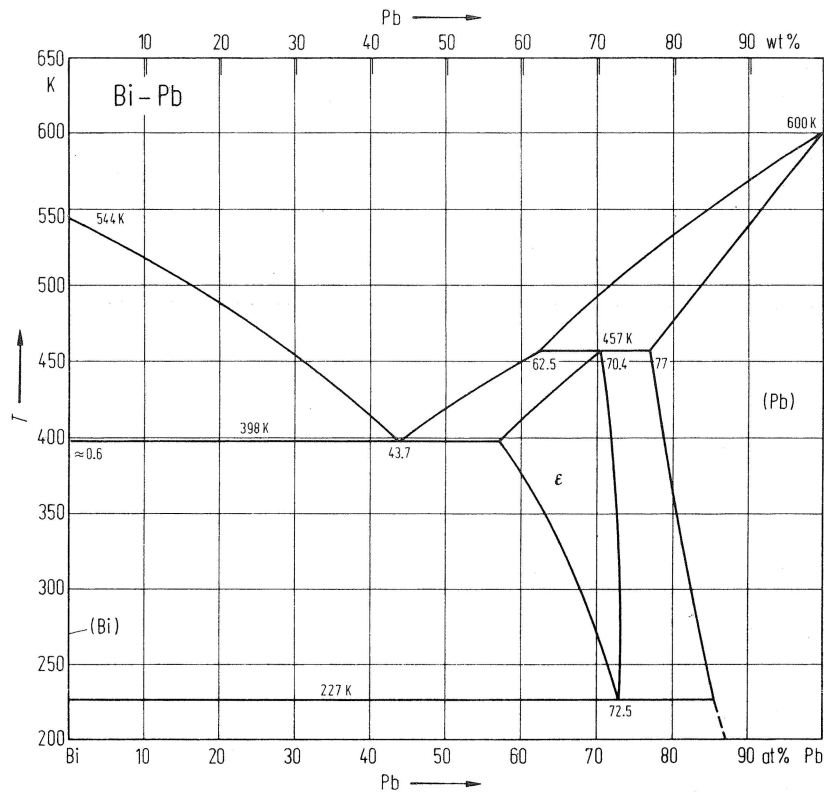


Figure 4: Bi-Pb phase diagram taken from [45]

Because of these beneficial properties it was decided to build a prototype LBE spallation target. Within the MEGAPIE Project (MEGAWatt Pilot Experiment) performed in 2006 at the Paul Scherrer Institute (PSI), Switzerland [48], such a LBE spallation target operating in the megawatt range was successfully built and operated. Being the target material for a period of 4 months, molten LBE was investigated concerning its feasibility as target material for future liquid metal spallation neutron sources and accelerator driven systems. As already mentioned in section 1.3, LBE is also foreseen as coolant and spallation material in the MYRRHA demonstration reactor [49]. Furthermore, the ESS project as well has considered LBE as a possible fallback solution [41]. Finally, Russia plans to construct LBE cooled nuclear fission reactors based on their long lasting experience with liquid LBE handling in experimental reactors [10] as well as in their alpha class submarines equipped with an LBE cooled reactors [50].

The use of LBE, however, does not come without certain drawbacks. As the alloy consists of more than 50% Bi, a considerable amount of ^{210}Po is formed within the liquid metal [9]. Additionally, a volume increase after solidification is observed for LBE, which may cause serious damage to the facility due to tube ruptures in case the liquid metal accidentally solidifies [51]. This effect is caused by a recrystallization of the inter-metallic compound Pb_7Bi_3 , referred as the ϵ -phase in the phase diagram shown in Figure 4. With decreasing temperature, the compound gets richer in Pb and the precipitating excess of pure Bi causes a volume expansion of the solid alloy in the order of 1%. This effect was observed to occur on very long timescales and was found to depend on the solidification velocity of the liquid metal [52]. Although a careful cooling of the metal may reduce stress to facility components in contact with Pb-Bi alloy, attention has to be paid at freezing/defreezing procedures to avoid any ruptures caused by the eutectic.

1.6.2 Liquid metal chemistry

Due to a large variety of nuclear interactions with protons, neutrons etc. the target material becomes highly radioactive. As already mentioned in section 1.4, for a target material with a atomic number Z , all elements from atomic number 1 to $Z + 1$ will be formed if the energy of the incident particle beam is well above the nucleon binding energy. The distribution of nuclear reaction products can be calculated [53] by means of well established empirical codes simulating the processes during spallation. The net radionuclide production depends upon the particle flux, the cross sections of the nuclides constituting the target material concerning the various nuclear reactions, and the irradiation time. The use of liquid metals in nuclear facilities thus results in the formation of large quantities of spallation and activation products within the liquid metal.

Directly after their formation, these nuclear reaction products will be present in the liquid metal in a highly excited monatomic state. After de-excitation, they in principle may remain dissolved in the liquid metal if the solubility limit of the corresponding chemical element at the temperature of operation is not reached. In case this solubility limit is reached, precipitation of the element can occur. The nuclear reaction products can also form chemical compounds with the solvent atoms, Pb and Bi, which are present in large excess. Although less probable, spallation and activation products can also form compounds between each other. Finally, the nuclear reaction products may react with impurities in the liquid metal, e.g. oxygen. Depending on their solubility in the liquid metal, the products of these chemical reactions may remain dissolved or they may separate from the liquid metal. In the latter case, they may float on the top of the liquid metal surface, remain dispersed as particulate matter within the liquid, or sink, depending on their density relative to the density of the solvent. Finally, insoluble species (elements or chemical compounds) may also deposit on the walls of the liquid metal vessel/loop. An overview on the spallation product concentration and their solubility in LBE at 500 K is given in Figure 5. Since only limited data on experimentally determined solubility of elements in liquid metals and alloys exist, a semi-empirical model has been proposed to quantitatively predict solubilities of the elements at various temperatures. By comparing these data with the calculated nuclide inventory provided by particle physics codes, it is possible to qualitatively assess the behaviour of spallation products in a liquid metal system. A detailed description of this topic may be found in [54].

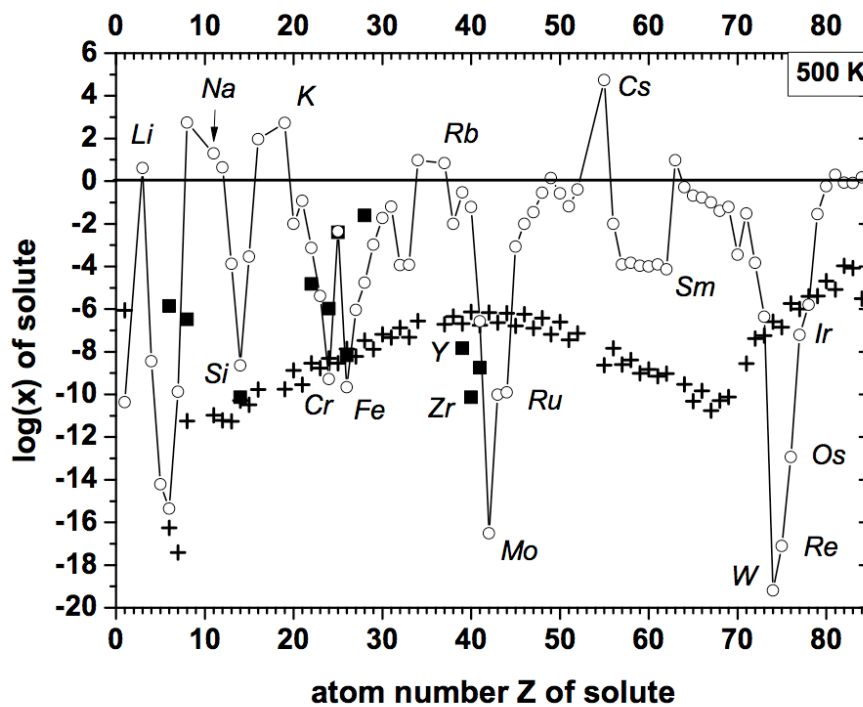


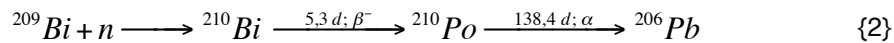
Figure 5: Molar fraction of the predicted [55] spallation product inventory (crosses) for the MEGAPIE LBE target and the measured (solid squares) and calculated (open circles) solubility of elements in LBE at 500 K; figure adopted from [56].

Apart from spallation products formed on irradiation, impurities also may originate from contaminations present in the liquid metal at start-up or from corrosion of steel structures during operation. Additionally, protons from the beam itself represent an intrinsic hydrogen source, as not all the protons injected into the system will be consumed by the spallation reaction. These protons will slow down and dissolve into the liquid metal as ionic hydrogen [57]. Depending on their concentration in the solvent, impurities may influence the behaviour of the system as a whole. It has, for example, been shown that impurities dissolved in Pb may significantly alter its oxidation behaviour [58].

Large quantities of liquid metal will be present in industrial nuclear facilities using a metallic liquid for cooling purposes. For safety and operation concerns it is important to understand chemical phenomena occurring within the liquid metal. The study on behaviour of spallation and neutron activation products is a challenging task, as each element will have its own peculiarities. Evaporation, adhesion to solid surfaces and many other physico-chemical effects will certainly increase the complexity of the system. A complete description of all processes occurring within a liquid metal used as spallation target is therefore out of reach. As a consequence, it is a convenient and scientifically reasonable approach to perform systematic studies on simpler systems containing only a few components in order to gain knowledge on the behaviour of single elements within a liquid metal environment.

1.6.3 The polonium problem

As already mentioned above, one important peculiarity arising from using Bi containing metallic liquids as spallation target material or reactor coolants is the formation of Po isotopes. In systems where high neutron or proton fluxes are present, considerable quantities of Po isotopes are formed as a product of (p, xn) and (n, γ) reactions with Bi:



While the neutron activation product ${}^{210}\text{Po}$ formed by reaction {2} is the major contributor to the total Po activity during operation, long-lived ${}^{208}\text{Po}$ and ${}^{209}\text{Po}$ isotopes produced by reaction {1} will be present long after shutdown of the facility. According to nuclear calculations, the ${}^{210}\text{Po}$ activity may reach up to 10^{11} Bq/kg in LBE under irradiation with high energy protons in a spallation facility [59]. In Table 2, the calculated MEGAPIE inventory for the most long-lived Po isotopes together with some of their decay data is summarized. Research on physical and chemical properties of Po has been performed in the past and the reader is referred to references [60-63].

Table 2: Half-life, decay mode and energy of the most long-lived isotopes of Po; additionally, the calculated [55] inventory for the MEGAPIE target after shutdown is given.

isotope	half-life	decay mode	α energy	calculated MEGAPIE nuclide inventory	
				mass [mg]	activity [Bq]
Po-206	7.7 d	EC 95% α 5%	5.22 MeV	2	6.1×10^{13}
Po-207	5.8 h	EC 100%	/	0.1	4.6×10^{13}
Po-208	2.9 y	α 100%	5.12 MeV	13	2.8×10^{12}
Po-209	102 y	EC 1% α 99%	4.88 MeV	2	1.4×10^{10}
Po-210	138.4 d	α 100%	5.30 MeV	758	1.3×10^{14}

Being a volatile α -emitter, Po represents a major concern if released into the surrounding enabling a possible uptake in the body. Especially ${}^{210}\text{Po}$ is extremely dangerous due to its high specific α -activity

(1.66×10^{14} Bq/g) [64]. The median lethal dose (LD_{50}) for acute radiation exposure is generally about 4.5 Sv [65]. For Po isotopes, the committed effective dose equivalent is $0,5 \mu\text{Sv/Bq}$ if ingested and $2,5 \mu\text{Sv/Bq}$ if inhaled [66]. Thus, the median lethal dose for ^{210}Po would be equivalent to 54 and 11 ng, respectively, making it about 250.000 times more toxic than hydrogen cyanide.

For the MEGAPIE experiment, calculations were performed to evaluate the radiological impact of Po release into environment in case of target leakage. From theoretical considerations, it was concluded that a complete release of the produced Po is hardly probable [67], [68]. Temperature functions of the equilibrium vapour pressure and evaporation rate of Po over dilute solution in LBE were conservatively estimated in [69]. Using such conservative estimations, it was proven to the licensing authorities that in accident cases only a very small fraction of the Po produced in MEGAPIE could be released into the environment. Nevertheless, several pathways for the release of Po seem to exist that still raise many questions in the scientific community. Apart from thermal evaporation, which has been studied in the past [70-73] and is believed to be understood with some certainty, the release of Po at low temperatures is still poorly investigated. Interaction of LBE containing Po with air or moisture was reported to result in the formation of the volatile species H_2Po [74].

Another possibility of Po to become airborne is attributed to an effect referred as aggregate recoil or self-sputtering [75]. It is based on the fact that during α decay, the recoiling daughter atom acquires enough kinetic energy to break several thousand chemical bonds within its host material [76], thus enabling the ejection of small particles from its surface. By such intrinsic irradiation, release of radioactivity from LBE surfaces containing α -decaying material, such as Po, may occur. This effect is independent of temperature [77] and would thus be largely driven by the amount of α activity present at the near surface region of either solid or liquid LBE. Po release caused by such a mechanism would require severe safety precautions while handling and managing the waste of solid LBE containing high amounts of Po isotopes. Po contamination was reported in incidents on Soviet Union alpha class submarines powered by nuclear reactors containing LBE [78]. These contaminations could possibly be explained by the occurrence of such volatilization mechanisms. Additionally, significant Po enrichment has been observed on surfaces of solid Pb and LBE [56, 79]. Such a surface enrichment could cause significantly increased volatilization of α , β and γ activity by sputtering effects.

In conclusion, much research is needed in order to understand the effects that are responsible for the release of Po from LBE. The fact that the pathways of Po volatilization are still not known with sufficient certainty still enlarges the demand for stringent requirements from safety authorities regarding facility licensing. Despite the efforts to understand the behaviour of Po in a nuclear facility, other suitable approaches to minimize the hazard caused by release of Po from such systems to the environment would be to decrease the amount of Po produced or to remove it from the liquid metal by chemical methods.

I.7 Motivation

The aim of this thesis is to provide physical and chemical data for lead-based alloys that are used in nuclear facilities in order to tackle the problems associated to the production of Po discussed above. Three different subjects have been studied within this thesis that cover different aspects of this topic. This research should give insights into possibilities of reducing the hazard of Po and serve for a better understanding of phenomena relevant for a safe operation of a liquid metal-based nuclear facility. A short description of these three topics is given below:

One way to minimize possible Po release to the environment from a liquid metal spallation target facility or an ADS would be to use a liquid metal that is free from Bi, thus reducing or completely avoiding the production of hazardous Po isotopes. Based on literature data for low melting Pb alloys, it was proposed to use Au as a substitute for Bi [80]. The resulting eutectic alloy of Pb and Au, LGE, has promising material properties to serve as a beneficial substitute for LBE. First material investigations and simulations revealed this material is an interesting candidate material for future spallation sources as, for example, the ESS spallation source [81]. Nevertheless, profound studies on its corrosion behaviour towards steels that are going to be used as construction materials for liquid metal spallation sources or ADS were missing. Within this PhD thesis, the corrosion behaviour of LGE towards steel

structures was investigated by chemical analysis of samples from an experimental liquid metal loop and compared to that of the better-studied LBE.

In case a reduction of Po production by choosing an alternative target material proves to be not feasible and one has to resort to LBE, other solutions for coping with the problems caused by Po in LBE in nuclear facilities have to be found. A possible way to face these problems can be a continuous removal of Po from the liquid metal. In literature, several possible techniques for Po removal from LBE have been discussed. One of the most promising techniques is a liquid-liquid extraction using fused alkali hydroxides. Within this thesis, systematic studies on the removal of Po from irradiated LBE using this extraction method were performed. Additionally, the alkaline extraction technique was studied concerning its efficiency for separating various nuclear reaction products from Pb, Bi and LBE samples containing a realistic mixture of spallation products. Apart from Po, the extraction of more than 30 other elements from these samples was investigated.

The approaches of solving the problems associated with Po production and release from liquid metals discussed above may prove not to be technically or economically feasible. Certainly, they are currently still not mature for an implementation in a large-scale facility. Thus, for the construction and licensing of facilities that are planned to be built in the near future, the need for a better understanding of the behaviour of Po in LBE persists. Consequently, more systematic studies of Po evaporation and release from LBE under various chemical conditions have been started [15]. The behaviour of Po in a solid LBE matrix has been considered to have minor importance for safety considerations so far. However, the discovery of Po segregation and surface enrichment phenomena in solid Pb and LBE [56, 79] can have a significant influence on the sputtering phenomenon discussed above. Therefore, the mechanisms and fundamental physicochemical parameters of the processes leading to Po surface enrichment should be studied to support safety assessments concerning future large-scale nuclear facilities using Pb-Bi. The third part of this thesis is devoted to provide a better scientific understanding on these surface enrichment effect.

II Stability of construction materials in lead-gold eutectic

II.1 Introduction

To avoid massive production of ^{210}Po as a neutron activation product of ^{209}Bi , it has been proposed to use Pb alloys free from Bi. Such an alloy should combine the beneficial properties of LBE and Hg while avoiding their specific pitfalls. For this purpose, a survey on existing Pb alloys was performed to elucidate a suitable alloying element. In Table 3 an overview on the possible alloys of Pb with 5d and 6p elements beginning from Ta are given. For comparison, the difference to the melting point of pure Pb is also listed in the table. As can be seen, the elements Ta to Ir, which have melting points above 2000 °C, do not form any intermetallic compounds with Pb. A wide miscibility range exists for alloys between Pb and Hg or Tl, but only alloys with Pt, Au and Bi exhibit melting points below that of their constituents. If the production of radioactive ^{210}Po is to be minimized, only alloys of Pb with Au or Pt are advantageous. Since the Pt containing alloy has a melting point depression of only 38 K compared to Pb, it is evident that the eutectic mixture of Pb with Au, lead-gold eutectic (LGE) is the most promising alternative to the Bi-based alloy.

Table 3: Overview on possible alloys of 5d and 6p metals with Pb

alloying element X	forms eutectic with Pb	eutectic composition at [at%] X	T_m [K]	$\Delta T = T_m(\text{Pb}) - T_m(\text{X})$
Ta, W, Re, Ir	no intermediate phases	/	/	/
Pt	yes	5.3	563	38
Au	yes	15.9	486	115
Hg	no, but miscible	/	234*	367
Tl	no, but miscible	/	577*	24
Bi	yes	56.3	398	203

* - melting point of pure element X

Based on this fact, LGE was suggested as a new candidate target material in neutron spallation sources [81, 82]. This proposal was based on different considerations and requirements towards a Pb-based alloy. First of all, the alloying element should be non-volatile and should have a high atomic number to be suitable as a spallation target material. Its eutectic with Pb should exhibit a considerably lower melting temperature than Pb and a high boiling point. All these requirements do apply to Au. However, physico-chemical, neutronic and fluid-dynamical properties of the alloy itself do also influence the use of a new material in a nuclear facility.

For LGE as potential target material, many of these properties are still not known and first investigations have been started in 2010 to shed light onto this exotic and expensive material. Up to now, investigative studies on the phase diagram [81], its physical properties [83] and calculations on nuclear characteristics [81, 84] have been performed. So far, no property excluding its usage for nuclear applications was found. Compared to LBE, LGE does not exhibit a volume increase in the solid state [81] while having similar neutronic performance. The accumulation of Po isotopes was calculated to be in the order of 10^4 less if no impurity Bi is present [81].

Nevertheless, the use of such a eutectic in nuclear applications is not only restricted to properties listed above. Handling of the alloy during operation, maintenance and final disposal have to be considered as well and require devoted investigations and tests under non-active and irradiation conditions. Substantial research and development has to be invested before any new liquid metal target material may be licensed for nuclear applications.

Among many others, one of these concerns is the evaluation of the corrosion behaviour of LGE towards structure materials. In order to test the behaviour of flowing LGE towards steel structures and to compare it to LBE, two identical isothermal test loops were built and operated in Salaspils by the

Institute of Physics of the University of Latvia (IPUL). Up to now, five campaigns operating at different temperatures were successfully carried out. The corrosion behaviour during these runs was investigated by applying two different methods. Analysis of steel specimens inserted in both loops was performed using scanning electron microscopy (SEM) in [85]. Within the work of this PhD thesis, the concentration of corrosion products present within both liquid metals was measured using inductively coupled plasma optical emission spectroscopy (ICP-OES). The result of this investigation will be presented here, together with recent findings of other studies on LGE.

II.2 Lead-gold eutectic

II.2.1 Properties of lead-gold eutectic

The eutectic alloy of Pb and Au (Pb: 84.1 wt%; Au: 15.9 wt%, [86]) is a shiny, silver-grey and brittle material which quickly becomes dark grey coloured if exposed to air due to oxidation of Pb. It has a melting point of 212.5 °C and a density of 12.2 g/cm³. Many properties such as boiling point, density or volume expansion of this material are currently not yet known. It is assumed to boil above 1700 °C [81]. A phase diagram of the binary system Pb-Au is shown in Figure 6.

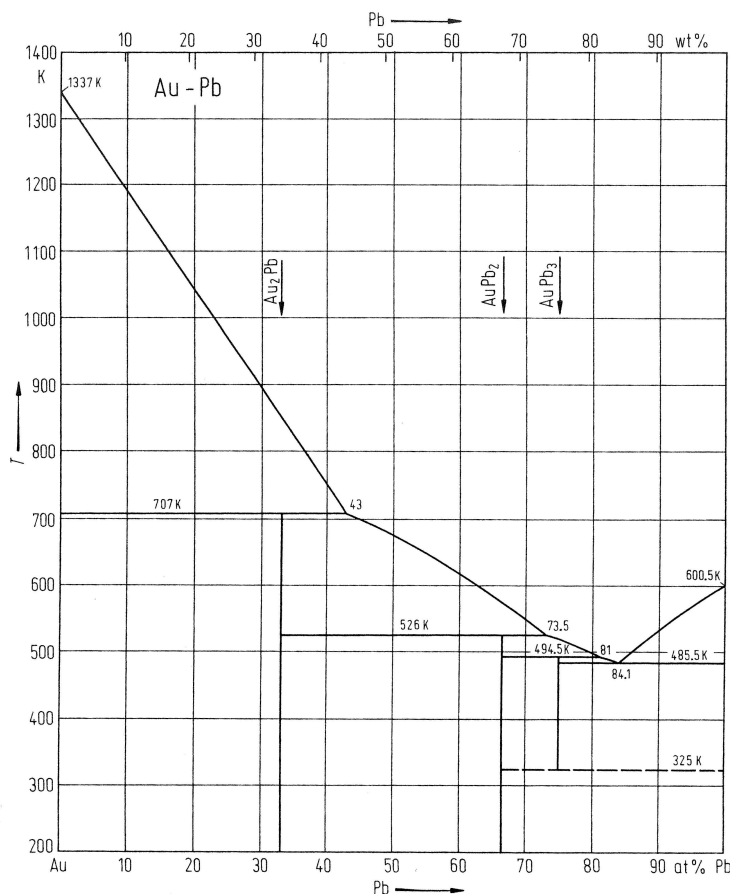


Figure 6: The binary phase diagram of Pb and Au taken from [87].

This phase diagram has been studied by [86, 88-92] and a summary on the experimental work done on the Pb-Au system may be found in [91]. Two inter-metallic compounds AuPb₂ and AuPb₃ were found to be present in the solid phase within the Pb-rich region of this system. If a mixture of both elements in eutectic composition is cooled below its melting temperature, the Au-rich phase AuPb₃ separates together with pure Pb. Thus, directly after crystallization, LGE represents a mixture of pure Pb crystals and the inter-metallic compound AuPb₃, which, however, has been shown to be an unstable compound on further cooling [81]. If the temperature drops below 325 K, AuPb₃ decomposes to Pb and AuPb₂, resulting in a recrystallization of the eutectic alloy in solid state, similar to that in the Bi based alloy.

This phase transition was, however, the topic of some debate as some scientists have either questioned its occurrence [86], or reported the transition to occur at a different temperature [91]. This feature was investigated in detail in experiments performed in [81], where the LGE phase transition was studied using x-ray diffraction. It was found that at room temperature, in contrast to earlier publications, AuPb₃ is the stable intermetallic compound in LGE. The occurrence of the AuPb₂ phase was only observed for samples with fast cooling, whereas a re-heating or a long storage at room temperature of such samples showed decomposition of AuPb₂. The occurrence of the AuPb₂ phase was not observed if a slow cooling of the liquid LGE sample is performed. These phase transitions have to be analysed in detail in order to understand the underlying processes and to gain knowledge on the correct phase diagram.

It was further shown in [81] that the transition of AuPb₃ to AuPb₂ and Pb in fast-cooled samples does not come with a volume change exceeding 0.2%, which is much lower compared to the effect known from LBE (see section I.6.1). Thus, problems arising from solid-state expansion of the spallation target material are minimized in case of LGE. The volume expansion during the phase transition from liquid to solid, however, has never been measured for LGE. Since Pb contracts on solidification and Bi, in contrast, exhibits a volume expansion, the volume change of LBE is often referred to be negligible [30].

The dependence of viscosity, surface tension as well as thermal and electrical conductivity on temperature has recently been investigated in [83]. An overview on known physical properties of LGE is given in Table 4 together with data on LBE and Pb for comparison.

Table 4: Overview on physical properties of LGE, LBE and Pb at 450 °C; taken from [83] and [37].

liquid metal	LGE	LBE	Pb
melting point [K]	485	398	601
boiling point [K]	n.d. ²	1943	2016
dynamic viscosity ¹ [Pa s]	3.4 x 10 ⁻³	1.4 x 10 ⁻³	2.0 x 10 ⁻³
thermal conductivity ¹ [W/m/K]	16.0	13.7	17.2
electrical resistivity ¹ [Ω m]	1.1 x 10 ⁻⁶	1.2 x 10 ⁻⁶	1.0 x 10 ⁻⁶
surface tension ¹ [N m]	0.49	0.39	0.44
volume expansion on solidification [%]	n.d.	≈ 0	-3.7
liquid density ¹ [g/cm ³]	n.d. ³	10.1	10.5

¹ at 450 °C

² not yet determined, but presumably >2000 K

³ not yet determined, presumably >12 g/cm³

II.2.2 Simulation of nuclear properties

Calculations on the neutronic performance of LGE as a liquid metal target were done with particle transport Monte Carlo simulations using the MCNPX2.5.0 code [81]. The aim was to compute the neutron energy spectrum, decay heat and the nuclide inventory under different boundary conditions. To compare a LGE target to other spallation materials already known in nuclear applications, simulations were also performed for LBE and Hg under similar conditions. The boundary conditions were operational considerations foreseen for the European spallation source (ESS), the main calculation parameters may be found in [81]. Figure 7 represents (a) the decay heat and (b) the radioactive inventory as a function of cooling time after facility shutdown. Additionally, in (c) the neutronic performance for LGE, LBE and Hg is shown.

The simulation revealed that LGE has very similar properties to LBE and Hg as far as the neutronic performance is concerned. No significant drawback excluding LGE as spallation material could be found by these computer simulations. The calculated radioactivity and decay heat originating from an LGE target is about a factor of 3 higher in the first 10 days after shutdown, if compared to LBE and Hg.

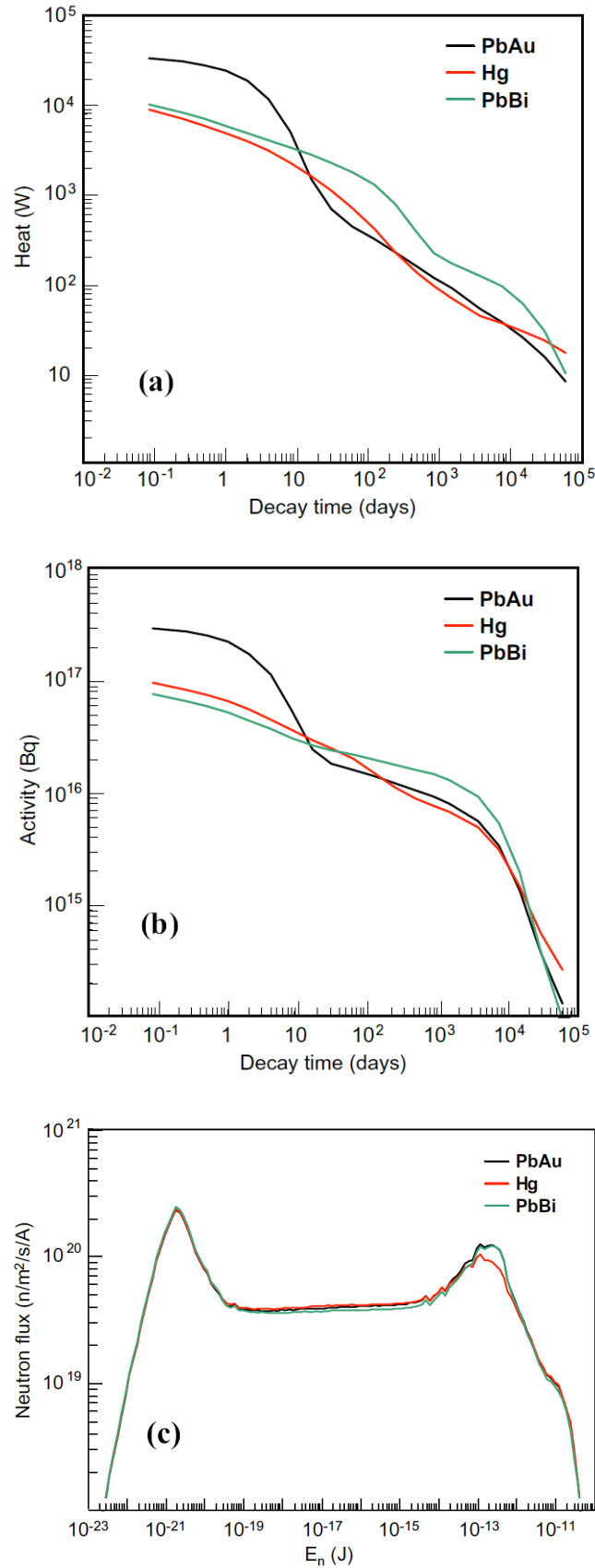


Figure 7: Calculated function of (a) decay heat, (b) activity with time after facility shutdown and (c) neutronic performance in the hydrogen moderator tank of a LGE, LBE and Hg in an ESS target. Graphs reproduced from [81].

This effect is caused by the production of the short-lived Au activation product ^{198}Au , which decays within weeks after shutdown. Afterwards, the heat dissipation and activity of an LGE target are similar or even slightly lower than an LBE and Hg target irradiated under similar conditions. Approximately 0.8% of Au was predicted to transmute into Hg during 40 years of facility operation. Apart from stable isotopes, one dominant radioisotope of Hg will be ^{194}Hg , which has a half-life of 440 years. Hg will cause a special issue in LGE targets, as it is a volatile element easily released to the environment. In LBE, 10 times less Hg is produced, and its volatilization from this liquid metal will fall behind that from LGE, mainly due to lower operation temperatures that can be used in LBE facilities.

For calculations on the total nuclide inventory and decay heat after facility shutdown, the authors in [81] have assumed that the impurity content of LGE is the same as in LBE, for which a detailed impurity analysis already existed, see Table 5. Despite the impurities coming from Pb, which may be assumed to be similar for both alloys, the purity of Bi and Au should obviously differ, as these metals originate from different refinement paths in metallurgical industry. The authors in [81], however, assumed the impurity content in LGE to be practically the same as for LBE, which is scientifically not justified. Arbitrarily, the LGE alloy was set to contain no Bi at all. However, Bi is known to be a prominent impurity accompanying Pb from metallurgical refineries.

Disregarding the Bi impurity, the accumulation of Po in LGE was calculated to be in the order of 10^4 less if compared to LBE. This is especially important for facility licensing and operation, as Po is associated with several issues due to its toxicity and volatility, see section I.6.3. A lower Po production rate in a liquid metal LGE target will certainly ease these issues resulting from the occurrence of this element. Nonetheless, more precise calculations assuming a reasonable Bi impurity content in LGE have to be performed in future.

Table 5: Impurity concentration for LGE and LBE used for Monte Carlo calculations in [81]

element	concentration [wppm] in	
	LBE	LGE
Ag	6.6	6.6
Au	0	152,300
B	1.7	1.7
Bi	550,000	0
Ca	0.39	0.39
Cd	0.6	0.6
Cr	0.4	0.4
Cu	2.1	2.1
Fe	0.2	0.2
In	28	28
Mg	0.2	0.2
Ni	2.4	2.4
Pb	450,000	847,700
Sn	113	113
W	2.7	2.7

In Table 6 an overview of the 10 radionuclides with the highest activity in LGE and LBE 10 years after facility shutdown is given. Interestingly, the radioisotopes itself do only differ by their position within the table, meaning these radioisotopes are the most prominent for both liquid metals, LBE and LGE. Disregarding ^3H , which represents the nuclide with the highest β^- activity in both materials, ^{207}Bi and $^{194}\text{Hg}/^{194}\text{Au}$ are those nuclides with the highest γ activity after end of facility lifetime. The isotopes ^{193}Pt , ^{204}Tl , ^{145}Pm and ^{148}Gd do either not or only emit weak γ radiation. This feature will play an important role for radiation safety concerns during disassembling or disposal works. Nevertheless, some of the last-named nuclides are also β^- or α emitters and should be taken into account while dealing with large quantities of material.

Table 6: Radioisotopes with the 10 largest activities in LGE and LBE 10 years after shutdown of the spallation facility. Table reproduced from [81].

Nuclide	$T_{1/2}$ [a]	Activity [Bq/kg] in	
		LGE	LBE
^3H	12.3	3.9×10^{11}	6.8×10^{11}
^{193}Pt	50	3.9×10^{10}	1.8×10^{10}
^{204}Tl	3.8	1.2×10^{10}	9.1×10^9
^{207}Bi	31.6	5.0×10^9	2.5×10^{11}
^{145}Pm	17.7	3.9×10^9	4.0×10^9
$^{194}\text{Hg}/^{194}\text{Au}$	520	2.8×10^9	2.8×10^9
^{148}Gd	74.6	1.8×10^9	1.8×10^9
^{90}Sr	28.6	1.5×10^9	2.4×10^9
^{133}Ba	10.5	1.5×10^9	1.6×10^9

II.2.3 Solution of elements in LGE

Up to now, no data on the corrosion behaviour of steels or other structure materials in LGE is known so far. Much research on corrosion was performed for the Bi-based alloy; here an appreciable amount of data is available in literature. For a Pb-Au alloy, such investigations have never been done in the past.

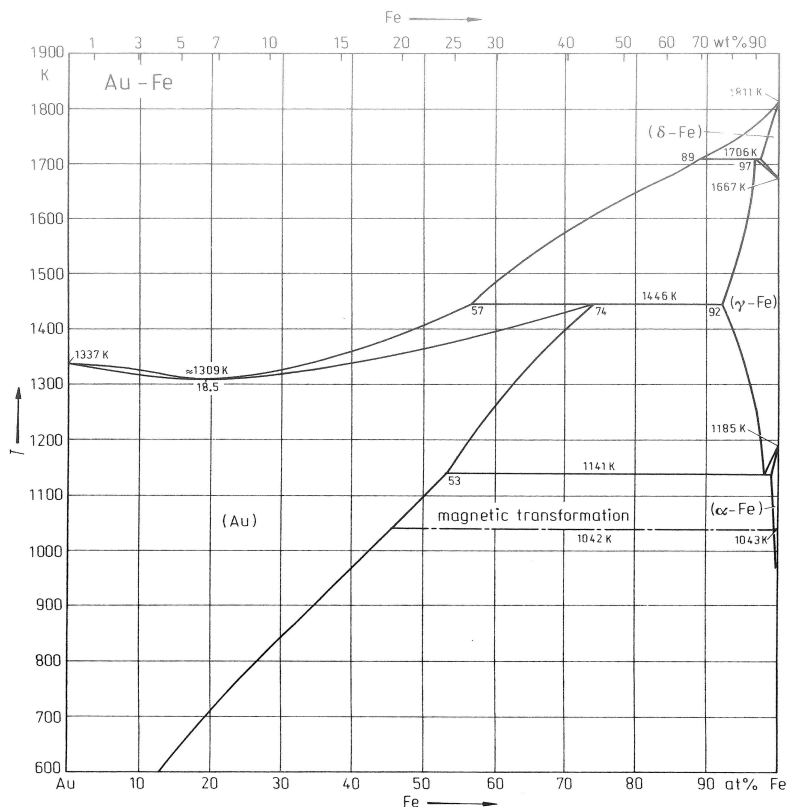


Figure 8: The Au-Fe phase diagram [87]

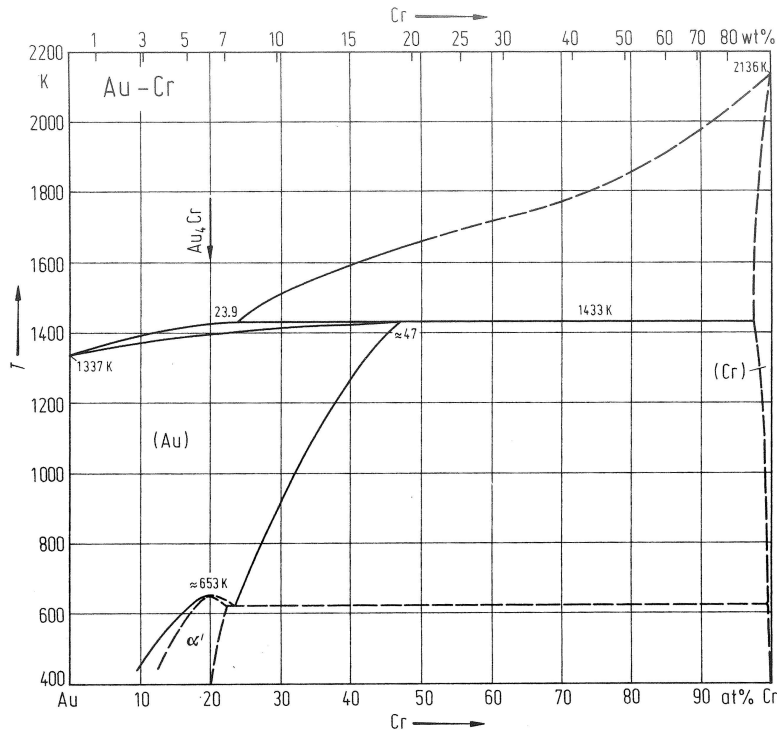


Figure 9: The Au-Cr phase diagram [87]

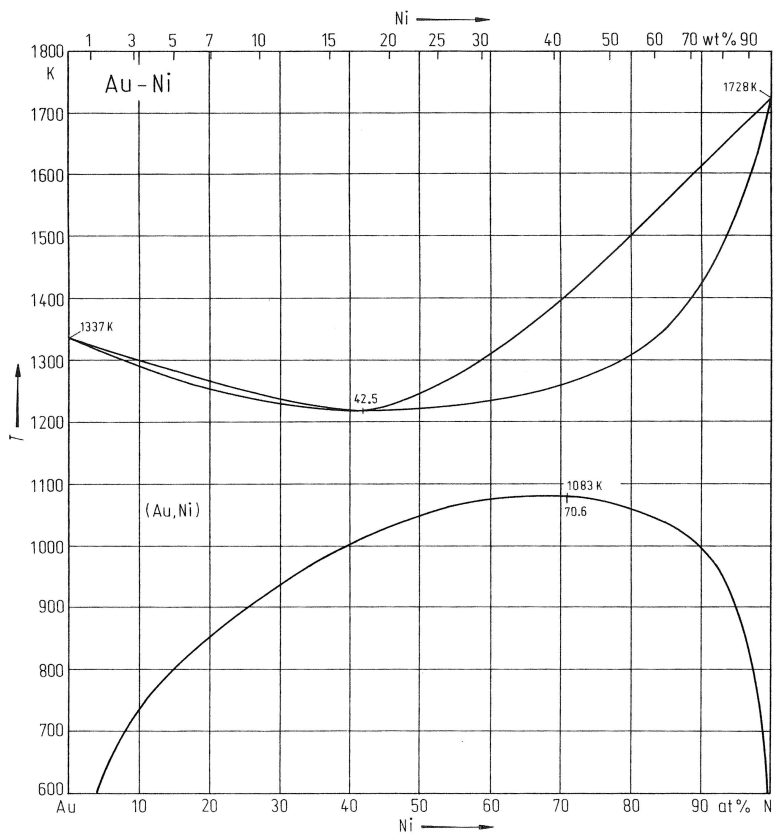


Figure 10: The Au-Ni phase diagram [87]

It is well known that Au easily forms stable alloys with several metals like Ag and Cu (jewellery), but also with Ni, Fe, Al, Cr and others [93]. Some of these metals show miscibility with Au in wide concentration ranges above its melting temperature. In Figure 8, Figure 9 and Figure 10 the phase

diagram of the Au-Fe, Au-Cr and Au-Ni systems are shown. From numerous investigations on binary Au alloys it is known that elements with melting temperatures exceeding 2500 °C such as W or Re do not form any Au alloys and are nearly insoluble in molten Au. These elements represent suitable container materials for handling molten Au and its alloys.

From the published liquidus lines in the phase diagrams it may be concluded, that above the melting temperature of Au, more than 10 wt% Fe and 30 wt% Ni dissolve in Au. The solubility of Cr is lower than that of Fe and Ni. All data published on the phase diagrams only apply to mixtures with relatively high contents of Fe, Cr or Ni at temperatures exceeding 1300 K. No data on the temperature function of the solubility of these elements in the near Au-region were found in literature.

II.2.4 Solubility of steel elements in molten Pb alloys

Studies on the corrosion effects of liquid metals on different steels date up to the early 1950ies. During the development of liquid metal cooled reactors, the corrosion behaviour of Pb, Bi and their eutectic alloy was the subject of several experimental studies [30]. These investigations were later extended towards studies on the solubility of pure elements in molten metals, where some data were already available either in metallurgical or physico-chemical literature. For example, the solubility data of Fe in Pb and Bi were only determined in the 1970ies, whereas corrosion studies on steels, where Fe is the main constituent element are available already from 1946. A lot of experimental work on solubility and compatibility of materials with liquid Bi was performed in the 1960ies during the liquid metal fuel reactor program in the US [94]. These works were also devoted towards evaluating the behaviour of fission products produced in Bi-U fuelled reactors.

Investigations have shown, that the maximum (or equilibrium) solubility c_s of element X in a solute Y can be described by the following equation:

$$\log c_s = A - \frac{B}{T}, \quad (2)$$

where A and B are constants determined experimentally and T the absolute temperature in K. Constant A usually refers to the dissolution entropy, whilst B is proportional to the heat of mixing between X and Y. In this simple model, the dissolution of element X in solute Y should not come with any formation of an intermetallic compound X_nY_m at any temperature within the range of interest. Data on solubility for the main steel alloying elements as Fe, Cr, and Ni in molten Pb, Bi, their eutectic alloy and pure Au is given in Table 7. A summary of data and reference to the original publications on the solubility of various elements in Pb, Bi and LBE may be found in references [57], [95] and [37].

The solubility of Fe in molten Pb and in its alloys of different composition was studied in detail by [47]. The amount and precision of collected data indicates that this investigation presents the most reliable data for Fe solubility in molten Pb in the temperature range between 400 and 850 °C. For Ni and Cr, solubility data were published by [96], and especially for Ni a wide set of data in the temperature between 370 and 1240 °C is available. Nevertheless, in some publications these numbers were either recalculated or adopted from literature referencing to [96], giving rise to different or slightly deviating values for Ni solubility in western and soviet literature. Up to now, data published in [96] represents the most reliable set of data for the solubility of Ni and Cr in molten Pb. Authors have also given numbers on Mo solubility, which was determined to be below 50 ppm up to the temperature of 1200 °C.

Data on the solubility of 19 elements in molten Bi were published by [97] and a review on data for 14 other elements is given in this work. For the determination of the Ni and Mn solubility, the authors note that these two elements form inter-metallic compounds with Pb that appear as peritectic points in the Ni-Bi and Mn-Bi phase diagram. Therefore, the solubility of these elements in Bi cannot be extrapolated to infinite dilution as required for the correct use of the thermodynamics [97]. For Mo in molten Pb, no data exists up to now.

Table 7: Experimentally determined fitting parameters for the solubility of steel alloying elements in Au, Pb, Bi and LBE. The saturation concentrations at 623, 673 and 737 K were calculated using equation (2).

solvent	solute	solubility equation $\log_{10}(\text{wt\% solute}) = A - B/T$		temperature range [K]	reference	equilibrium solubility [wppm] at		
		A	B			623 K	673 K	723 K
Pb	Fe	0.34	3450	673 - 873	[47]	0.06	0.16	0.37
	Cr	3.88	6949	1181 - 1473	[96]	5×10^{-4}	4×10^{-3}	2×10^{-2}
	Ni	1.30	1381	645 - 1350	[96]	1211	1770	2454
	Mo	2.92	10554	> 1473	[98]	9×10^{-11}	2×10^{-9}	2×10^{-8}
	Mn	2.02	1825	748 - 1273	[99]	1232	2034	3132
Bi	Fe	1.69	3490	698 - 998	[100]	1.22	3.19	7.29
	Cr	2.26	3580	673 - 973	[100]	3.26	8.72	20.34
	Ni	2.496	1465	753 - 903	[100]	13947	20854	29493
	Mo	no data available			/	< 1 ppm below 1073 K		
	Mn	3.804	2177	613 - 719	[97]	20399	37088	/
		2.214	1030	719 - 783	[97]	/	/	61572
LBE	Fe	2.01	4380	823 - 1052	[47]	0.10	0.32	0.90
	Cr	-0.02	2280	673 - 823	[101]	/	3.91	6.71
		1.07	3022	643 - 813	[102]	1.66	3.80	7.77
	Ni	5.2	3500	603 - 688	[103]	3820	9986	/
		1.7	1000	753 - 823	[101]	/	/	20743
	Mo	no data available			/			
	Mn	no data available			/			
Au	Fe				[87]	6.1 wt% at 1309 K		
	Cr				[87]	7.7 wt% at 1430 K		
	Ni	no data available			[87]	18.0 wt% at 1220K		
	Mo				/			
	Mn				[87]	11.6 wt% at 1233 K		

From the solubility-temperature curve in a binary system, one can estimate the heat and entropy of solution (ΔH and ΔS). For bcc metals in liquid Pb, the value of ΔH was found to be related to the melting point of the solute and decreased to zero at a melting point slightly above 2500°C. Thus, all metals with melting points greater than 2600°C were totally insoluble in Bi. These metals were also found to be fully corrosion-resistant to Pb in the absence of oxygen [94].

In LBE, solubility of Co, Cr, Cu and Ni has been measured by [101] in the temperature range between 400 and 550 °C. For Fe, systematic investigations were performed with a near-eutectic composition of Pb and Bi by [47]. The numbers given in [47] have been used to interpolate parameters A and B in equation (2) for the exact eutectic composition (55 wt% Bi and 45 wt% Pb) and were published in some recent publications as new data. Their origin, however, seems questionable, as numbers and even the valid temperature range published by [104] or [105] are very similar to data reported more than 40 years ago by [47]. It is reasonable to assume that the numbers published by J.R. Weeks in 1969 are the only measurements of the Fe solubility in Pb-Bi alloys and later reports do directly, indirectly or do not even refer at all to this investigation. No successful investigation on the solubility of Mo and Mn in LBE has been reported yet.

Some additional measurements on the Ni and Cr solubility at temperatures as low as 350 °C have been reported recently [102, 103]. In [103] a review on existing data for Fe, Ni and Cr solubility is given, the reader may refer to this publication as the most up-to-date. An overview on solubility data for a big variety of elements in molten Pb, Bi and LBE may be additionally found in [37, 95].

From data in Table 7 one may conclude, that molten Bi will show significantly more dissolution attack towards steel structures than pure Pb. For every solute element in Table 7, the solubility in molten Bi is calculated to be higher than that in Pb for temperatures between 623 and 773 K. This finding was confirmed by investigations done by [47], where mixtures of Pb and Bi at different compositions were analysed concerning their relative corrosion rates towards steels. The result of this investigation is presented in Figure 11. For alloys with a high Bi content the relative corrosion rate drastically increases. This dependence, however, is not linear, and the corrosivity at the eutectic composition does not change significantly compared to pure Pb.

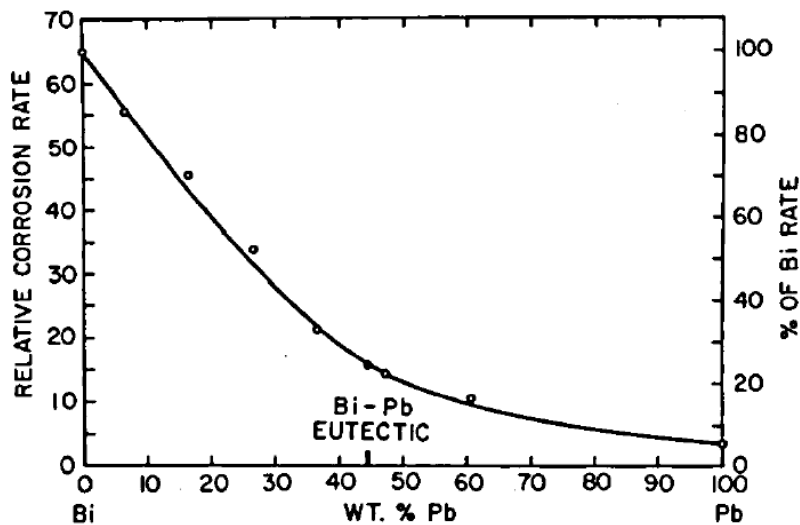


Figure 11: The relative corrosion rate of steels in Pb-Bi mixtures of different composition; reproduced from [47].

Data given in Table 7 indicates that the most soluble species in Au will be Ni and Mn. A similar picture may be drawn for the solubility of these elements in Pb. One may now postulate that this finding should also apply to the binary alloy LGE, nevertheless such a statement has to be taken with care. For Au, nearly all solubility data were obtained at temperatures exceeding 900 °C and reliable data on the solubility of Fe, Cr, Mn and Ni in LGE at much lower temperatures may not be straightforwardly extrapolated. Additionally, it is known that some properties of Au alloys may significantly alter if compared to properties of the pure elements [83].

Therefore, a study on the dissolution of steel alloying elements in LGE is done by analysing the behaviour of this material towards steel structures and comparing it with that of LBE under stringently equivalent conditions. As corrosion by LBE is the by far better studied process, a comparison with LBE is of crucial importance for a quick assessment of the suitability of LGE as target material. For a detailed investigation on this topic, a corrosion experiment was started in 2010 at IPUL in the frame of a material research program for ESS. LGE and LBE were tested in two identical loops for their behaviour towards steel specimen inserted in both loops. The results of this investigation should show if there are significant peculiarities for LGE regarding corrosivity and how this new material will behave under experimental conditions.

II.3 Experimental

II.3.1 Preparation of LGE

For the preparation of the eutectic Pb-Au mixture a special mixing apparatus was developed by IPUL, where molten Pb was added to molten Au in a controlled manner. It consists of three heated vessels connected in a row to ensure an easy mixing of both metals while molten. The layout of the mixing device is shown in Figure 12. The first vessel (pos. 1 in Figure 12) was built of 304 stainless steel and used to melt Pb under an Ar atmosphere. A certain mass of molten Pb was transferred to a second heated vessel (2) where the amount of Pb was determined by a balance. In order to avoid any transfer of Pb oxides, molten Pb was taken only from the bottom of the first vessel.

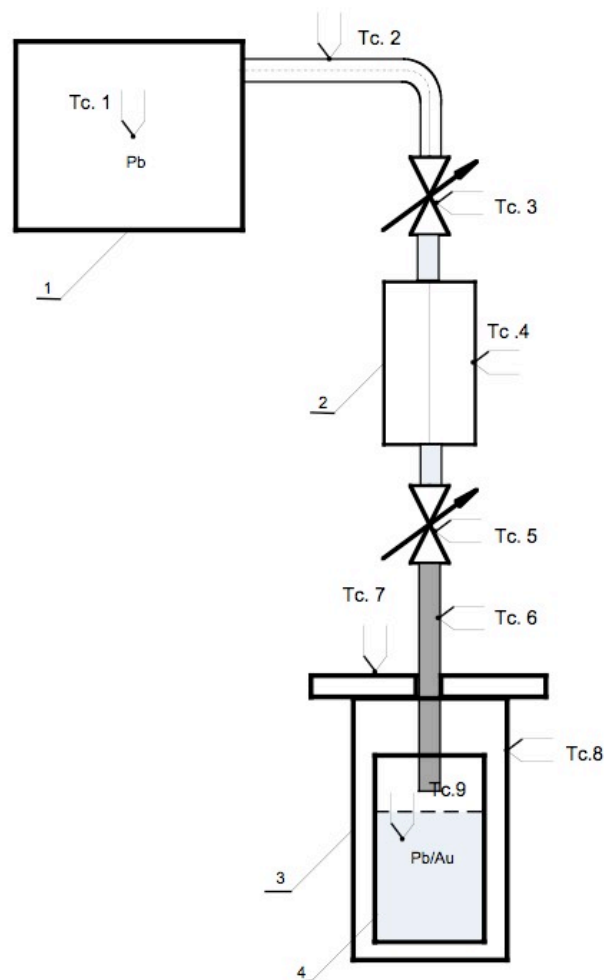


Figure 12: Mixing device used for the preparation of LGE; points referred as “Tc.” represent positions of installed thermocouples, positions 1-4 are described in the text.

Au was molten in a ceramic Alsin Al₂O₃ crucible (4) to ensure that no metallic impurities are transferred to the molten Au. Before mixing, all vessels were evacuated and filled with Ar in order to avoid any oxidation of Pb during the mixing process. After the second vessel was filled with the desired amount of Pb, a valve was opened to allow Pb at 520 °C to be drained into the mixing vessel containing molten Au heated to 1100 °C.

In order to obtain a homogeneous alloy, the liquid metal in the ceramic crucible was thoroughly mixed by means of an electro-magnetic rotary induction stirrer (3). By this procedure, 862 g of Au, 99.99% purity, provided by Valcambi Inc., were mixed with 99.9% Pb, GMH Jost-Hinrich Stachow GmbH, to obtain 6 kg of LGE in three subsequent batches.

The concentration of impurities inside the initial metals was determined by a procedure described in section II.3.3. The eutectic composition of the final product was confirmed by differential scanning calorimetric measurements. The appearance of a plateau at 216°C during heating and cooling of the alloy coincided well with the expected LGE melting temperature.

II.3.2 The experimental loop

Corrosion experiments were performed using two identical isothermal liquid metal loops. A schematic layout of this twin-loop is shown in Figure 13.

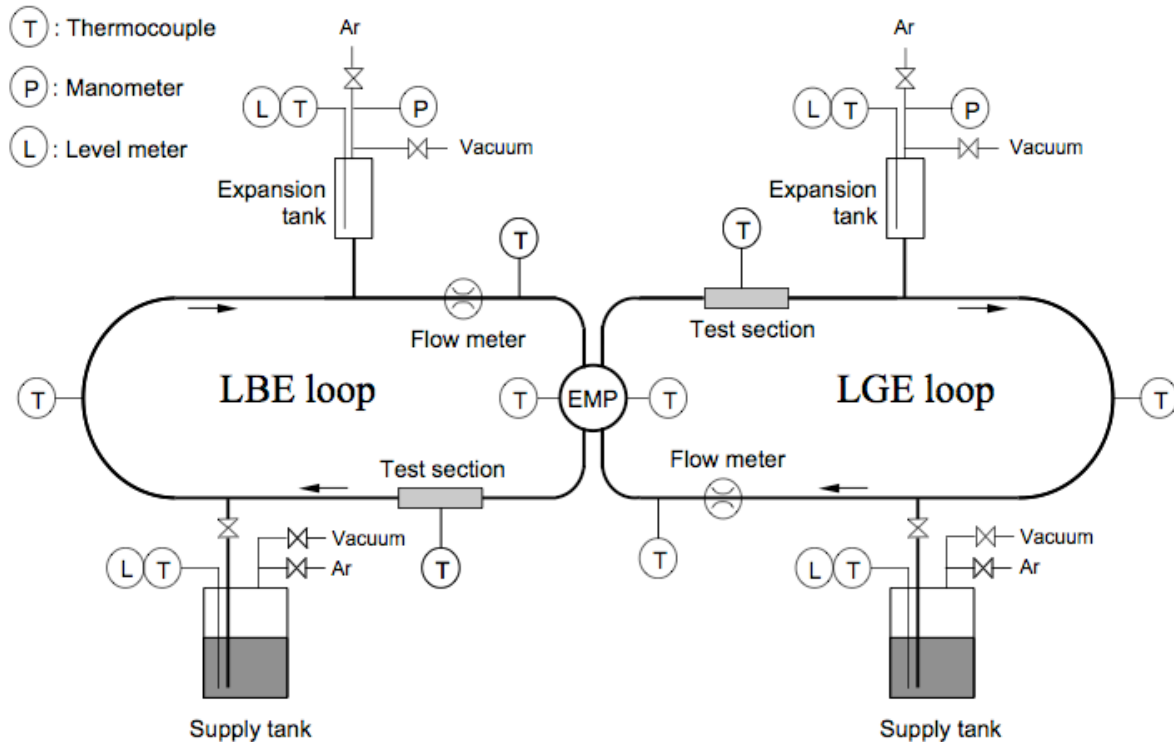


Figure 13: Layout of the twin-loop

The tubing of the twin-loop was made of 316L stainless steel and had a length of approx. 2.5 m with an inner diameter of 10 mm. Each loop was filled with approx. 250 ml of liquid metal from a supply tank. An electromagnetic pump (EMP) with a pumping power of 1 kW circulated the metals at a speed of 1 m/s during four subsequent campaigns performed between 350 °C and 450 °C. At the end of each campaign, both alloys were drained back into the supply tanks, cooled down and solidified. There was no exchange of the alloys; each test run was performed with the same material used in the run before. No oxygen sensor was present in either of the loops.

Additionally, a material test section was installed in each loop in order to investigate the corrosion behaviour of LGE and LBE towards austenitic 316LN and martensitic T91 stainless steel specimens. In total, three 316LN and three T91 specimens were placed in each test section. After each run, a maintenance break allowed the exchange of these specimens. The retrieved samples were finally analysed by SEM, the results of these investigations are reported in [85].

At the end of each test campaign, samples of the two eutectics with masses ranging from 1 to 5 g were taken and transferred to PSI for chemical analysis. For the first two campaigns, the sample-taking procedure was accomplished by draining a small portion of the liquid metal into a sealed and evacuated steel tube connected to the loop. After cooling the sampled liquid metal, the tube was cut off and again sealed with a welding torch. In the remaining test runs, the liquid metal samples were retrieved together with the material test section, subsequently being molten out by heating.

Within the first campaign, which was performed at 400 °C, LGE samples were taken immediately after start-up of the loop (0 h), after 900 h and at the end of the first run (1800 h). LBE samples were only obtained for 1800 h, the initial impurity content for LBE is therefore not known. For the 2nd, 3rd and 4th campaign at 450, 350 and 400 °C, LGE and LBE samples were obtained after 1300 h, 3000 h and 3000 h, respectively. Data on the temperatures and duration of each experimental run are given in Table 8. Samples of the 5th experimental run were not available up to the end of this PhD work and no analysis was done on these samples. Data on this last run is only given for information purpose.

Table 8: Overview on operation temperature and duration of each experimental campaign performed at the twin-loop

run number	temperature	start date	end date	total accumulated time [h]
1 st	400°C	10-Feb-2010	27-Apr-2010	1800
2 nd	450°C	31-May-2010	28-Jul-2010	1300
3 rd	350°C	16-Oct-2010	24-Feb-2011	3000
4 th	450°C	18-March-2011	25-Jul-2011	3000
5 th	400°C	18-Oct-2011	17-May-2012	5000

II.3.3 ICP-OES measurements

From each retrieved sample, approx. 250 mg were cut and dissolved in 5 ml of 7 M HNO₃. LGE required an additional dissolution step, as Au does not dissolve in nitric acid. It remained as a brown sludge and was separated from the solution by centrifugation. The sludge was washed twice with 5 ml of distilled water, again centrifuged, dried, weighed and finally dissolved in 2 ml of aqua regia. This procedure was necessary because in aqua regia, large quantities of Pb would cause massive precipitation of PbCl₂, which has to be omitted for a precise determination of trace elements. Samples of pure Pb and Au, which were used for the preparation of LGE, were dissolved in 7 M HNO₃ and aqua regia, respectively. Additionally, steel samples of 200 mg were taken from the SS316L tubing of the loop and dissolved in aqua regia.

For each analysed sample, a 5-fold repetition was made to decrease uncertainties. Together with blank solutions of 7 M HNO₃ and aqua regia, all aqueous solutions were analysed via ICP-OES. Before each measurement, the samples were diluted with 0.2 M nitric acid solution. The elements of interest were Fe, Cr, Ni, Mo and Mn as steel alloying elements as well as Ag, Cu and Bi as typical impurities in LGE and Ag and Cu for LBE. Analysis was done using a Vista Pro AX simultaneous ICP-OE spectrometer from Varian Inc. Emission lines used for the determination of Fe, Cr, Mn and Mo were 238.20, 267.72, 257.61 and 202.03 nm, respectively. The concentration of Ni was calculated by averaging the counts at 216.56 and 231.60 nm. For the determination of Ag, Cu and Bi the lines at 328.07, 327.40 and 223.06 nm were used. Standard solutions of the analysed elements were measured in order to perform a calibration of the spectrometer.

The final concentration of each element was calculated by averaging data over all repetition measurements, subtracting the background of the blank solutions.

II.4 Results

The concentrations of relevant trace elements found in both investigated alloys and their quantification limits are given in Table 9. Additionally, the measured composition of the structure material of the loop (316L stainless steel) is given.

Table 9: Impurity concentration of elements dissolved in both investigated alloys for different loop temperatures and sampling times. Values denoted by “<” were below the quantification limit of the ICP-OES spectrometer. The overall errors were in the range of $\pm 20\%$.

loop temperature	sampling time after startup	analysed alloy	impurity concentration [mass ppm]							
			Fe	Cr	Ni	Mo	Mn	Ag	Bi	Cu
quantification limit			1	0.5	3	3	0.3	1	5	1
initial metals used for the preparation of LGE		Pb	68	17	9	<	1	20	116	13
		Au	24	<	3	<	<	34	<	17
400°C	0h	LBE	18	1	2	<	<	5	/	3
		LGE	29	7	6	<	1	14	97	7
	900h	LGE	16	4	83	<	2	26	114	13
		LBE	13	4	146	<	3	26	139	14
1800h	LBE	4	2	14	<	<	5	/	3	
	450°C	1300 h	LGE	86	134	537	<	53	25	106
LBE			15	2	74	<	<	5	/	6
350°C	3000 h	LGE	66	29	166	7	5	22	err. ¹	54
		LBE	20	3	93	5	1	6	/	10
450°C	3000 h	LGE	100;25 ²	173;30 ²	168;96 ²	10;< ²	35;6 ²	25	124	76
		LBE	26	6	69	11	1	10	/	28
316L stainless steel composition [%] ³			64.3	17.4	13.1	2.6	1.7	<	<	0.3

¹ the Bi content in LGE could not be determined due to high blank values

² the distribution of steel alloying elements was not homogeneous in this analysed batch

³ the precision for these data is in the range of $\pm 1\%$

The concentrations of Ag and Bi may be used to evaluate the precision of measurements in each experimental campaign. Silver is a noble metal that is easily dissolved in Pb alloys [106]. This element is not present in relevant amounts inside the steel structure, nor does it precipitate from the liquid metal or adsorb on the steel tubing surface at any studied temperature. In Hg, it was indeed observed in laboratory experiments [107] and also in the Japanese SNS Hg target [108], that Ag remained dissolved in the liquid metal and did not adsorb to tubes and pipes. Similar behaviour was found concerning the Ag distribution in proton irradiated LBE retrieved from different positions of the solidified MEGAPIE target [109]. This implies that the concentration of Ag inside both liquid metals

should not change over the whole period of test campaigns by dissolution or deposition processes. A similar postulate may be made for Bi dissolved in LGE.

Based on this assumption, the overall precision of the analysis data was estimated to be in the order of $\pm 20\%$. By averaging the measured concentrations, the mean impurity contents of Ag and Bi were calculated to be 5 ± 1 ppm Ag in LBE and 23 ± 6 ppm Ag and 114 ± 18 ppm Bi in LGE. Both last-named values coincide well with impurity concentrations found in Pb and Au before the preparation of LGE.

The determined concentrations for the most important steel alloying elements Fe, Cr, Ni and Mn are plotted against the accumulated operating time in Figure 14. In addition, the operating temperature with time is shown in the upper section of the graph.

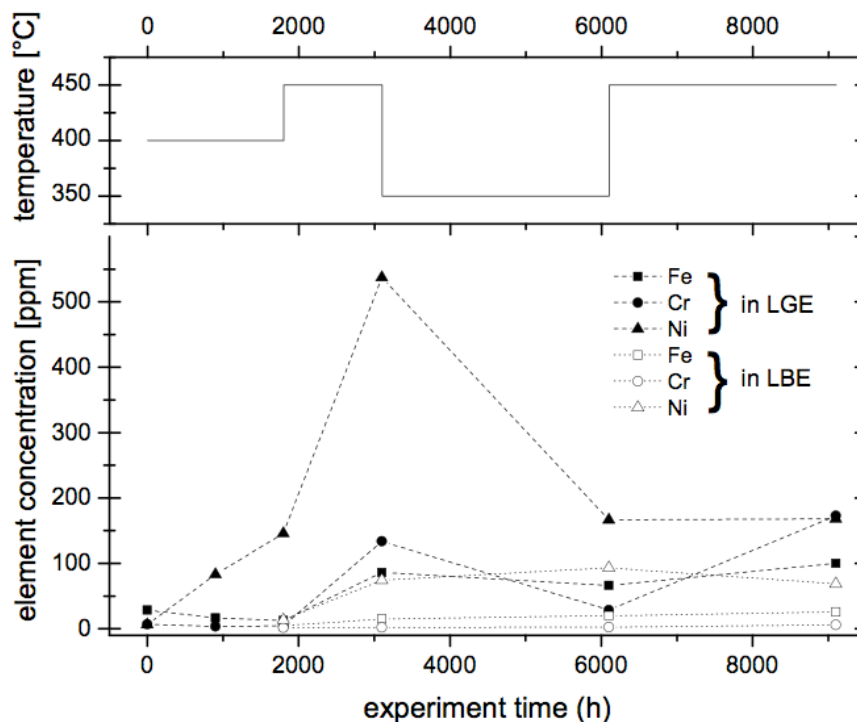


Figure 14: The mass concentration of Fe, Cr and Ni in ppm found in LGE and LBE as function of accumulated experiment time. In the upper graph the operating temperature is shown, where temperature offsets represent maintenance breaks for both loops.

In the initial LGE material, 29 ppm Fe was found. The concentration of Fe was even higher in Pb used for the preparation of its alloy with Au. This contamination may originate from the mixing device used for preparing LGE, where molten Pb was in contact with steel structure materials at temperatures exceeding 500 °C.

As indicated in Figure 14, the dominant impurity that was preferentially dissolved in LGE was Ni. Its concentration continuously increases with longer operation times of the loop at 400°C. Compared to LBE, there was a clearly larger dissolution effect of Ni - after 1800h the concentration of Ni in LGE was ten times higher than in the Bi containing alloy. For Mn, this enhanced corrosion behaviour was less pronounced, but was still clearly visible. Interestingly, the concentration of Fe and Cr inside the loop decreased for longer operation times at 400 °C. At the end of the first test campaign, their concentration decreased 5-fold compared to the content present in pure Pb and Au metals used for the preparation of the initial LGE. This behaviour may possibly occur if these elements are present as clusters in the liquid metal and are trapped by magnetic forces near the pump. High concentrations of Fe-Cr agglomerates were found for samples retrieved near the electro-magnetic pump of the JLBL-1 loop [110].

The concentration of corrosion products within both alloys drastically increased in the second loop experiment that was performed at a higher temperature (450°C). Here, LGE again showed stronger dissolution attack to the steel structure, resulting in concentrations of 86 ppm for Fe, 53 ppm for Mn, 134 ppm for Cr and 537 ppm for Ni. The corrosion behaviour of LBE at 450°C was far less pronounced; however, significant dissolution of Ni was also observed. For both investigated alloys, this element was the dominating impurity. No Mo dissolution was found either in LGE or in LBE.

The 3rd run was operated under the lowest investigated temperature at 350 °C. Data in Table 9 indicate that within LGE the concentration of Fe, Cr, Ni and Mn decreased, which implies the precipitation of these elements due to over-saturation. The authors of ref. [110] have indeed observed Ni-rich and Fe-Cr precipitates on parts of their non-isothermal loop. This behaviour was not observed for the Bi-based alloy, where the concentrations still slightly increased. Surprisingly, several ppm of Mo were found in both liquids at the lowest temperature. The origin of this impurity is not yet clear; possibly mechanical stress of Ni-depleted surfaces may have caused the release of steel “clusters” containing this element.

Analysis of LGE samples from the 4th run revealed that the concentration of steel alloying elements largely deviates throughout the investigated batch. As the determined concentrations of Ag, Bi and Cu did not show such variances, errors resulting from sample preparation and measurement can be ruled out. This implicates that the distribution of steel alloying elements was not homogeneous throughout the obtained batch of LGE samples from the 4th run. A more detailed view of this finding is presented in Figure 15.

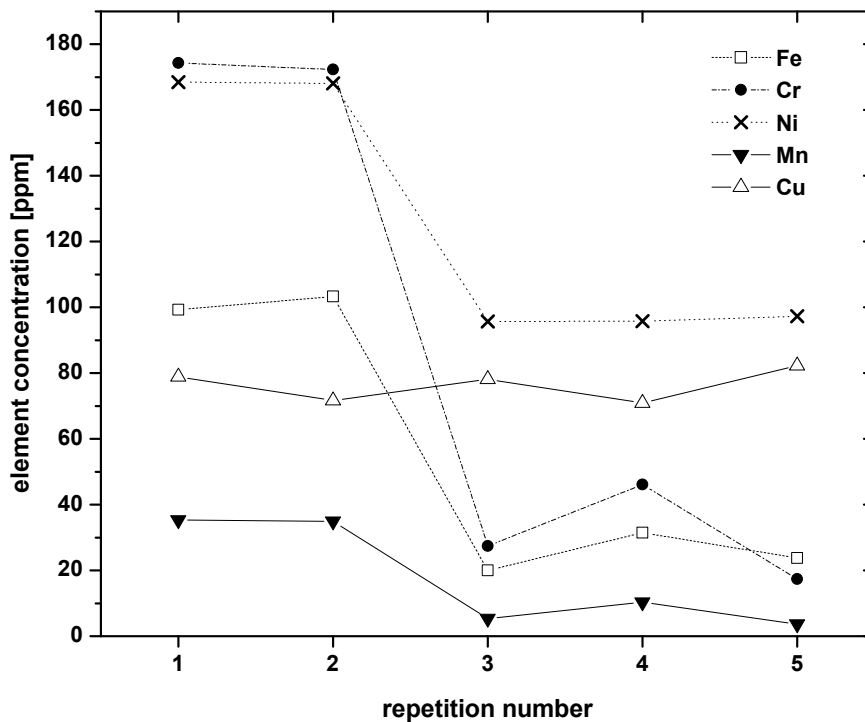


Figure 15: Graph showing measured concentrations of Fe, Cr, Ni, Mn and Cu in LGE after the 4th experimental run at 450 °C for each of 5 repetition measurements.

It shows the analytical results for concentrations of steel alloying elements and Cu for each repetition measurement. As already stated before, the distribution of Cu in each repetition sample was found to be nearly homogeneous, leading to a mean value of 76 ppm. For steel alloying elements, data in Figure 15 indicates that only samples 1 and 2 seem to give conclusive results for every investigated element, whereas lower concentrations with larger deviation are observed in samples 3 to 5. Interestingly, this does not apply to Ni, its concentration is again homogeneous throughout samples 3 to 5, but deviates from that found in 1 and 2. The concentrations of Fe, Cr and Mn, in contrast, show a large spread, but seem to correlate to each other throughout the analysed repetition batch. It was found that the relative concentration ratio remained nearly constant at $c(\text{Fe}) : c(\text{Cr}) : c(\text{Mn}) \approx 3:5:1$.

This may indicate that solid, crystalline precipitates containing these elements were formed inside the liquid metal. They may be present in different amounts in each analysed sample, depending on their crystal size, growth time, liquid metal cooling rate etc.

In order to explain the observed measurement results, it is important to specify the origin and treatment of every LGE sample obtained from the 4th run. Unfortunately, this information is not available and therefore it was impossible to find out the cause for the discrepancies within this campaign. The results for this analysis are therefore given in concentration ranges (min to max, see Table 9) without pretending to provide quantitatively precise data.

For LBE samples, which all were homogeneous, a slight increase for Fe, Cr and Mo concentrations compared to the 3rd run was found. The Ni concentration levels out and is comparable to that found at the 2nd run operating at the same temperature of 450 °C.

II.5 Discussion

From investigations on the corrosion behaviour of LBE it is known, that the concentration of oxygen dissolved in the alloy is a crucial factor influencing the corrosion behaviour [111]. Since no oxygen sensor was installed in either of the loops, a detailed analysis of the underlying mechanisms is not possible in the present study. Therefore, only a comparison between the corrosion properties of both liquid metals will be made.

The origin of impurities inside both liquid metals, apart from those present already at the beginning, is mainly the twin-loop tubing material. The contact area of the stainless steel 316L tubing of the loop towards the liquid metal is much higher if compared to that of specimens within the test section. Considering an inner diameter of 10 mm and a total length of the loop of approximately 2.5 m, the total contact area would correspond to about 800 cm². The size of the steel specimens inside the material test section is comparatively small (about 1 cm² per specimen, 6 specimen in total). Thus, the source of steel alloying elements that are found as impurities either in LBE or LGE should mainly be the tubing material. The large difference in contact area suggests that the influence of the material specimen on the impurity concentration in both liquid metals may be neglected.

From temperature functions given in Table 7, it may be concluded that in LBE, Ni is the most soluble species of the discussed elements, with solubility limits ranging from 10⁴ to 2 x 10⁴ ppm at 400 and 450 °C, respectively. The solubility function for Cr yields much lower values ranging from 4 to 8 ppm. For Fe, however, an extrapolation from functions obtained at higher temperatures [47] has to be made. From such extrapolation, a solubility of Fe in LBE in the order of 1 ppm at the highest investigated temperature of 450 °C is obtained. The solubility of Mo in molten Pb and Bi was determined to be below 1 ppm for temperatures up to 800 °C.

Apart from the knowledge on the solubility of these elements in a liquid metal alloy, information on the rate at which a solid goes into solution is of importance. Equation (3) describes the dissolution kinetics of a solid in a liquid metal under isothermal conditions [37]:

$$\frac{dc}{dt} = \frac{\alpha S}{V_l} (c_s - c_v), \quad (3)$$

where S is the total surface of the solid in contact with a liquid metal of volume V_l with a concentration c_v of the solute. The value c_s is the solubility of the solute in the liquid metal (see section II.2.4) and α the temperature dependent dissolution rate. If $c_v \ll c_s$, the concentration increase per unit of time becomes proportional to the solubility c_s , assuming S , V_l and α remain constant.

Indeed, for Ni and Mn in LGE, the data obtained for 400 °C indicates an approximately linear behaviour. This finding indicates that the concentrations observed in the present experiments may be far below the saturation concentration for these two elements in LGE at 400 °C. Thus, one may postulate from the numbers given in Table 9 that the solubility of Ni in LGE is greater than its solubility in LBE.

From the facts discussed above it may be concluded that the measured Ni concentration in LBE and probably also in LGE is far below the saturation concentration at all studied temperatures. The dissolution of Ni from the steel surface is a relatively slow process dependent on the temperature and time of contact with the liquid metal. From the available data it is concluded, that much longer test runs would be needed in order to obtain Ni saturation. On the other hand, the Ni dissolution is mitigated by the depletion of Ni at the steel surface for longer operation times. Diffusion of Ni atoms from the steel bulk to the liquid metal – steel interface becomes the rate-determining step for Ni dissolution. Such a depletion of Ni and Mn was indeed observed during investigations of the SS 316LN specimens from the material test sections from the twin-loop. It was shown by SEM combined with energy dispersive X-ray analysis that for SS 316LN specimens in contact to LGE a depletion of Ni content from 10.2 wt% to 2 wt% had occurred at the surface of the specimen throughout a penetration layer of 10 – 40 μm thickness [85]. A cross-section of a 316LN specimen is shown in Figure 16 and the corresponding

results of EDX analysis at different depths is depicted in Table 10. One can see substantial diffusion of LGE into the bulk material and the diffusion zone has a sharp front. The depth of the diffusion zone varies between 10 and 40 μm . Table 10 indicates that compared to the initial composition, the Cr, Ni and Mn concentrations decreased significantly within the diffusion zone, while for Fe and Mo no such pronounced decrease is observed. As already discussed in section II.2.3, the presence of 16 wt% Au in LGE may explain this behaviour, since Au easily alloys with many transition metals. Outside the diffusion layer, the elemental composition of the specimen practically stays unchanged. Since the loops are constructed from the same material (316L) and were operated isothermally, a similar depletion can be expected for the inner tubing surfaces of the whole LGE loop.

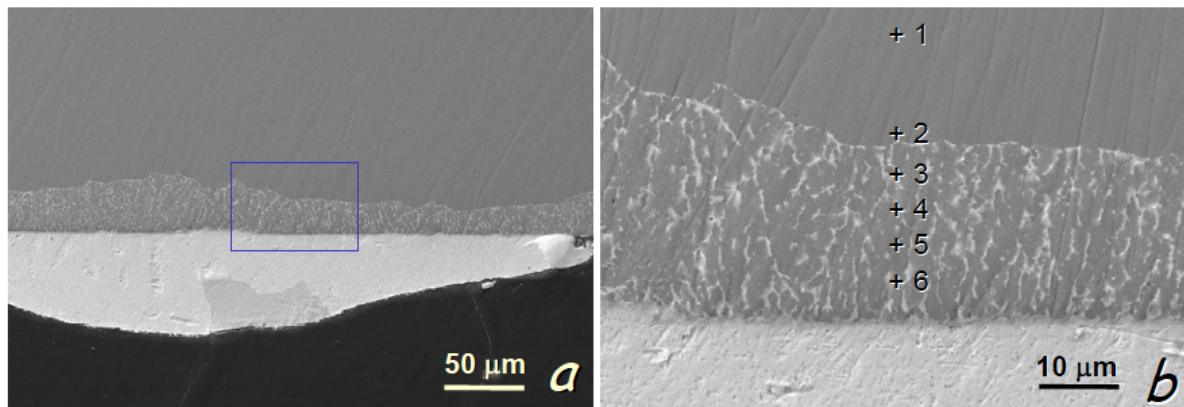


Figure 16: SEM micrograph showing (a) the cross-section of a 316LN specimen exposed to LGE at 450°C for 1300h and (b) the EDX analysis to determine the elemental composition at various sample depths; reproduced from [85].

Table 10: Elemental composition determined by EDX analysis of the sample shown in Figure 16; data taken from [85].

position	relative concentration [wt%] of element				
	Fe	Cr	Ni	Mn	Mo
1	68.6	16.7	10.2	2.3	2.2
2	67.4	15.8	10.1	2.0	2.2
3	53.9	5.0	2.4	0.1	1.3
4	76.9	5.8	3.0	0.0	2.6
5	77.4	6.5	3.4	0.1	3.2
6	57.9	5.7	2.4	0.0	2.3
Initial	64.3	17.6	13.1	2.6	1.7

The decrease in the concentration of Fe in LGE during the experiment at 400 °C may indicate that this element was already present at the start of the experiment at concentrations exceeding the saturation solubility. These high concentrations at start-up can be explained by an extended contact of the Pb used for preparation of the eutectic alloy with the surface of a steel melting pot at temperatures higher than 500 °C. However, the decrease in Fe concentration could also be explained by the formation of magnetic iron clusters in the liquid metal that are precipitated within the electromagnetic pump. Such cluster formation was indeed observed in Hg, where cluster growth inside the liquid metal is occurring on the submicron scale [112]. Together with Cr, these clusters might then be trapped by magnetic forces near the pump. For example, high concentrations of Fe-Cr agglomerates were found for samples retrieved near the electro-magnetic pump of the JLBL-1 loop [110], supporting this assumption. Yet another indication for the formation of steel clusters is the detection of Mo in our analysis. Because of low solubility, the presence of Mo in the sample cannot be explained by dissolution of the element, but only by the release of solid clusters originating from steel corrosion.

Such small sized particles are transported with the metal flow and certainly will be detected if no filtering of the liquid metal is performed.

The concentration of dissolved Cu continuously increased for both investigated Pb alloys with cumulative duration of the corrosion experiments. For LGE, the Cu content did not change significantly from the initial during the first run at 400 °C, as impurity Cu coming from both metals used for the preparation of LGE should be in the order of 14 ppm. Only the measurement done with the initial LGE material ($t = 0$ h) revealed a lower Cu concentration, which, probably, is an erroneous measurement. As soon as the loop temperature is raised, a pronounced increase in Cu concentration was observed. This additional Cu should certainly originate from the 316L stainless steel material, where 0.3 wt% Cu is found by the ICP-OES analysis as given in Table 9. As the solubility of Cu in Pb is in the same order of magnitude as that of Ni (see references [47] and [101]), and Au easily forms stable alloys with this element in all concentration ranges, no precipitation of Cu is assumed to occur during maintenance breaks, where LGE was allowed to cool down and solidified. Thus, the concentration of Cu should increase with cumulative experiment time at every temperature studied. This behaviour was indeed observed for LGE, where the Cu content increased more than 5-fold after the end of the 4th run. A similar behaviour was observed for Cu in LBE. At higher temperatures and corrosion rates, the amount of dissolved Cu increased.

In order to better understand these phenomena, several additional investigations should be performed in the future. Samples from the vicinity of the electro-magnetic pump should be retrieved in order to prove if a magnetic trapping of Fe-Cr rich precipitates is occurring. Steel samples from the tubing material have to be studied in a similar manner as the material test samples in [85].

From the obtained analysis data it is also concluded that a suitable filtering system for liquid metal samples retrieved from the test loops becomes mandatory. To assure that no solid clusters distort measured solute concentrations, a stringent sample taking procedure is very important. For any future study on the corrosion performance of liquid metals, careful liquid metal sample taking at controlled conditions should be done. The purity of the alloy has to be controlled as well because it directly influences the dissolution rate. Additionally, oxygen sensing has to be maintained during the whole measurement campaign. As corrosion studies on LBE have shown, different oxygen concentrations in the liquid metal do provoke diverse corrosion mechanisms. This feature is likely to be observed also in Pb-Au based systems.

II.6 Summary

The corrosion behaviour of liquid LGE in contact with SS316LN stainless steel is significantly worse compared to that of LBE at the same operational conditions. Substantial dissolution of Ni was observed at temperatures of 400 and 450°C. These findings call for detailed investigations looking for steels with higher corrosion resistance toward LGE. Before taking LGE seriously into consideration as a target material, extended chemical, physico-chemical and materials studies have to be undertaken to guarantee the safety of the selected material. Such studies imply the investigation on mechanical properties of materials previously in contact with flowing LGE as well as studies on the corrosion mechanism similar to those done for LBE.

Independently, investigations on steels and other materials with higher resistance towards LGE have to be undertaken to find a suitable tubing material for experimental LGE loops. One possibility to mitigate corrosion implies a protection by special coatings resistant to liquid metal deterioration [37]. Another possibility is the use of structure materials made of Ta or Mo, as these elements have shown to be nearly insoluble in Pb, Bi and Au. Corrosion investigations should be performed under controlled conditions concerning the purity of the alloy. All material and corrosion studies should also incorporate reliable measurements of the oxygen concentration inside the liquid metal, as this was found to be a crucial factor for material corrosion in LBE systems. If these investigations confirm the possibility to use LGE as alternative target material with certain steel types resistant to corrosion, the materials should be tested under irradiation conditions. Material damage should be investigated to assure reliable statements on the sustainability of steels under an intense irradiation environment present in a spallation target.

Apart from research on the corrosion resistance, the behaviour of spallation and activation products in a LGE target has to be investigated as well. Calculations in [81] revealed that after proton irradiation of LGE the Po inventory will be by a factor of 10^4 smaller if compared to the Bi based alloy. These calculations assumed that LGE is free from Bi. Our measurements have shown that the Bi content in LGE used for the present investigation exceeded 100 ppm. The amount of Po formed within LGE with such a concentration of Bi would be certainly higher than predicted by [81]. Careful calculations supported by experimentally data should be done to analyse the amount and behaviour of spallation products inside LGE.

Another peculiarity of LGE arises from the formation of Hg due to nuclear transmutation of Au. As spallation facilities using LGE as target material will have higher operating temperatures than similar ones using LBE, the evaporation rates of radionuclides formed within the liquid metal will be enhanced. As a result, the total release of isotopes of Hg will be higher from LGE if compared to the Pb-Bi alloy, whereas the Po release may not be necessarily lower due to higher operating temperatures. A suitable hot off gas treatment system has to be installed to deal with this problem. Consequently, dedicated studies on the release of volatiles from LGE are mandatory and cover gas filtering systems have to be developed in order to assure a safe operation of the spallation facility.

The market price of Au is another factor that makes the use of LGE questionable as target material. With a market Au price of 1500 €/oz., the net price for a 20 ton liquid LGE target would be around 150 M€ for the Au alone, which is around 10% of the total budget of the ESS project, according to [16]. The advantages of LGE will have to be outstanding to warrant this cost within any future spallation facility project. Finally, the choice for a target material also depends on the time to complete essential studies that would qualify it for selection. In case of LGE it would certainly take several years to complete detailed investigations on corrosion, irradiation and release. It has to be kept in mind that many key facility design decisions hinge upon target choice.

The qualification of the recently proposed eutectic alloy of Pb with Au, LGE, as potential target material in spallation sources, thus lacks the economical and scientific basis. Although first studies have shown promising results concerning its properties, our investigations clearly indicate that corrosion rates of Ni-based steels are significantly lower if in contact with the Bi-based alloy. Apart from this, many physical parameters of this new material are not yet known and time-consuming investigations are needed. Considering the available database and long-lasting experience present for

LBE, Hg and Pb, the amount of available information certainly will affect choice and funding to the disadvantage of LGE.

III Extraction of radionuclides from liquid metals

III.1 Introduction

In nuclear facilities using LBE, the recycling and handling of the target and coolant material will be one of the essential issues for a continuous operation. The release of spallation and activation products from LBE represents a major radiological impact in case of a leakage of the liquid metal. One way of dealing with the radiotoxic nuclides is to remove the potentially hazardous elements from the target and bind them in a stable chemical form. These separated nuclides could be then safely contained in appropriate storage vessels until their radiation levels sink to a tolerable background. During facility operation a continuous production of numerous isotopes occurs in LBE. One approach for dealing with the produced radioactivity could be to reduce the concentration of the radiotoxic nuclides in the liquid metal to sufficiently low levels by an online separation technique. Another approach could be their extraction within long maintenance breaks or after shutdown of the facility.

For isotopes of Po, which are considered to be the most problematic in facilities using LBE, several methods for their separation from the liquid metal were already discussed in the past [113, 114]. The separation techniques differ by the physico-chemical pathway, although all methods avoid any chemical attack on the liquid metal itself to enable its continuous reuse.

III.1.1 Polonium separation from liquid metals

In the early years of Po production, the distillation of Po from the liquid metal was proposed as a suitable method to obtain purified ^{210}Po in large quantities for military and scientific purposes. As Po is a volatile metal with a boiling point of 962 °C, there is a large difference in vapour pressure between Pb or Bi and Po. The distillation method represents an efficient, but energy-consuming pathway to separate Po isotopes from the irradiated metal. Many publications are available dealing with Po distillation from liquid Bi or LBE. In studies [115], [71] and [116] a significant Po release from molten LBE or Bi at temperatures exceeding 700 °C was found. To maximize Po separation in a technical process, the surface of the molten metal has to be large and formed vapours containing Po should be removed by condensation at a cold surface.

However, such a separation apparatus needs stringent safety requirements in order to avoid any release of Po vapours into the surrounding. Additionally, potential disadvantages for applications of the distillation method toward ton amounts of irradiated LBE metal include the necessity for creating and maintaining industrial scale high vacuum systems for handling large amounts of toxic Po vapour. The high corrosivity of molten LBE at temperatures to be used for distillation (700 – 900 °C) is yet another problem concerning the utilization of the volatilization process. Expensive construction materials are required to contain LBE metal reliably at these temperatures.

Another separation method, which up to now has only been studied in theory, represents the stripping of Po isotopes with gaseous hydrogen. This technique relies on the formation and separation of the unstable gaseous hydrogen polonide H_2Po . Some authors state that this compound is formed when H_2 gas is forced into contact with Po dissolved in LBE [113]. Another possible formation reaction for Po hydride was reported in the presence of moisture [117]. A technical implementation of this method is based on the capture of H_2Po in an alkaline aqueous solution, thus trapping the polonide and releasing hydrogen gas recirculating in a mass exchanger.

There are, however, contradictory observations on the formation [118], stability [119] or even the existence of H_2Po . Latest theoretical extrapolations of thermodynamical data indicate that large amounts of H_2Po are not formed in such a system [120]. Even if this process could be proven to work, it would demand safety precautions similar to Po distillation, as large amounts of toxic Po and Po-hydride vapour will be formed. Since volatilization pathways of Po are currently not yet fully

understood, any technical implementation of such a separation technique will fail to pass licensing given the current state of knowledge.

Another approach for the separation of Po from LBE that has been discussed theoretically is the use of rare earth metals as getters for Po. This method is based on the fact that rare earth metals form stable polonides with high melting points. For example, DyPo and YbPo have melting points exceeding 2000 °C [119]. These data suggest that it might be possible to decrease the rate of release of Po by dissolving lanthanides in LBE, hence promoting the formation of a species with a lower volatility than Po itself. Incorporation of rare earth metals into suitable filters could represent a suitable method to separate Po from irradiated LBE. However, the high neutron absorption cross-section of lanthanides, their oxygen affinity and the lack of sufficient studies on the involved method make an industrial application unsuitable.

Yet another possibility of Po separation from LBE is the zone melting process. This method comprises of a partial melting of a cylindrical irradiated metal ingot where Po separates due to impurity concentration effects. Po has a strong tendency to segregate on surfaces of LBE samples and to concentrate on grain boundaries, as will be discussed in section IV.1.3. Thus, the Po impurities will concentrate at the end of a metal ingot the melting zone is moving to. This separation process was performed and investigated on a small scale (100 g) by [121] with a Bi ingot. These experiments showed the practical feasibility of physical Po separation of up to 90 % during several melting runs and different melting zone velocities. This technique is rather inappropriate for large scale reactor coolant purification as the contaminated liquid metal have to be first solidified and treated in a separate zone melting process. Rather poor Po separation yields are another disadvantage of the method.

A different approach for the extraction of radionuclides from liquid metals represents the method of direct adsorption. In [122] the sorption of various elements onto metallic surfaces immersed into irradiated Pb was investigated. It was found that adsorption is extremely specific to the metal immersed – isotopes of Mo, Ir, Tl and Pt may be selectively separated depending on the sorbent material. Based on the selectivity of the chemisorption process, this method could be applied for the separation of other elements as well. There is no investigation existing on the sorption of Po isotopes from an irradiated liquid metal target and a careful study of this promising technique still remains to be done.

Finally, the separation of Po by the action of molten alkali metal hydroxides has been in principle successfully applied for the separation of Po from pure Bi metal on a laboratory scale [123]. This technique represents a non-aqueous liquid-liquid extraction at elevated temperatures. As a secondary liquid, molten hydroxides are used as extraction medium. This method, however, has been poorly studied in the past. Nevertheless, it was recently proposed as a technique for the purification of LBE serving as coolant and target material in large scale nuclear facilities [78]. It is the goal of this thesis to shed some more light onto the fundamental physicochemical characteristics of this process to validate this proposal.

III.1.2 Properties of molten hydroxides

Sodium and potassium hydroxide are white, solid and highly hygroscopic materials easily soluble in water. Especially KOH exhibits a high potential of binding moisture and is thus used for gas blanket drying applications. Due to their high hygroscopic properties, solid NaOH granulate may contain up to 2%, KOH up to 15% of water depending on their exposure time to wet air. The removal of water can be accomplished by heating both substances to temperatures above 450 °C or by the addition of Na₂O or K₂O [124]. Both solids have comparable physical properties that are given in Table 11.

The eutectic mixture of both hydroxides exhibits a lower melting temperature of 443 K [125]. The eutectic composition was found to be at 50:50 at% of NaOH and KOH, respectively [126]. The liquid density of molten NaOH-KOH eutectic is approximately 1.7 g/cm³ [127], which is roughly 6 times smaller than that of LBE.

Table 11: Physical properties of NaOH and KOH

substance	molecular weight [g/mol]	melting point [K]	boiling point [K]	solid density at 20 °C [g/cm ³]
NaOH	40	591	1661	2,13
KOH	56	633	1593	2,04

When liquid, both hydroxides and also their eutectic mixture have highly corrosive properties. There are few materials that are resistant to molten hydroxides under inert gas conditions, e.g. Fe, Ni, Cr, Zr, noble metals such as Au or Pt, some Zr/Al oxides or graphite. When exposed to molten alkali hydroxides, Al, Zn and other less noble metals are violently attacked forming H₂ and the corresponding aluminates or zincates. Nearly every kind of glass or ceramic material such as boron/silicon carbide or nitride is readily dissolved in molten hydroxides. It has been reported that in the presence of air, most metals suffer serious corrosion damage when exposed to fused hydroxides [128]. KOH exhibits even higher corrosive effects than NaOH under air due to oxygen uptake, forming peroxides resulting in Fe, Cr and Ni to lose their resistance towards hydroxide melts at higher temperatures ($T > 500$ °C) [129].

III.1.3 Literature overview on alkaline extraction of polonium from liquid metals

The pyrochemical extraction by alkaline melts represents a promising method for the separation of various impurity elements from liquid metals. Much knowledge exists on this technique from its industrial implementation for the purification of crude Pb and Bi from impurities. There also exist several publications on alkaline extraction of Po from metals like Bi or Pb [123], [130], [131]. Unfortunately, only few experimental studies exist that deal with extractions of impurities from LBE [132, 133]. Since physical and chemical properties of Pb and Bi are comparable to properties of the eutectic, it is reasonable to assume that in analogy, available data on the behaviour of impurities in Pb and Bi would also apply to LBE.

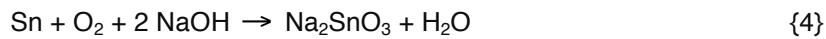
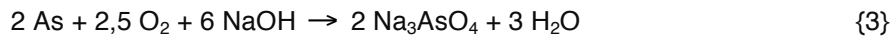
Additionally, the chemical behaviour of Po is comparable to its group VI homologue, Te. Both elements are known to form similar chemical compounds with comparable crystal structures (as, for example PbTe and PbPo). Some data is available on the behaviour of Te in the system molten Pb – molten NaOH. Based on the chemical similarity it can be therefore argued that the chemical processes responsible for the extraction of Te would also apply for Po.

In the following sections, the current knowledge on the extraction of Po and its lighter homologue Te from liquid Pb, Bi and LBE will be summarized. This literature review should serve as a foundation for the experimental and theoretical work performed within this thesis.

III.1.3.1 Extraction of impurities from molten Pb metal

In metallurgy, several purification steps are needed to extract impurities like Ag, Cu, Sn and Sb from Pb originating from Pb-rich ores. Since the early 1930ies the metallurgical purification of Pb was done by a pyrochemical extraction referred to as the Harris process [134]. Published in a patent in 1919, the author described the possibility of purifying Pb from impurities like Sb, Sn and As by the addition of NaOH. Only elements less noble than Pb can be extracted from the metal using this technique. Large-scale purification plants based on this technique were operational in the metallurgical industry.

During the Harris process, Pb is pumped through NaOH at temperatures around 450°C. For the extraction of Sb, Sn and As, an intensive air blow through the melt is maintained to assure oxygen ingress. In order to increase the oxidation potential, NaNO₃ is added to the hydroxide phase. It is argued that chemical oxidation is the driving force for all three elements to transfer into the alkaline melt thus to be extracted from molten Pb [135, 136]. The main reactions are:



The extraction is occurring in several steps. First element to be extracted under these conditions is As. With descending As concentration, the oxidation of Sn begins, subsequently removing this element from the Pb phase. Finally, Sb is extracted to the hydroxide phase. Due to intensive air ingestion, Pb is also oxidized to some extent, but this reaction only occurs in noticeable amounts after all Sb is extracted from molten Pb, as the tendency for oxide formation decreases in the sequence $\text{As} > \text{Sn} > \text{Sb} > \text{Pb}$.

A systematic investigation on the transfer kinetics of As, Cd, Sb, Sn and Zn from pure Pb into molten NaOH while applying the Harris process was performed in [137]. The results of this study confirm the gradual transfer of impurities as was described above. Zn transfers even more easily than As, whereas the oxidation of Cd occurs after that of Sb. This tendency is graphically shown in Figure 17.

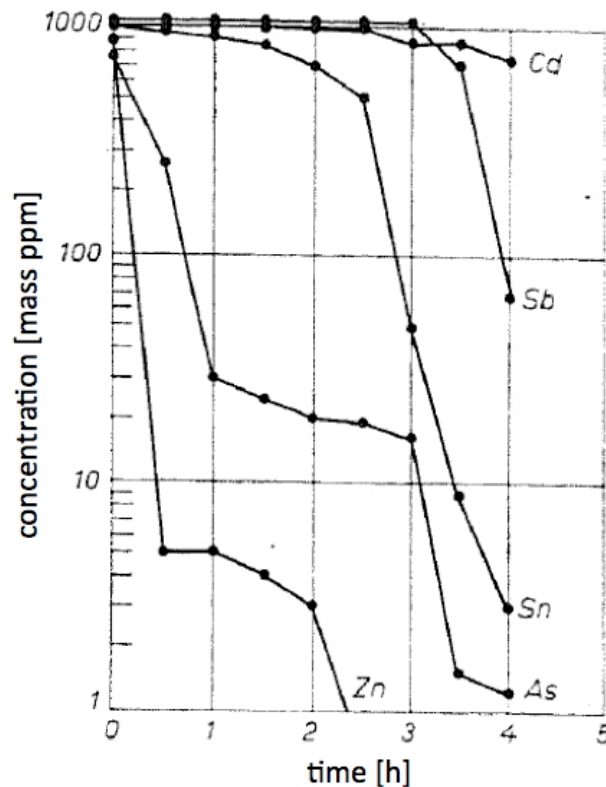
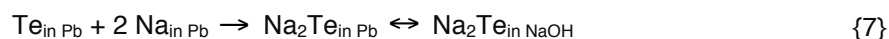


Figure 17: The gradual transfer of impurities from molten Pb at 420 °C applying the Harris process; figure taken from [137].

The extraction of Te within the Harris process is also performed with NaOH, but under different conditions. Improvements on the Harris process revealed that Te is extracted under inert conditions and not by oxidation [138]. The reaction for the removal of Te from Pb is usually given as:



However, it has been further shown that the addition of metallic Na into molten Pb enhances Te separation. The ingress of oxygen reduces Te transfer [138]. The extraction is believed to occur according to the following reaction:



Na_2Te is readily dissolved in the hydroxide, leaving the metal phase nearly free from Te. The purification is done under ambient air and no inert gas atmosphere is needed for complete Te removal. The extraction of Te is believed to occur by the same chemical principle. For Po as a homologue of Te, a similar behaviour may be expected.

This process was used to purify large quantities of molten Pb from impurity Zn, Te, As, Sn and Sb. No Ag removal is possible with this procedure, and Cu and Bi will also remain in the metal phase. For these metals other purification steps exist such as the Parkes or the Knoll—Betterson process [138, 139]. The Harris process is also applicable for the purification of Bi metal, but was mainly performed for the refining of crude Pb.

III.1.3.2 Extraction of impurities from molten Bi metal

Based on this metallurgical knowledge, first experimental studies on the extraction of Po, the homologue of Te, were performed in the early 1960s, purifying Bi foreseen as coolant in nuclear reactors. Extraction of Po from molten Bi with fused NaOH was first reported by [140] in 1953. These experiments were performed in vacuum at 500 °C, using few grams of Bi containing kBq activities of Po. Later on the possibility of extracting Po activities up to 10^{15} Bq from 200 kg batches of irradiated Bi metal was described [123, 130]. In these experiments, temperatures between 400 and 500 °C were used under inert atmosphere for the alkaline extraction step. Systematic experiments on Bi to NaOH phase ratios, extraction time and gas blanket effects were made [123]. A quantitative extraction of Po was obtained over a wide range of extraction conditions. The main scientific outcome of these studies confirmed that it is in principle possible to almost completely extract Po from irradiated Bi metal at temperatures around 400 – 500 °C if the presence of oxygen is avoided.

In addition to the alkaline extraction of Po from Bi, other salt melts were studied for the removal of fission products from liquid metals. For example, distribution constants of several rare earth metals between molten Bi and LiCl – LiF eutectic were analysed [141]. The purpose was the reprocessing of high-burnup metal reactor fuel, where extensive extraction studies were performed for a thorium containing molten salt reactor fuel at Idaho National Laboratory. Investigations on the extraction behaviour of more than 20 elements from irradiated Bi with fused LiCl-KCl were performed by the authors of [142-144]. Po was found to be poorly extractable with eutectic LiCl-KCl at temperatures between 400-500 °C.

A large scale feasibility study was performed for a reactor containing 800 ppm U fuel in a closed molten Bi loop [145]. Extractions of ^{137}Cs , ^{140}Ba , $^{89/91}\text{Sr}$, ^{143}Ce and ^{133}I were successfully performed using a LiCl – KCl – MgCl_2 eutectic salt mixture at temperatures around 500 °C. It was shown that the elements ^{95}Zr , ^{103}Ru , $^{238/235}\text{U}$ and ^{210}Po have poor extraction rates under these conditions.

III.1.3.3 Extraction of impurities from molten LBE

III.1.3.3.1 Extraction of polonium from molten LBE

To use of an alkaline melt for LBE reactor coolant purification was initially proposed by Russian scientists. They also proposed to use the low melting NaOH – KOH mixture. A short note of successful Po extraction was given in [78]. Furthermore, a basic scheme of an extraction facility was proposed and tested using Te as chemical analogue of Po [146]. Similar experiments were performed using Te in a LBE / NaOH extraction system for several extraction runs at 427 and 500 °C [113]. These experiments on LBE extraction techniques were performed at Idaho National Laboratory in the last decade [147]. All reported investigations were done at temperatures above 400 °C with NaOH and 10^3 ppm amounts of Te using atom absorption spectroscopy (AAS) for the determination of the Te distribution. No systematic investigation on the extraction of Po from LBE has been published until recently [133].

To overcome this lack on conclusive data and to extend the studies to the element that is of relevance, i.e. Po, a study on the extraction of Po from irradiated LBE samples was performed in preparation for this thesis and was published recently [133]. As a part of this investigation, the temperature dependence of Po extraction was studied together with the influence of the gas blanket. Additionally, an influence of the water content on the extraction performance of the alkaline melt was observed in this study. The result on temperature dependency and water content is graphically presented in Figure 18.

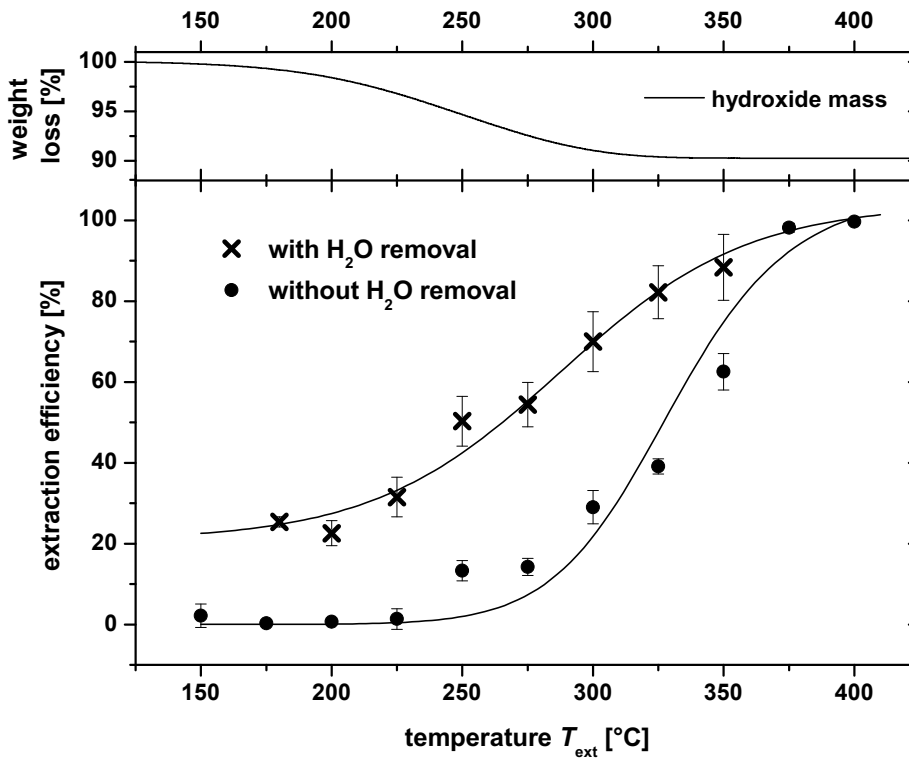


Figure 18: Influence of temperature and water content on the Po extraction performance; extraction time 30 min; N₂ gas blanket; NaOH/KOH to LBE mass ratio 2:1; taken from [133].

For the investigated (NaK)OH-Po-LBE system, an increase in temperature results in higher extraction. For temperatures exceeding 400°C, the extraction of Po from LBE can be assumed to be complete for both moisture containing and dry systems. At lower temperatures the extraction performance is depending on the water content within the hydroxide phase and large differences are observed within a temperature range of 180 to 350 °C. According to the thermo-gravimetric measurement, the net water content in the alkaline phase decreases with increasing temperature exactly in this temperature range. This investigation has shown that for an efficient Po removal, the hydroxide phase should be dried to obtain best possible results.

As an additional effect, a strong dependence of the extraction efficiency on the oxidation potential of the cover gas was found. Compared to inert gases, a clearly lower extraction ratio of approx. 20 % was found in O₂ and air, which is in agreement with earlier works on the extraction of Po from Bi [123] and Te from LBE [146]. For reducing hydrogen, the effect on the extraction ratio is opposite. For both extraction runs, about 90 % of Po were removed from the liquid metal to the alkaline phase, resulting in significantly higher extraction ratios compared to inert blanket gases like N₂ or He. The result of these experiments is shown in Figure 19.

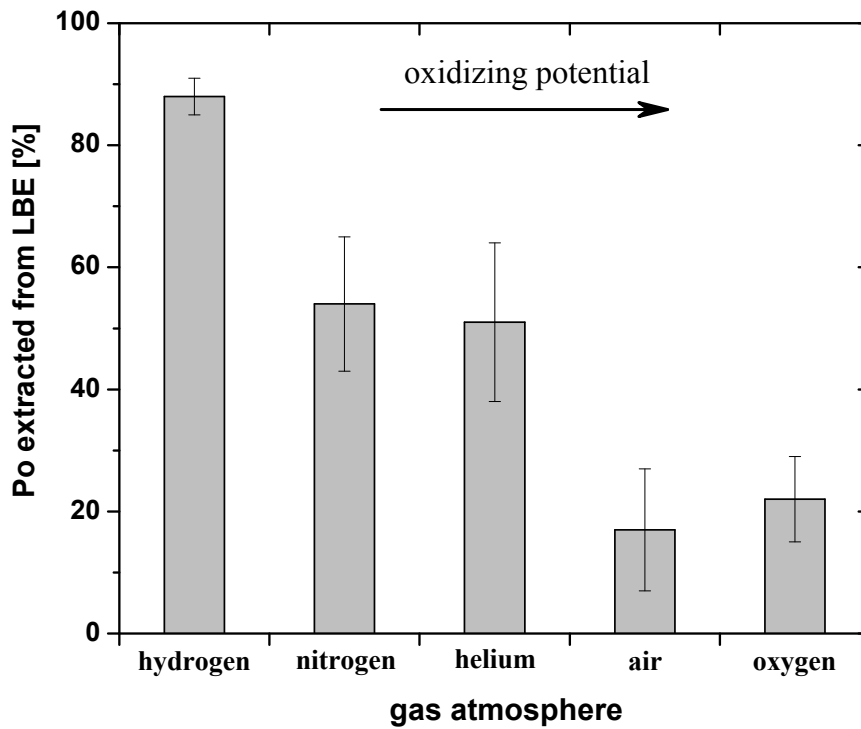


Figure 19: Percentage of Po extracted from LBE under different gas blankets; extraction time 30 min; extraction temperature 250 °C; mass ratio 2:1; taken from [133].

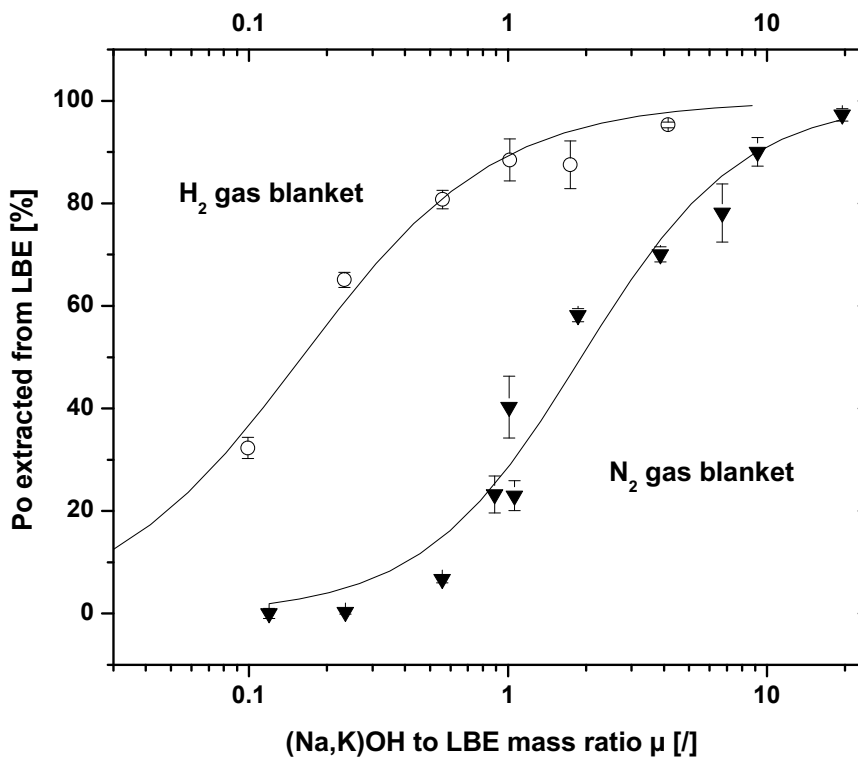


Figure 20: Dependence of Po extraction from hydroxide to LBE mass ratio for H₂ and N₂ gas blankets at 250 °C; extraction time 30 min; taken from [133].

Finally, the extraction performance was measured as function of the hydroxide to LBE mass ratio at a constant temperature of 250 °C. The result of this investigation is shown in Figure 20. The extraction process is increasingly less efficient at a lower mass ratio, as would be expected from extraction thermodynamics. Comparing H₂ and N₂, there is again a pronounced difference in Po extraction performance when an equal hydroxide to LBE mass ratio is used. Generally, about 10 times more hydroxide is needed to achieve the same efficiency under inert gas conditions compared to hydrogen at 250°C.

Summarizing, the experimental results obtained in [133] indicate that Po can be efficiently removed from LBE using molten NaOH/KOH eutectic if reducing conditions and a high temperature are maintained. This work has clearly shown that the pyrochemical extraction represents a suitable possibility to separate Po from LBE. The results are in agreement with data obtained for the removal of Te from Pb in industrial refining. This work represents the first systematic investigations on this method of separation of Po from liquid LBE.

Nonetheless, still no study exists which describes the physico-chemical parameters, e.g. distribution coefficients and kinetic constants, of the transfer process of Po from the metallic into the hydroxide phase. If a Po extraction apparatus is to be implemented into the design of a nuclear facility using a liquid metal, where Po should be efficiently extracted, then the knowledge on these thermodynamic and kinetic parameters is of crucial importance. Based on the findings presented above, follow-up experiments investigating the Po transfer under defined conditions had to be performed. Such conditions may be achieved by assuring that chemical equilibrium is actually established for the determination of distribution coefficients, and providing a defined geometry, contact surface and flow conditions in the two liquids creating proper conditions for studies on the Po transfer kinetics.

In the investigation published in [133], a steady mixing of both phases was realized to enlarge the contact area of both liquids to reach a fast Po equilibrium. For the subsequent study presented here, the Po transfer was additionally studied under stagnant conditions to reduce contact area and decelerate the establishment of equilibrium, thus slowing down the extraction process to enable systematic kinetic investigations. Complementary to these kinetic experiments studying the time dependence of the Po transfer to the alkaline melt, temperature dependent studies of the distribution of Po between the two liquid phases under verified equilibrium condition should give insights into thermodynamics of the underlying process and allow the determination of distribution coefficients.

III.1.3.3.2 Extraction of various nuclear reaction products from molten LBE

As explained in section I.6.2, the liquid metal in a spallation system will be contaminated with a large variety of different radioactive impurities. These impurities may be potentially hazardous by themselves. Furthermore, the presence of these impurities in principle may also have an influence on the efficiency of Po extraction. Therefore, in addition to studies on the extraction of Po from “pure” liquid LBE, the behaviour of other elements concerning the possibility of their extraction from the liquid metal and their influence on Po extraction is also of interest. For such studies, three samples were available from different sources that contained a wide spectrum of radioactive trace impurities. These samples provided a unique opportunity to study the alkaline extraction of various chemically very different radionuclides from liquid metals at the same time, thus allowing to establish systematic trends in their chemical behaviour and drawing conclusions that should be valid for complex mixtures such as those expected in spallation systems.

III.1.4 Objective of this work

Based on the state of knowledge described above, within the course of this PhD thesis the following studies were performed on the alkaline extraction technique with the objective to obtain a better understanding of the underlying fundamental kinetic and thermodynamic parameters:

1. Studies on the transfer of ²¹⁰Po from molten LBE to a molten eutectic NaOH/KOH mixture under stagnant conditions, thus providing a defined contact surface between the two liquid phases. These

studies were performed under systematic variation of contact time of the two liquids and at different temperatures, with the goal of determining kinetic parameters of the extraction process.

2. Experiments under identical conditions, but with stirring, should provide reference data on the Po equilibrium distribution at the same temperature, allowing for the determination of distribution coefficients.

3. In parallel, qualitative investigations concerning the efficiency of the alkaline extraction method towards the removal of various radionuclides of elements other than Po were performed on material from existing proton or heavy ion irradiated Pb-, Bi and LBE-targets from PSI and CERN, containing a realistic mixture of radionuclides representative for a spallation target.

The extraction of hazardous nuclides such as Po isotopes from LBE using salt melts could ease many of the problems concerning safety and licensing of spallation sources based on LBE. The studies performed within this thesis shall provide some of the fundamental knowledge that is required for the development of a technical scale implementation of the method in future nuclear systems. In this way, by demonstrating the possibility of Po removal by alkaline extraction and evaluating advantages and disadvantages of this method, the obtained results contribute to the evaluation of the environmental compliance issues resulting from the operation of a liquid LBE spallation target.

The evaluation of the alkaline extraction process for more complex samples, representative for the radionuclide inventory expected for spallation systems not only shall reveal if and how Po extraction is influenced by the presence of other impurities, but should also give a qualitative overview on the systematics of the behaviour of many chemically very different elements in the alkaline extraction process, possibly allowing a classification of these elements according to their chemical properties and deriving conclusions on the underlying chemical reactions.

III.2 Experimental

III.2.1 Sample preparation

III.2.1.1 LBE samples containing polonium

Po containing LBE samples were produced by neutron irradiation of Pb-Bi ingots at the SINQ spallation neutron source of the Paul Scherrer Institute. The impurity content of LBE used in this investigation is given in Table 16 in section IV.2.1. If not otherwise stated, LBE of batch number 03A124 was used to study Po extraction.

For the irradiation, typically, 4 g LBE samples were put in polyethylene capsules and transferred into the irradiation position using the pneumatic NAA facility. The irradiation time was one hour at a maximum thermal neutron flux of $\Phi_{th} = 3 \times 10^{12} \text{ n cm}^{-2} \text{ s}^{-1}$. After irradiation, the samples were stored for at least 30 days to yield sufficient ^{210}Po accumulation resulting from ^{210}Bi decay. The samples were then diluted with 10 times the mass of non-active LBE at 600°C under a continuous H_2 flow (see [116] for further details). No substantial loss of Po was observed under these conditions in repeated heating experiments.

III.2.1.2 Samples containing a mixture of spallation products

Three different samples originating from earlier experiments and containing a realistic mixture of spallation products were available for extraction studies.

A Pb sample weighting 42.7 mg originating from Target 4 of the PSI SINQ spallation neutron source was cut from a bigger specimen available at the PSI hot-laboratory. It had the designation D10-4, originating from Rod 3 of Target 4 irradiated between 2000 and 2001, which was retrieved in 2006 after 5 years of cooling. The sample had a distance of 27 mm to the centre of the proton beam and received an estimated total proton dose of $2.7 \times 10^{25} \text{ p/m}^2$ [148]. For details on the position of the rod, its irradiation history and the performed investigations such as the analysis of the Pb purity, the reader is referred to reference [149]. After cutting, the sample was stored under air and was used with no further treatment.

A proton irradiated LBE sample was available from an experiment that was performed at the ISOLDE facility at CERN to analyse the release of volatile nuclear reaction products formed within the liquid metal under irradiation. Approximately 500 g of LBE with the batch number 03A124 were irradiated with 1 – 1.4 GeV protons for two weeks in 2004 and 2005 (see [150] for further details). This target was later transferred to PSI, and the LBE retrieved from it serves now as a reference material for investigations on the chemical behaviour of spallation products and their inventory in proton irradiated LBE. From this source, a sample weighting 462.3 mg was cut from the bulk and stored under air prior to its use for the extraction experiment.

Finally, a Bi sample weighting 3.04 g was retrieved from an irradiation experiment performed with a high-energy ^{40}Ar beam described in [151]. The irradiation of seven 0.1 mm thick Bi foils with 220 MeV ^{40}Ar ions ($I = 200 \text{ nA}$) for 3,5 h was performed at the PSI Philips cyclotron. The foils were purchased from Sigma Aldrich and had 99.99% purity, the exact impurity composition is not known. The main purpose of the irradiation experiment was the production of ^{209}At for thermochromatographic investigations. For the separation of ^{209}At all foils were joined and heated to 1000°C for 30 min in a pure He stream. After this experiment, the sample was stored under air and used for the extraction experiment 21 days after irradiation.

Due to the final shutdown of the PSI Philips cyclotron facility, no further irradiated metallic samples were available for additional extraction experiments.

III.2.1.3 Preparation of the hydroxide mixture

NaOH and KOH pellets obtained from Fluka AG were dried under P_2O_5 in a desiccator for 10 days prior to the experiments. The water content of each compound was determined from the weight loss after heating to 500°C for 30 min. It was found to be 1% for NaOH and 8% for KOH. For the preparation of the eutectic hydroxide mixture, 4 g of NaOH and 6.3 g of KOH were put into a grinding vessel and ball-milled for 5 minutes to give a homogeneous powder mixture, which was kept in the desiccator until used.

To perform additional studies investigating the influence of reducing additives to the hydroxide melt, two hydroxide mixtures containing 0.01 or 0.1 wt% NaH were prepared. For this purpose, 1 or 10 mg of the chemical were added into the grinding vessel holding 4 g of NaOH and 6.3 g of KOH. After milling, both mixtures were kept in the desiccator until used.

III.2.2 The extraction device

All extraction experiments were performed in a device displayed in Figure 21. It consists of a 20 cm long quartz tube with a NS29 ground-glass joint. A glassy carbon crucible (Sigma-Aldrich) is placed inside and serves as reaction vessel. The crucible is heated by a 400W HC503 (Electrothermal) heating cord, which is coiled around the quartz tube and is connected to a temperature control system.

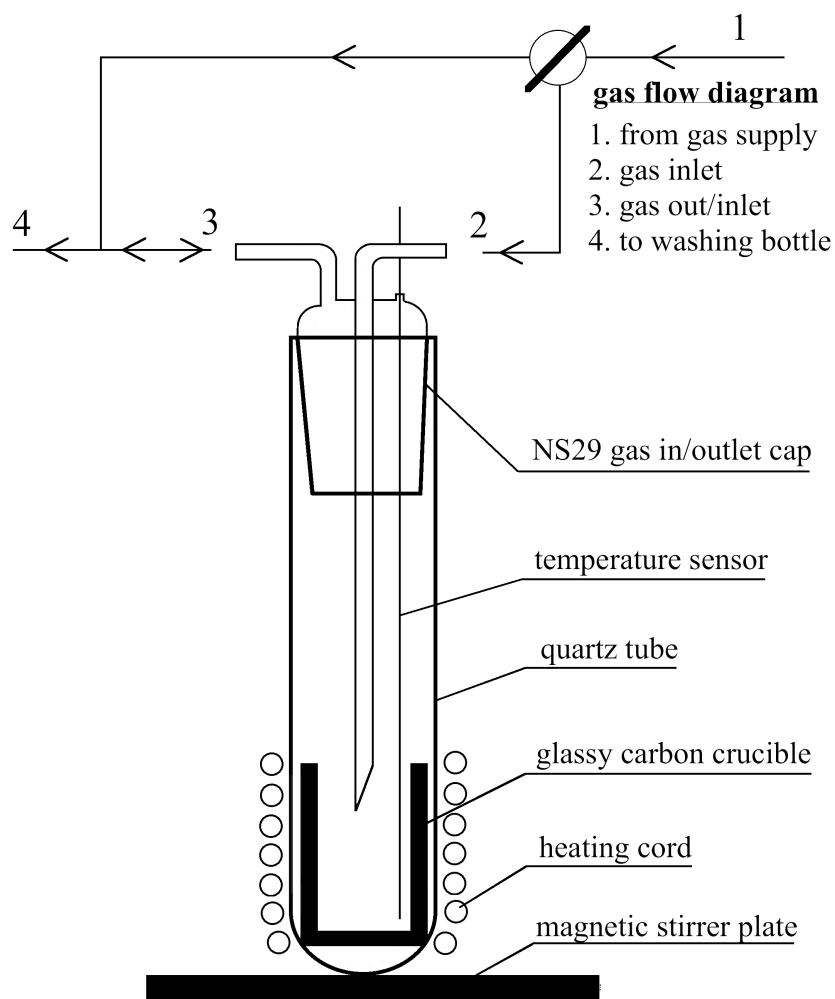


Figure 21: A schematic view of the extraction device

The upper part of the extraction device comprises a gas purging NS29 cap made of glass with a hole for introducing a temperature sensor. This cap provides an airtight enclosure to the inner part of the quartz tube. During extraction experiments, a continuous gas flow N_2 with a flow rate of 100 ml per min was maintained over the extraction vessel using a TECAN CAL 601 mass flow controller. Messer AG, Switzerland, provided nitrogen with 5.0N purity. No further gas purification was performed in the initial stages of this thesis, as the concentrations of water and oxygen were considered to be sufficiently small.

Three identical extraction devices were built and operated to increase the number of extractions and investigative output. In the later stages of this thesis it became apparent that the ingress of oxygen and/or moisture might have an influence on the results obtained. One additional device was installed in an inert gas glove box to minimize the ingress of impurities. Although the inert gas box allowed operations under exclusions of air, it had a rather primitive design without any gas purification or an impurity monitoring system. The oxygen partial pressure inside the box was measured with an oxygen sensor to be around 0.1 vol%. Sicapent powder, obtained from Fluka, served for trapping water vapour. The moisture content was in the order of 5% relative humidity, determined with a commercially available hygrometer.

For a continuous mixing of LBE and the hydroxide melt, a magnetic stirrer bar with a PTFE coating could be introduced into the crucible. This assured a steady agitation of both liquids during the experiment, if desired. However, the presence of the stirrer bar limits the maximum operating temperature of the extraction device, as PTFE quickly deteriorates above 350°C. For experiments under stagnant conditions no PTFE stirrer was used, enabling extractions at higher temperatures.

As shown in Figure 21, the gas flow can be reversed by dismantling the connection of the gas inlet hose at position 2. The diameter of the gas injection tube at this position was chosen to be large enough to enable charging of LBE samples and the magnetic stirrer bar into the crucible against a gas counter flow. This allows adjusting the temperature of the hydroxide melt to the desired value prior to the contact with LBE and avoids the ingress of oxygen into the system during charging of the alloy.

III.2.3 Modifications on the extraction device

At the beginning of the investigations performed on the extraction of Po from liquid LBE with the procedure described below in section III.2.4, a frequent failure of the temperature sensor was observed. This failure was caused by the fact that during the extraction runs, the sensor was immersed into the molten hydroxide and thus suffered intense corrosion attack. The sensor was later placed above the melt touching the carbon crucible. This avoided the temperature sensor failure problem but had a significant influence on the precision of the temperature measurement.

To overcome these problems, a hole was eroded into the glassy carbon crucible using the spark discharge erosion method. Due to excellent electrical conductivity of glassy carbon, this method allowed precisely eroding a vertical hole, 3 cm deep and 1.5 mm in diameter, into the wall of the crucible where the temperature sensor could be inserted. By using this procedure, a precise temperature measurement and control of the system with no contact to the alkaline melt was achieved.

To record and analyse the temperature profile for different placements of the temperature sensor, four temperature sensors were inserted into the extraction apparatus at different positions as shown in Figure 6. The first sensor (T1), which also served as input for the temperature control system, was directly inserted into the melt consisting of 2 g NaOH/KOH mixed by a stirrer bar. The second sensor was placed into the eroded hole (T2). The third one (T3) was adjusted in such a way that it touched the carbon crucible but had no contact to the hydroxide melt to avoid corrosion, as it had been done in the investigation published in [133]. Another sensor (T4) was placed at the outer wall of the crucible. All thermocouples were connected to a Voltcraft K204 meter that enabled data logging. The temperatures for all thermocouple positions in the extraction device were recorded in a test run at temperatures set to 200, 300, 400 and 500 °C. The results of these measurements are given in Figure 22.

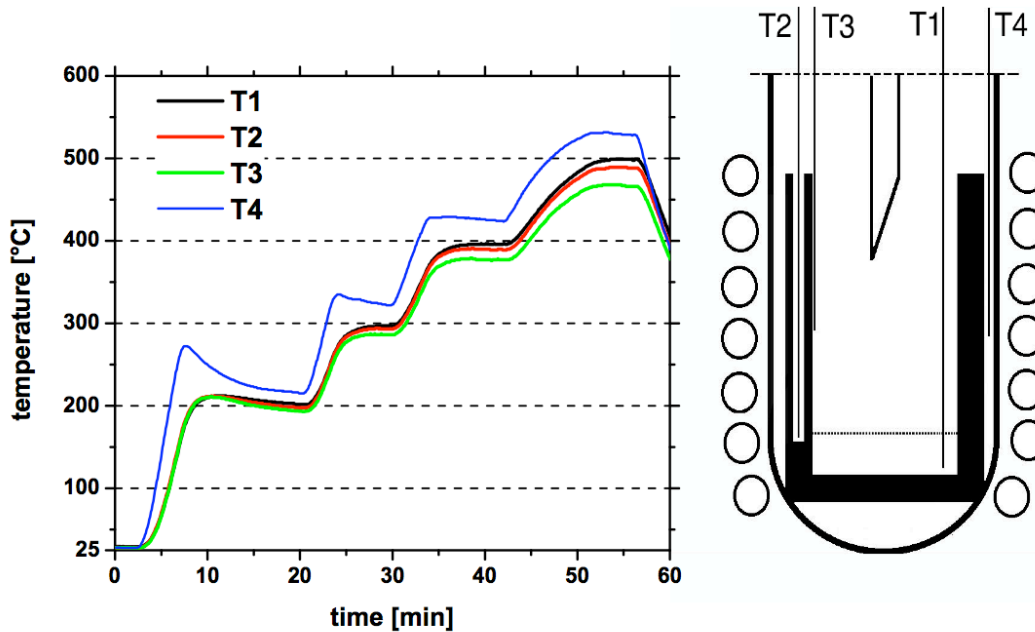


Figure 22: A comparison of recorded temperatures at different positions inside the extraction device.

The difference between the temperature of the melt and the one recorded in the eroded hole did not differ by more than 8 K in the temperature range between 25 and 500 °C. In contrast to this, there was a notable discrepancy between actual and measured temperature, exceeding 25 K, at sensor position T3. The stream of cold gas entering the device likely caused this effect. The change in sensor position represented an improvement with respect to the original setup described in [34], and thus the extraction experiments described within this thesis were always performed with the sensor installed at T2.

As an additional measure to avoid the ingress of oxygen and/or moisture from the cover gas into the extraction device, additional experiments were performed under vacuum. For this purpose, the gas-purging cap shown in Figure 21 was replaced in favour of a NS29 cap with one single stopcock connected to a vacuum manifold. A Teflon-bearing fitting was installed to enable an airtight implementation of the temperature sensor. With this setup, a pressure of 10^{-2} mbar could be maintained inside the extraction vessel during extraction runs performed under vacuum conditions.

III.2.4 Experimental procedure

III.2.4.1 LBE samples containing polonium

In order to analyse the efficiency of ^{210}Po extraction as a function of temperature, contact time and under stagnant or stirring conditions, several sets of experiments were performed, systematically varying each of the above parameters. The NaOH/KOH to LBE mass ratio was held constant at 2:1 for all the experiments performed. Before each experiment, the hydroxide mixture was dried by a preheating step performed at 500 °C.

The first three sets of extraction experiments were performed at stagnant conditions, varying the extraction time while keeping a constant temperature. The duration of each extraction varied between 1 min and 8 h. For each set of extractions, the temperature was maintained at 200, 350 or 500 °C, respectively.

For experiments under stirring, similar variations of the parameters were chosen. However, the temperature was not raised above 350 °C due to deterioration of PTFE. For this reason, no stirring experiment was performed at temperatures exceeding 350 °C. Additional extraction runs were

performed under vacuum with and without stirring. The NaOH/KOH to LBE mass ratio was again held constant at 2:1. All experimental series were carried out with initial Po activity concentrations ranging from 0.8 to 2 kBq per gram LBE.

Each extraction run was performed according to the following procedure: the hydroxide mixture with a mass of approximately 1 g was put into the glassy carbon crucible. The latter was introduced into the quartz tube, which was subsequently closed using the gas injection cap. The temperature sensor was then inserted into the hole inside the wall of the crucible (see section III.2.3). The system was purged with nitrogen for at least 15 minutes prior to heating.

The hydroxide mixture was then heated to 500°C to remove water. The end of the drying process could be visually determined, as water condensing in the upper part of the system disappears, being carried away by the flowing gas. After drying, the melt was cooled to the desired temperature for the extraction experiment and the gas stream was reversed to the counter flow regime as described in section III.2.2. For experiments where stirring was required, the magnetic stirrer bar and approximately 0.5 g of neutron activated LBE was added into the carbon crucible and the nitrogen stream was switched back to normal operation. For stagnant experiments, the addition of the stirrer bar was omitted. Two screening experiments were performed without preheating the hydroxide mixture for water removal.

If vacuum was to be used, the hydroxide mixture was allowed to cool down and to solidify after the removal of moisture at 500°C. When the temperature of the crucible dropped below 100 °C, the gas injection cap was opened and LBE and, if needed, the stirrer bar are placed into the crucible. Then the system was closed by the NS29 vacuum cap and immediately evacuated to avoid moisture or oxygen take-up by the solid hydroxide as good as possible. Then, the temperature was raised to the desired value for the extraction. In contrast to the described procedure using a nitrogen flow, in experiments under vacuum the LBE and hydroxide phase already maintained contact while the system was still heated to the desired temperature. This circumstance was an additional source of uncertainty concerning the extraction time for experiments under vacuum. The starting time of each vacuum extraction was considered as the point in time when the mixture had reached the desired temperature.

At the end of the experiment, the carbon crucible was taken out of the glass tube and both phases are separated while molten. During this procedure, the reaction vessel was opened and the crucible was taken out and tilted to let the metallic droplet “fall” out of the crucible leaving behind the hydroxide melt. This operation lasted about 30 seconds and was performed under air except for those experiments that were performed in the glove box in the later stages of this thesis.

The hydroxide phase was dissolved in 20 ml of distilled water and LBE was dissolved in 7M HNO₃. Both fractions are analysed via LSC as described in section III.2.5.1. The extraction efficiency was calculated by averaging the Po activity found in (Na,K)OH and the loss of activity in LBE. The values are in the following given in percentage of the initial ²¹⁰Po activity. The error bars given correspond to the standard deviations on the mean values determined from repetition experiments. For a general overview on all extraction experiments performed within this investigation, the reader may consult Table 21 in the Appendix.

III.2.4.2 Samples containing a mixture of spallation products

The Pb sample from PSI-SINQ was fused with 355.5 mg of NaOH/KOH at 350 °C for 0.5 h at inert conditions under stirring in the extraction device shown in Figure 21. Additionally, an active charcoal filter was connected between the device and the washing bottle at position 4 in order to capture evaporating Hg isotopes (e.g. ¹⁹⁴Hg) during the extraction experiment. The proton irradiated LBE sample was fused with 0.9 g of eutectic NaOH/KOH. The extraction was performed at 300°C under agitation for one hour under a nitrogen stream. The Bi sample was fused with 1.03 g of eutectic NaOH/KOH mixture. The extraction was performed for 2 h at 350 °C under a nitrogen stream.

For each of these experiments, both phases were separated while molten under air. The solidified hydroxide phase was dissolved in 20 ml of water and both phases were measured by γ -spectroscopy directly after the extraction experiment.

III.2.5 Analysis techniques

III.2.5.1 Liquid scintillation counting

For determination of the ^{210}Po content before and after each extraction experiment, small pieces of up to 80 mg were cut from the sample and dissolved in 1 ml 7M HNO_3 . After mixing with 6 ml of distilled water, 1 ml of the solution was mixed with 9 ml Aquasafe 500 plus scintillator solution (Zinsser Analytics) in a 25 ml PE vial and shaken for homogenization. Similarly, 1 ml of the hydroxide solution was mixed with 9 ml scintillation cocktail. The total ^{210}Po activity of both solutions was measured via liquid scintillation counting (LSC) using a PerkinElmer 3110TR analyser. The initial Po activity concentration in LBE used in the extraction experiments was in the range of 0.8 – 2 kBq/g. In order to obtain sufficient counting statistics with the resulting activities of the measured aqueous samples, the measurement time of the liquid scintillation counter was set to 60 minutes.

III.2.5.2 Measurements using γ spectrometry

To enable a qualitative analysis of the performance of NaOH/KOH for the extraction of various radionuclides present in the metallic samples from CERN, SINQ and the Philips cyclotron irradiation, a γ -spectrum was measured before and after the extraction experiment.

Before each extraction, a measurement using γ spectrometry was performed of each sample described in section III.2.4.2 via a high purity germanium (HPGe) detector with subsequent qualitative analysis on the nuclides present in the samples. The HPGe detector was equipped with standard electronics and connected to the Genie2000 software provided by Canberra Inc., USA. Energy and efficiency calibration was done using a commercially available standard calibration source of ^{152}Eu . The detector allowed a reliable energy and efficiency calibration from 100 keV to 2.5 MeV. The decay data search engine [152] provided by the University of Lund, Sweden, served as reference database for the assignment of detected γ -lines to the corresponding isotopes. After the experiment, the metal samples were measured with the same geometry again for 24 h on the same detector in order to detect remaining nuclides. Similarly, the hydroxide solution was also placed on the HPGe detector and measured 24 h for an analysis of its content of extracted nuclides. In order to correct for the background radiation, a background measurement was performed and the recorded spectrum was subtracted from the spectra of each sample.

As the recorded γ -spectrum of the irradiated Bi sample was very complex because of the presence of an extremely large number of radionuclides, additional spectra of the metal sample after extraction and the corresponding hydroxide phase were recorded 15 d and 158 d after the extraction experiment. This procedure allowed the determination of long-lived isotopes of weak activity, since because of the decay of short-lived ($T_{1/2} < 15$ d) nuclides with a considerable number of γ -lines, such as ^{172}Lu or ^{206}Bi , the recorded spectrum was simplified and allowed the detection of much weaker γ -lines. Applying this procedure, additional nuclides such as ^{75}Se and ^{144}Pm could be identified.

For the experiment performed with irradiated Pb from the SINQ spallation facility, the active charcoal filter used to capture Hg was also measured to check for captured volatile species.

III.3 Results

III.3.1 Extraction of polonium from liquid LBE

The first extraction experiments were performed under stagnant and stirring conditions at the lowest possible temperature of 200 °C. In experiments performed under stirring, it was found that at very short contact times, i.e. below 5 min, the extraction efficiency of Po is above 90%. With increasing extraction time, this value drastically decreases down to 10% within the first 30 min of the extraction. It then does not change significantly with longer extraction time. A very fast and efficient extraction of Po is also observed in experiments under stagnant conditions. For longer experiment times, a decrease similar to that observed in stirring experiments is also observed under stagnant conditions, however the decrease in efficiency occurs over a much longer timescale. This behaviour is shown in Figure 23. The solid and dashed lines in the following figures do not represent physical functions and should only serve as guidance for the eye. For the longest experimental run of 8 h, a decrease from 99 to 30% of extracted Po from LBE was measured in stagnant experiments. Obviously, at 200 °C Po is initially extracted from the liquid metal to the hydroxide phase very fast and efficiently, but over time a back-extraction to the metallic phase occurs.

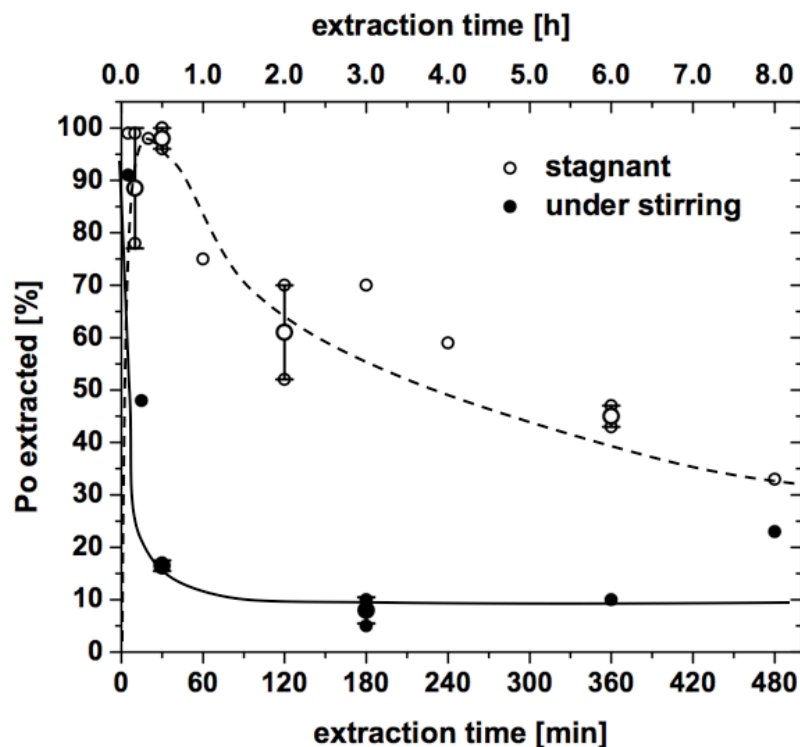


Figure 23: Comparison of Po extraction performance at 200 °C under stagnant and stirring conditions as function of time; N₂ gas blanket; mass ratio 2:1; phase separation was performed under air.

If the temperature is raised to 350 °C, again a near quantitative transfer is observed for short extraction times under stagnant and stirring conditions (Figure 24), similarly to the data obtained at 200 °C (Figure 23). However, for longer extraction runs a behaviour different to that at 200 °C is observed. In contrast to the experiments performed at 200 °C, more than 90% of Po remains in the hydroxide phase at this temperature, independent of the duration of the experiment, as illustrated in Figure 24. This observation is made for extractions under both stagnant and stirring conditions.

Similar results were obtained for the highest investigated temperature of 500 °C. At this temperature, only stagnant experiments were performed due to the maximum operating temperature of the PTFE stirrer bar. The Po extraction behaviour at 500 °C is similar to the one measured at 350 °C with no

significant changes of the Po distribution between NaOH/KOH and LBE with increasing extraction time. A comparison of the results obtained for stagnant experiments under nitrogen at different temperatures is depicted in Figure 25.

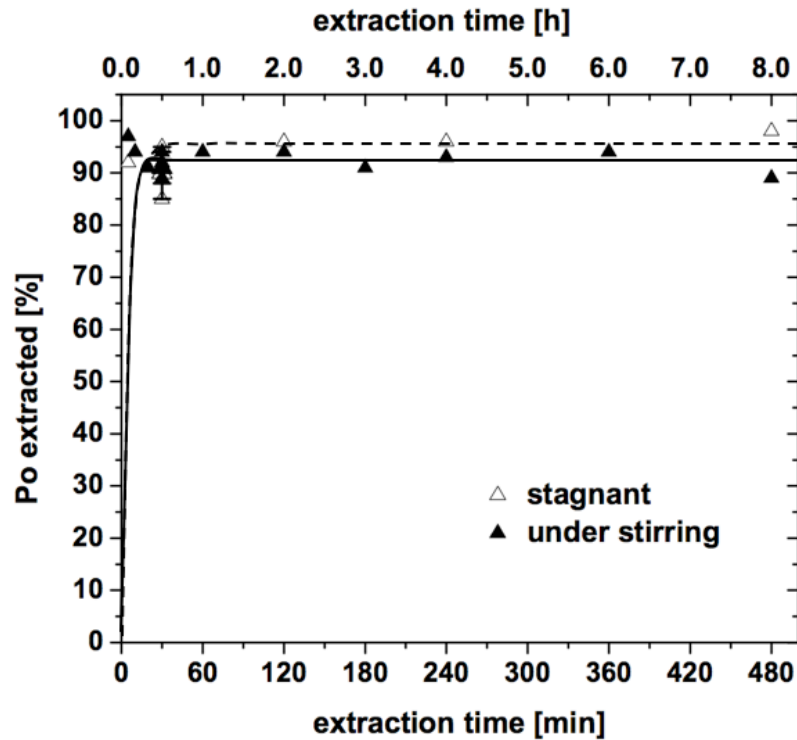


Figure 24: Comparison of Po extraction performance at 350 °C under stagnant and stirring conditions as function of time; mass ratio 2:1; phase separation under air.

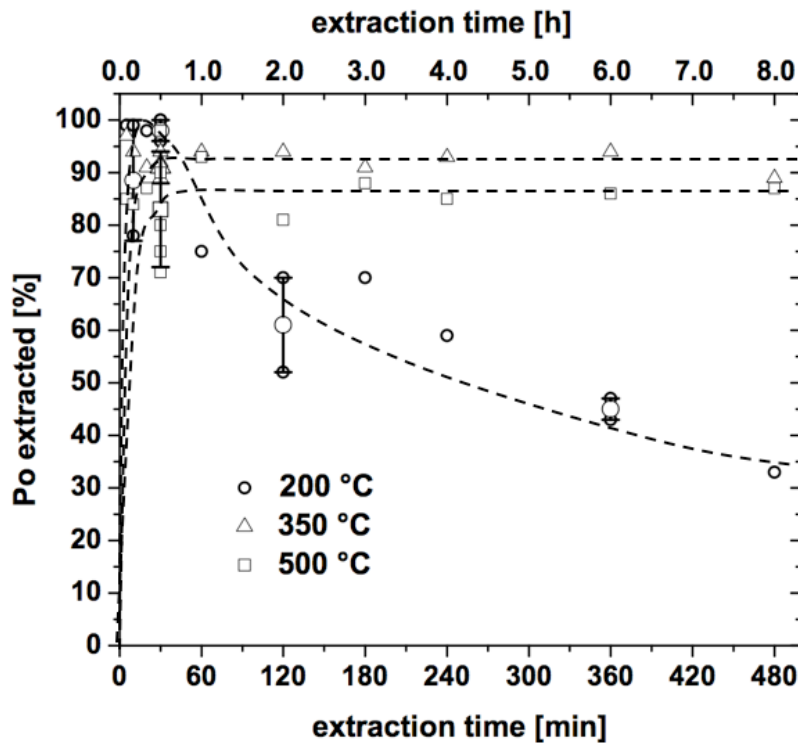


Figure 25: Po extraction performance under stagnant conditions as function of extraction time and temperature; N₂ gas blanket, mass ratio 2:1; phase separation under air.

From Figure 25 a clear difference in Po transfer at different extraction temperatures is observable. While at 200°C, the percentage of extracted Po runs through a maximum at near 100% for very short times and then decreases with increasing experiment time, at 350 and 500°C the percentage of extracted Po remains more or less constant in long term experiments up to 8 h. The final extraction percentages observed at 350 and 500 °C are approx. 93 and 87 %, respectively.

Another graphical representation of the results on extractions performed at different temperatures and mixing conditions is given in Figure 26. Here all measured data for the Po separation experiments with a duration of 30 min, similar to experiments in the investigation published in [133], is summarized. Under stirring, one can observe the following dependence: the higher the extraction temperature, the higher the transfer of Po from LBE into the alkaline phase. While at 200 °C only 15% of Po is transferred, it increases to 90% at 350 °C. This tendency has already been reported in the published investigation [133] and described in III.1.3.3 (for comparison, see Figure 18). The extraction behaviour with increasing temperature under stagnant conditions, however, is of more complex nature. Going from 200 to 250 °C, the Po transfer efficiency drops from 95 to 70%. From 300 °C it again continuously rises to 95% at 350 °C, practically remaining constant for higher temperatures. At 500 °C, however, a drop is again observed. This deviation from near complete Po transfer will be explained later in the text.

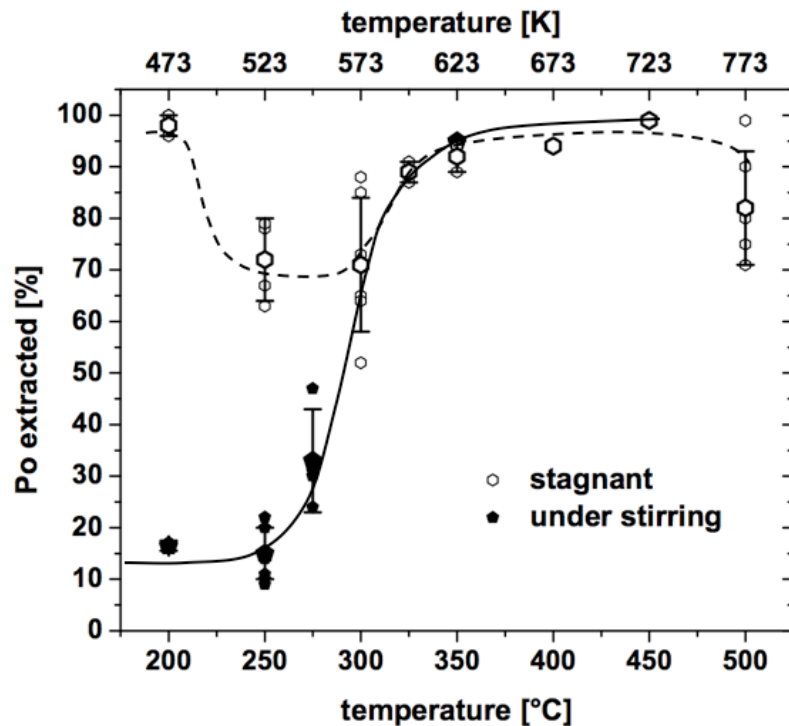


Figure 26: Summary of data obtained for different temperatures under stagnant and stirring conditions under N_2 and 30 min extraction time; for all experiments, phase separation was done under air.

Summarizing the results of the first set of experiments, a clear indication was found that the processes underlying the Po extraction under these conditions are of a complex nature. Experiments under variation of the extraction time indicate that no steady state Po distribution is reached for extractions lasting 30 min and extraction temperatures below 350 °C. Additionally, a significant difference between stagnant and stirring conditions was observed at these low temperatures. However, at 350 °C and 500 °C a steady state is reached, and the results of stagnant and stirring experiments do not differ significantly at these temperatures.

To explain the discrepancy between stagnant and stirring experiments at low temperature, first it had to be excluded that a deterioration of the Teflon stirrer bar and associated chemical reactions could have an influence on the obtained results. This was proven by stagnant experiments where the bar

was present in the melt. No difference to stagnant experiments without the stirrer bar was observed. Taking these facts into account, it was concluded that traces of oxygen or moisture penetrating into the reaction vessel might have a crucial influence on the Po transfer process.

At first, a contamination originating from the cover gas was suspected. Therefore, it was decided to perform further experiments under vacuum conditions. Another reason for the complex behaviour observed may be the brief contact of the sample to air during the separation of the alkaline and metallic phases. Therefore, it was decided to transfer the extraction apparatus into a simple inert gas glove box available in our laboratory to exclude the influence of oxygen and possibly moisture during this separation step as good as possible.

The results on extractions performed under vacuum at 200, 350 and 500 °C are graphically presented in Figure 27. Similar to results obtained under a nitrogen cover gas, the Po transfer is much less efficient under stirring at 200 °C if the extraction time is longer than several minutes. For $t > 60$ min, the Po extraction efficiency remains at around 20%. Compared to stirring conditions, stagnant experiments still lead to higher values of the extraction efficiency in experiments lasting up to 6 h. Nevertheless, at 200 °C a decrease in efficiency with time is observed, similar to findings presented in Figure 23. No such behaviour was found at higher temperatures of the experiment. For vacuum experiments at 350 and 500 °C the transfer of Po remained above 80% at every experiment time investigated. All these findings imply that applying vacuum to the extraction vessel does not significantly improve the poor extraction yields observed under stirring for prolonged times at 200 °C. If ingress of moisture or oxygen should be indeed the reason for the poor extraction efficiency under these conditions, one could suspect that even under the vacuum conditions as applied here, small amounts of moisture and/or oxygen might diffuse into the extraction device.

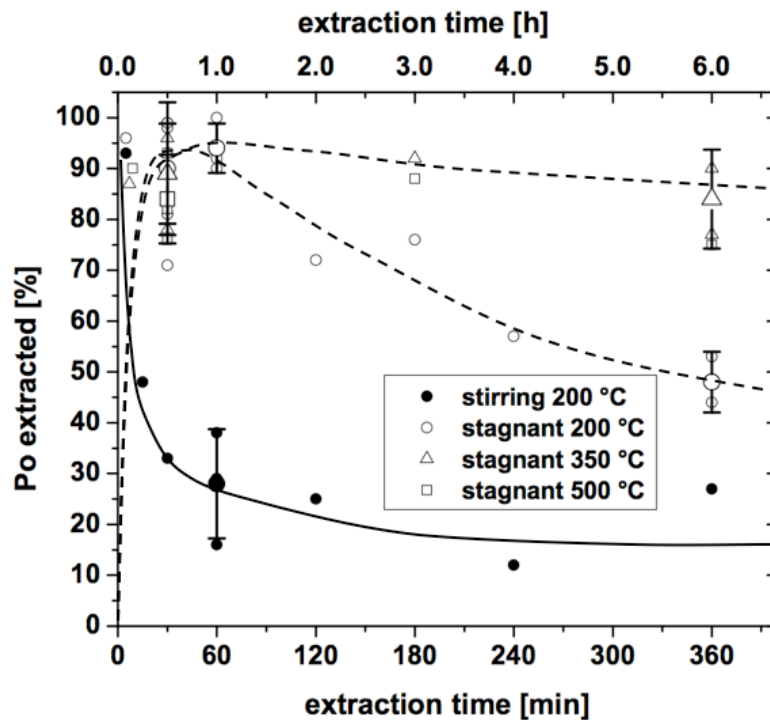


Figure 27: Summary of data for extractions performed under vacuum; mass ratio 2:1; phase separation performed under air.

In order to circumvent possible problems with ingress of oxygen or moisture as well as to avoid contact with air during the separation of the two liquid phases, it was finally decided to transfer one extraction apparatus into a glove box filled with N_2 . As already mentioned in section III.2.2, the glove box had a rather primitive design without any gas purification system. Thus, the quality of the inert gas atmosphere must be considered to be rather poor. Nevertheless, the separation of the metallic and the alkaline phase from now on could be performed with exclusion of atmospheric oxygen.

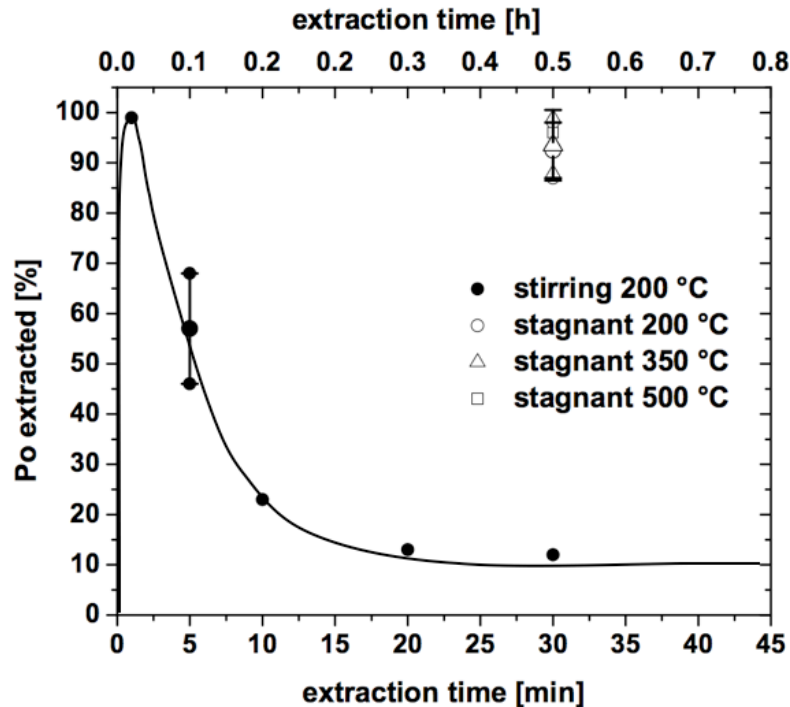


Figure 28: Summary of data for extractions performed inside the glove box filled with N_2 ; mass ratio 2:1; phase separation performed under N_2 in the box.

Again, stagnant and stirring experiments were accomplished inside the glove box, where operations turned out to be more complicated due to the difficult handling of hot parts of the extraction device and the highly corrosive liquids. A summary of the obtained data is given in Figure 28. Despite substantial effort, the obtained results indicate that at 200 °C, there is still a pronounced decrease in Po transfer with time if both liquids are stirred. Substantially higher extraction yields are obtained under stagnant conditions for every studied temperature at 30 min. The data is practically similar to that found under vacuum and under N_2 , except the fact that a near quantitative transfer of Po was observed at 500 °C.

Summarizing, the second and third set of experiments performed under vacuum and inside an inert gas glove box could not resolve the question why low extraction yields for stirring conditions and a back-extraction of Po from the hydroxide phase to the liquid metal are observed at 200 °C. Even with the improved experimental setup, avoiding ingress of impurities together with the cover gas flow and avoiding contact to the ambient air, the experimental results still are very similar to those observed under a nitrogen flow. This could indicate that even with the improved setup, it was still not possible to achieve conditions clean enough to avoid the back-extraction of Po.

Some additional screening experiments were performed to elucidate the nature of the impurities influencing the extraction. In Table 12 an overview of the conditions and the results of these additional experiments is given. A high temperature (500 °C) extraction performed in the inert gas glove box yielded near quantitative Po transfer. Performing the same experiment, but doing the LBE / hydroxide separation under air, lowered the efficiency to 76%. A third extraction experiment exposing the reactants to ambient air for half of the experiment duration (15 min) revealed that the Po transfer drastically reduced to 3% if the reactants were subjected to air for longer periods of time.

These findings indicate that contact with ambient air indeed decreases the efficiency of total Po extraction through a back-extraction of Po to the liquid metal. They also explain why quantitative transfer of Po is never observed at high temperatures if the separation of hydroxide and liquid metal phase is done under ambient air. They finally show that the back extraction is a moderately slow process in the sense that the back-extraction is not complete when the samples are exposed to ambient air only for a short time, i.e. the duration of the hydroxide/metal separation, which was in the order of 30 seconds. For longer times of exposure to air, an almost complete back-extraction of Po to the liquid metal is observed. The results of these three qualitative experiments support the assumption

that oxygen or moisture from the ambient air could be the cause of both back-extraction of Po from the hydroxide to the liquid metal with increased contact time at 200 °C and possibly also incomplete Po extraction observed at higher temperature. Overall, the results are also consistent with the behaviour observed within the three series of experiments performed under a flow of nitrogen, vacuum and inside an inert gas box when one assumes that even very small traces of oxygen or moisture ingressed through the cover gas flow and through leaks in the vacuum apparatus can have a significant influence on Po distribution between the two liquids.

Table 12: Overview on some additional extraction experiments done to elucidate the influence of oxygen and moisture on the Po transfer.

temperature [°C]	condition	extraction yield [%]
500	30 min, stagnant, 2:1, inside glove box	99%
500	30 min, stagnant, 2:1, N ₂ ¹	76%
500	15 min, stagnant, 2:1, under N ₂ , then 15 min with open vessel (under air) ¹	3%
200	30 min, under stirring, 2:1, N ₂ ¹	25%
200	30 min, under stirring, 2:1, N ₂ , + 0.01 wt% NaH ¹	49%
200	30 min, under stirring, 2:1, under N ₂ , + 0.1 wt% NaH ¹	92%
200	30 min, under stirring, 2:1, N ₂ no water removal	1%
200	30 min, stagnant, 2:1, N ₂ no water removal	46%

¹ LBE / hydroxide separation under air

In a second series of screening experiments, 0.1 or 0.01 wt% NaH, a strong reducing agent, was added to the grinding jar during the preparation of the hydroxide mixture. Three subsequent extractions under stirring were performed under nitrogen with these two mixtures and for comparison also one containing no NaH. As the results in Table 12 show, a significant difference is indeed measured for the Po distribution between LBE and NaOH/KOH in these three experiments. While 25% of the Po is transferred into the hydroxide phase containing no NaH, the addition of 0.01 wt% of NaH doubles the amount Po transferred. Increasing the concentration of NaH to 0.1 wt% subsequently raises the Po transfer to 92%.

A third group of tests were performed under stirring and stagnant conditions with no preheating of the hydroxide melt, thus without water removal. Nearly no Po was transferred to the hydroxide melt under stirring, while almost half of it was extracted from the liquid metal without agitation.

Finally, some qualitative experiments have been performed with different LBE batches to ensure that the extraction behaviour is not influenced by different impurities present within the LBE. No statistically significant difference in Po transfer was observed between LBE batch 03A124 and 05B124.

III.3.2 Experiments with extraction of spallation products

The vast number of detected isotopes of different elements and their extraction behaviour from the analysed metallic samples makes the presentation of the data rather complicated. In order to properly visualize the obtained results, a periodic chart of elements will be given for each investigated system. In this chart, all elements that were detected by γ -spectroscopy will be highlighted in colour. Elements marked green were successfully extracted from the metal (> 90% extraction efficiency), red coloration

indicates no or poor transfer (< 10% efficiency). Nearly every detected isotope had a clear tendency either to remain in the metallic matrix or to be transferred into the hydroxide phase.

III.3.2.1 Extraction of radionuclides from irradiated Bi

As can be seen in Figure 29, the spectrum of reaction products formed by the $^{40}\text{Ar} + ^{209}\text{Bi}$ reaction is very broad. In total, 45 radioactive isotopes of 31 elements with $Z = 20$ to $Z = 84$ were detected by γ spectroscopy. A list of all detected radionuclides with their corresponding half-life may be found in Table 22 in the Appendix. The most γ -active radionuclides found in the Bi sample before the extraction experiment were ^{46}Sc and ^{48}V . Both of these elements were quantitatively transferred into the hydroxide phase. After the experiment, isotopes with the highest activity remaining in the metal were ^{205}Bi and ^{206}Bi . Isotopes with the longest half-life were

- in the Bi-phase: ^{207}Bi ($T_{1/2} = 31$ a), $^{110\text{m}}\text{Ag}$ ($T_{1/2} = 250$ d) and ^{102}Rh ($T_{1/2} = 207$ d)
- in the hydroxide phase: ^{60}Co ($T_{1/2} = 5.3$ a), ^{125}Sb ($T_{1/2} = 2.8$ a) and ^{75}Se ($T_{1/2} = 120$ d).

There are many elements in Figure 29 that were suitable radionuclides could not be detected and thus no information on their extraction behaviour is available. This has two distinct reasons. At first, the Bi sample was heated to 1000°C in a prior experiment [151] and thus, elements volatile at this temperature have been evaporated. These elements are marked in grey in Figure 29. Furthermore, some elements do either not have isotopes emitting γ radiation or their half-life is so short that they decayed prior to the experiment.

Due to the existence of different mother-daughter pairs, the evaluation of a successful transfer to the hydroxide phase was in some cases not easy. For example, a considerable activity of ^{206}Bi was found in the hydroxide phase, which is puzzling at first glance. The analysis of the γ -spectrum revealed that in fact its mother nuclide, ^{206}Po , was successfully extracted. The decay of ^{206}Po explains the build-up of ^{206}Bi in the hydroxide phase. The $^{172}\text{Hf}/^{172}\text{Lu}$ or the $^{194}\text{Hg}/^{194}\text{Au}$ are other examples of mother-daughter relationships, where a careful interpretation of the γ -spectra is mandatory.

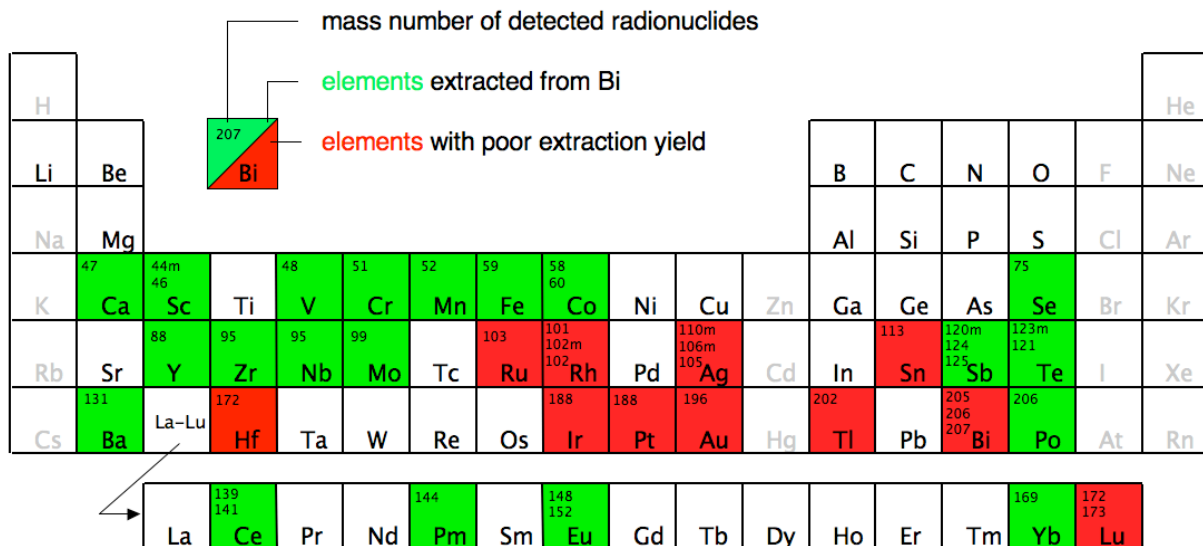


Figure 29: Chart of detected elements in the irradiated Bi sample indicating their extraction behaviour; elements given in grey were evaporated by a heat treatment at 1000°C in a prior experiment.

As a general trend one can observe that lanthanides and the less noble 3d and 4d metals (Sc-Co, Y-Mo) have good extraction efficiency. They may be successfully extracted into the alkaline melt. Metals

more noble than Bi remain in the metallic phase. Members of the chalcogen group are also transferred to the alkaline melt. However, due to their different chemical properties compared to the electropositive metals, a reductive extraction process is assumed [133]. The behaviour of Lu is surprising, as from a chemical point of view one would not expect a drastic change in chemical behaviour from Yb to Lu. Similarly, the fact that the electropositive Hf is not extracted to the alkaline melt was not expected.

III.3.2.2 Extraction of radionuclides from irradiated LBE

In total, 10 radionuclides of 7 different elements were identified in the γ spectra of the initial LBE sample: ^{60}Co , ^{101}Rh , $^{102\text{m}}\text{Rh}$, $^{108\text{m}}\text{Ag}$, $^{110\text{m}}\text{Ag}$, ^{133}Ba , ^{172}Hf , ^{172}Lu , ^{173}Lu and ^{207}Bi . Except for ^{172}Lu , which is the radioactive daughter of ^{172}Hf , all radionuclides have half-lives $T_{1/2} > 1$ y. Short-lived isotopes are missing in the spectra since they all have decayed due to the long decay time of the sample of approx. 5 years. Other radioisotopes present in the sample, e.g. ^{208}Po , ^{148}Gd or ^{129}I , may only be detected by other techniques like α -spectroscopy or accelerator mass spectroscopy (AMS). ^{207}Bi represents the nuclide with the highest activity. Table 23 in the Appendix lists all detected nuclides with their corresponding activity and half-life.

A part of the recorded spectra for the LBE sample before and after the extraction experiment as well as for the (Na,K)OH phase is shown in Figure 30. All radionuclides that initially were detected within the starting LBE material are found in one of the two phases after performing the extraction experiment. Some elements remain in the liquid metal, while others are transferred to the hydroxide phase. This fact is graphically represented in Figure 30 by the presence or absence of the specific γ -lines of the corresponding nuclides in the recorded spectra. The corresponding chart of detected elements can be found in Figure 31.

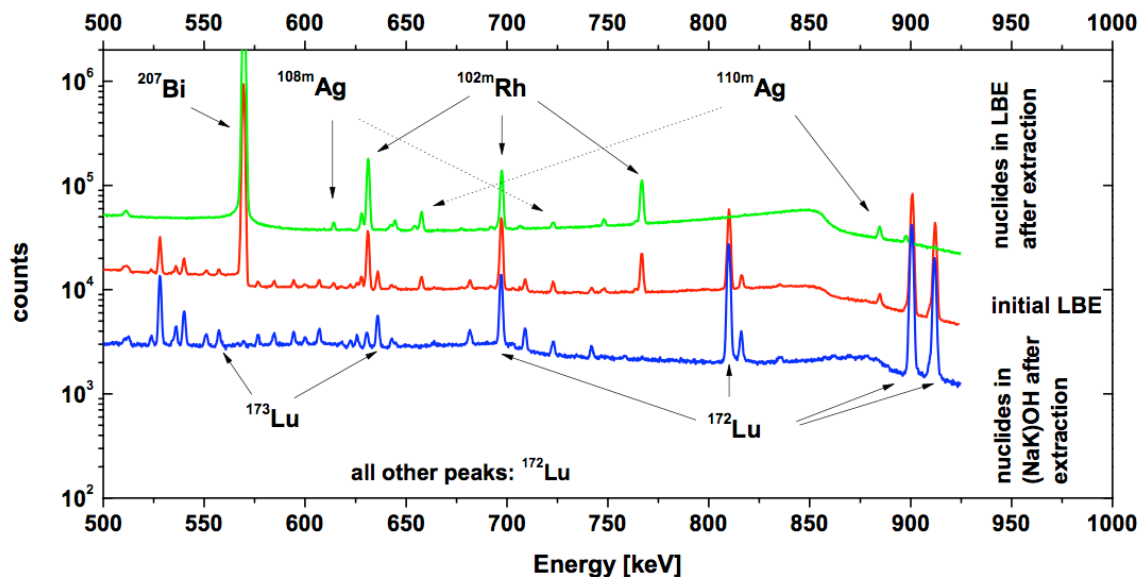


Figure 30: A section of the three γ -spectra recorded from the irradiated LBE sample before and after the extraction experiment and the alkaline phase; the green and blue spectrum are plotted with an offset; nuclides corresponding to recorded peaks are also given in the figure.

In agreement to the study performed with pure Bi, Ag and Rh do not transfer to the hydroxide phase since they are not oxidized under the given conditions. They remain dissolved in the liquid metal and are not observed in the (Na,K)OH spectrum.

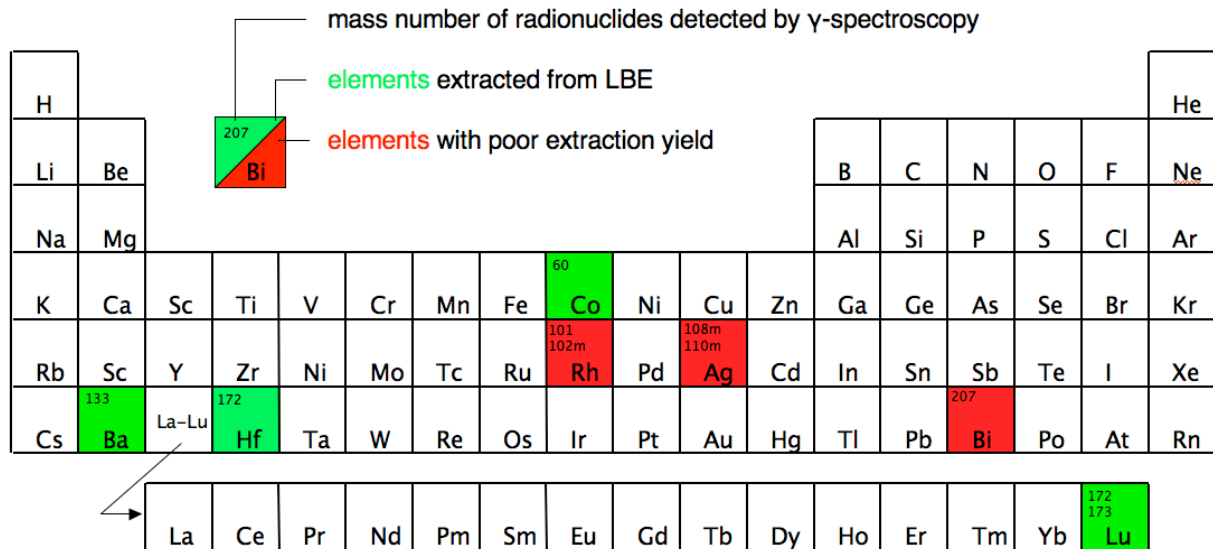


Figure 31: Chart of detected elements in the irradiated LBE sample indicating their extraction behaviour.

The nuclides ^{60}Co , ^{133}Ba , ^{172}Hf , ^{172}Lu , and ^{173}Lu were quantitatively extracted into the hydroxide phase. For ^{60}Co and ^{133}Ba , this finding is in agreement with the study done for the extraction of radionuclides from the heavy ion irradiated Bi sample. In contrast to the former study, for the mother-daughter pairs $^{172}\text{Hf}/^{172}\text{Lu}$ and ^{173}Lu we observed a different behaviour. Both elements did not transfer into the hydroxide phase from metallic Bi, but are easily removed from LBE under inert conditions. Either this effect is caused by the presence of Pb in LBE or by traces of oxygen due to the long storage time of the ISOLDE target under ambient conditions exposing it to oxygen present in air. The weight loss for the sample during extraction was measured to be 2.0 mg. This indicates that approx. 0.5% of its total weight was present as oxides, because they easily dissolve in the alkaline melt. Possibly Lu and Hf were already oxidized before the extraction experiment.

III.3.2.3 Extraction of radionuclides from irradiated Pb

The result of the extraction experiment on the irradiated Pb sample is graphically shown in Figure 32. As can be seen, the spectrum of detected radionuclides is comparable to the one found in the irradiated LBE sample from the ISOLDE facility. The qualitative isotope identification also revealed similar results to those obtained in 2006 from two similar samples originating from rod 3 of SINQ target 4 [149].

Similar to results obtained for irradiated LBE, 16 γ -active isotopes with half-lives exceeding 1 y were detected. Taking into account the cooling time of 10 years, the occurrence of ^{42}K , ^{172}Lu , ^{194}Au and ^{202}Tl , all having a half-life below 14 d, may only be explained by the presence of their long-lived mother nuclides in the analysed sample. Similarly to irradiated LBE, the isotope with the highest activity in proton irradiated Pb is ^{207}Bi . A list of detected nuclides, activities and half-life is given in Table 24.

As shown in Figure 32, the radionuclides of the alkali and alkaline-earth metals are efficiently extracted into the hydroxide phase. However, care must be taken with the interpretation of this finding, since the hydroxide phase contains massive amounts of stable Na and K isotopes. Due to isotope exchange between $^{39/41}\text{K}$ in KOH and ^{42}K in Pb, an efficient extraction could have been imitated. Such an effect would only apply to Na and K or impurity elements that are present in sufficiently high concentrations in the hydroxide phase. To check whether such isotope exchange effects indeed occur, additional extraction experiments could be helpful. Such experiments could involve the use of a neutron activated alkaline metal hydroxide such as $^{24}\text{NaOH}$ that is fused with inactive LBE, Bi or Pb. After the extraction experiment, the distribution of ^{24}Na is determined between the metallic and the hydroxide phase.

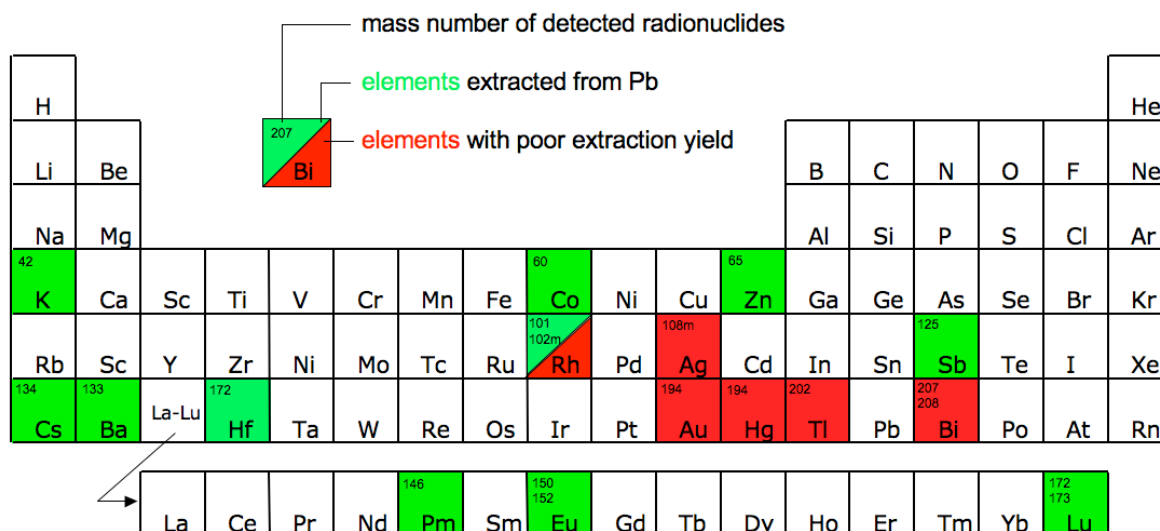


Figure 32: Chart of detected elements in irradiated Pb indicating their extraction performance.

All detected lanthanides and ^{172}Hf were observed to transfer into the hydroxide phase, similarly to detected nuclides of the 3d metals and ^{125}Sb . In agreement with earlier extractions with LBE and Bi, elements that are nobler than Pb such as Ag, Au, Hg and Tl may not be extracted from the metallic phase.

The behaviour of Rh in this experiment was rather unexpected. In contrast to a clear preference of the vast majority of analysed elements to remain in one single phase, 40% of this element was observed to transfer into the caustic phase. The reason for this behaviour is rather unclear, since Rh was observed to completely remain in the metallic phase in experiments with irradiated Bi and LBE. It should be mentioned that both isotopes ^{101}Rh and $^{102\text{m}}\text{Rh}$ showed similar behaviour.

The analysis of the charcoal filter installed to catch volatile species indicated that solely ^{194}Hg has been trapped. No $^{194}\text{Au}/^{194}\text{Hg}$ was detected in the hydroxide phase, showing that Hg is removed from irradiated Pb by evaporation and is not retained in the alkaline melt. A rough estimate of the ^{194}Hg quantity in Pb before and after the experiment indicated that approx. 15% of ^{194}Hg has been released during the extraction experiment performed at 350 °C for 30 min, corresponding to approx. 100 kBq.

III.4 Discussion

III.4.1 Results on polonium extraction from LBE

During the course of this investigation, more than 200 single experiments were performed with the set of extraction devices described in section III.2.2. It should be stated that based on the number of repetition measurements and the balance for Po activity found in both reactants, the overall precision of the data is in the order of $\pm 25\%$.

The first important conclusion based on the presented results is that the Po transfer from the liquid metal to the alkaline melt occurs very fast. In experiments with short contact times as low as 1 minute, a surprisingly high transfer of Po even at the lowest temperature of 200 °C was observed. Such a fast transfer found in experiments without stirring was rather unexpected. In the investigation published in [133], it was argued that under stirring, contact of both phases for 30 min is sufficient to reach equilibrium. By agitation, a huge increase in contact area and material transport by forced convection is generated, substantially reducing the influence of natural convection and diffusion on the Po transfer process. It was therefore expected that under stagnant conditions it would take longer to reach a steady-state Po distribution.

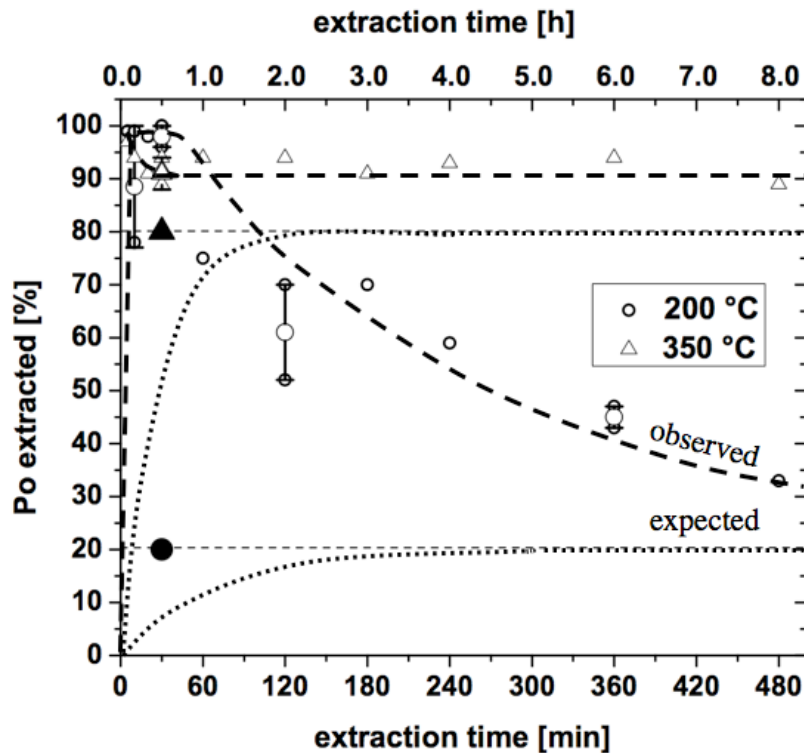


Figure 33: Graphical representation of expected and observed Po transfer kinetics under stagnant conditions; both filled symbols are data obtained in [133], whereas open symbols represent data from the present investigation; large points denote the average of values given as small symbols.

A graphical representation of this aspect is given in Figure 33. The two data points shown as large filled symbols represent data from [133] for the extraction efficiency at 200 (circle) and 350 °C (triangle) for experiments with a duration of 30 min under stirring (efficiency of 20% and 80%, respectively). If a steady-state Po distribution is assumed for extractions under stirring after 30 min, then the Po transfer with time at stagnant conditions should take longer to reach a similar steady state. The black dashed lines shown in Figure 33 illustrate this expected behaviour, i.e. a slow increase with time of the fraction of Po extracted from the liquid metal to the alkaline melt.

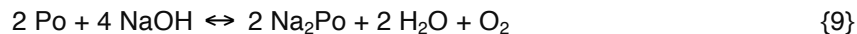
The open symbols connected with dashed lines represent the observed extraction yield for stagnant experiments as a function of time. They show that basically the Po extraction mechanism is a two-step process that completely deviates from the expectations formulated at the beginning of this work. The first step occurs fast, with complete transfer of Po into the hydroxide phase. Within a second step, a back-extraction occurs, forcing Po back into the metal phase. The rate of the second step was found to depend on the temperature involved. At 200 °C, contact times of 8 h are not sufficient to reach a steady state, whereas at 350 °C and 500 °C, a contact of less than 30 min are sufficient.

The obtained results clearly indicate that here at least one additional process is occurring that influences the equilibrium. Based on the knowledge gained from the previous investigation [23], it was assumed that oxygen might cause the observed effects. An attempt for an interpretation of these findings and the potentially occurring chemical reactions will be given.

As was already mentioned in [133], the chemical reactions occurring in the alkaline extraction of Po may be written as:



This disproportionation reaction is based on the chemical similarity of Po to Te and was adopted from metallurgical literature [136]. From experience on Pb refining it is known, that in inert media Te is extracted by reduction and not by oxidation [153]. In [23] it was observed that Po is most efficiently extracted from the liquid metal to the alkaline melt under reducing conditions. The corresponding reaction under inert and reducing media would be:

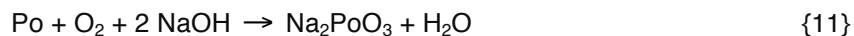


Since the direct oxidation of oxygen by elemental Po, as supposed by reaction {9}, seems improbable, another reaction is proposed to describe the undergoing process under inert conditions. Since metallic Pb is present in large excess, its participation in the extraction process could be explained via the reaction:



In some papers, Po is indeed assumed to be present as PbPo in the LBE phase [113], as it forms a stable compound with Pb [154]. Nevertheless, the existence of discrete diatomic molecules in a metallic melt, as reaction {10} indicates, seems questionable. Alternatively, the mixture can be regarded as a solution of Po in the liquid eutectic, where Po atoms are coordinated with a number of metal atoms as typically observed in liquid metals. There may be a preference of either Bi or Pb in the coordination sphere of Po, and based on electronegativity considerations, the Po atoms are probably slightly negatively polarized. Reaction {10} should therefore not be regarded as a discrete chemical reaction itself, but is referring to a process at the metal / hydroxide interface.

At oxidizing conditions, reaction {9} is reversed and Po is oxidized to its elemental form, facilitating its back-extraction into the metallic phase. The presence of excess oxygen might result in further oxidation of Po via reaction {11}:



However, in a system, where Po is in contact with an excess of Pb, reaction {11} would not occur, since it can be expected that due to the much higher stability of PbO (or $\text{Na}_2\text{PbO}_2 = \text{Na}_2\text{O} \cdot \text{PbO}$), the formation of $\text{Na}_2\text{PoO}_3 (= \text{Na}_2\text{O} \cdot \text{PoO}_2)$ is unlikely. Under these conditions, the formation of PbO (or $\text{Na}_2\text{PbO}_2 = \text{Na}_2\text{O} \cdot \text{PbO}$) would be favoured. Thus, due to the higher oxygen affinity of Pb compared to Po, an oxidation of elemental Po will not occur. Instead, PbO is formed. This claim is strengthened by the following thermodynamic calculation:

Consider a hypothetical reaction of PbO with a metal X resulting in metallic Pb and the oxide of X as products. If the oxidation state of X in the oxide is $2n$, then the reaction may be written as:



Standard laws of thermodynamics will describe the state of the equilibrium between the reactants and the products. By consulting tabulated thermodynamic data it should be possible to predict the tendency of oxide formation relative to that of Pb. The equilibrium constant K of reaction {12} is given as

$$K = \frac{a(\text{XO}_n) \cdot a(\text{Pb})^n}{a(\text{X}) \cdot a(\text{PbO})^n} \quad (4)$$

where a denotes the thermodynamic activity of each species participating in the reaction. With $K > 1$, the equilibrium of the above reaction is shifted to the right-hand side towards the products, i.e. the oxygen affinity of X would be higher than that of Pb. The constant K is given by the relationship

$$-RT \ln K = \Delta^\circ H_R - \Delta^\circ S_R \cdot T \quad (5)$$

with R being the ideal gas constant, T the absolute temperature, and $\Delta^\circ H_R$ and $\Delta^\circ S_R$ the standard enthalpy and entropy of reaction {12}. The latter can be calculated from tabulated data [155] on the formation enthalpy and entropy of the compounds participating in reaction {12}. Data for Po has been taken from [120]. The standard formation enthalpy for pure elements is zero by definition. From the tabulated data, the standard enthalpy and entropy of a given reaction is calculated by balancing $\Delta^\circ S$ and $\Delta^\circ H$ of the products against that of the educts. Inserting these data into equation (5) yields the equilibrium constant K for reaction {12} involving different metals X and temperatures T . An overview on the tabulated data and the results of the performed calculations is given in Table 13.

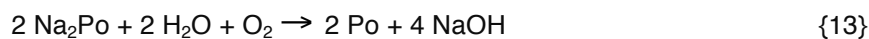
Table 13: Tabulated and calculated thermodynamic data for reaction {12} for different reactants and temperatures according to equation (5)

element X	oxidation state, + 2n	$\Delta^\circ S$ [J mol ⁻¹ K ⁻¹]		$\Delta^\circ H$ [kJ mol ⁻¹]	calculated equilibrium constant K [] at		
		X	XO _n		298 K	500 K	700 K
Pb	2	64.8	68.7	-218.1	1	1	1
Bi	3	56.7	151.5	-573.0	1.4×10^{-13}	7.8×10^{-8}	2.1×10^{-5}
As	3	35.7	117.0	-654.8	7.5×10^1	6.8×10^1	6.5×10^1
Sb	3	45.5	110.5	-690.0	4.8×10^6	1.4×10^4	1.2×10^3
Sn	4	51.2	52.3	-580.8	1.0×10^{25}	5.9×10^{14}	2.8×10^{10}
Se	4	42.3	66.7	-225.4	8.3×10^{-37}	7.0×10^{-22}	1.4×10^{-15}
Te	4	49.5	74.1	-323.4	1.3×10^{-19}	1.3×10^{-11}	2.9×10^{-8}
Po	4	54.4	74	-253.3	3.7×10^{-32}	3.3×10^{-19}	9.3×10^{-14}

As data for the equilibrium constant in Table 13 show, reaction {12}, with X being Sn, Sb and As, is shifted to the side of the products. These metals are exactly those impurities that are oxidatively extracted from Pb in the industrial Harris process [137] (see section III.1.3.1 and Figure 17). In contrast, for Bi and the chalcogenes, the oxygen exchange reaction isn't thermodynamically favoured. This relation clearly indicates that the process responsible for the transfer of chalcogenes is not oxidation. Po may thus not be extracted from metallic Pb, Bi or LBE under oxidative conditions.

In molten hydroxides, reactions {9} and {11} represent parts of reaction {8}. However, reactions {9} and {11} are favoured in completely different environments regarding oxygen concentration. For chalcogenes, the species X^{2-} and XO_3^{2-} were indeed observed by electrochemical measurements in molten NaOH/KOH eutectic [156]. These species, however, were found to exist only in different environments generated by anodic and cathodic reactions.

In summary, the most probable reaction describing the Po transfer from metallic LBE into NaOH/KOH would be {10}. A reverse transfer can proceed by the back-reaction of {9}:



The two-step extraction process found in our investigation at 200 °C may be explained by assuming these two reactions occurring at different stages of the experiment. The thermodynamically favoured reaction {10} is occurring very fast to an almost complete transfer of Po into the hydroxide in the first step. This behaviour is found for all investigated temperatures under both stirring and stagnant conditions. If, however, the hydroxide mixture is continuously stirred, an uptake of oxygen and moisture from the gas stream or leaks in the vacuum apparatus occurs. Po is then oxidized according to {13} and transferred back to the liquid metal. A similar effect is observed without stirring, but on a much longer timescale, as depicted in Figure 23. Stirring thus facilitates the ingress of oxygen and moisture, leading to a fast back-extraction of Po that is represented by the reverse reaction {13}. It should be stressed that the concentration of Po in the system is in the order of 10^{-13} mol%, whereas trace amounts of O₂ and H₂O will certainly be present in considerably higher concentrations.

As it was found at 350 and 500 °C, the influence of diffusing trace gases vanishes, and high extraction efficiencies are observed at these temperatures. This can have several reasons. At first, the solubility of water vapour in molten hydroxides drastically reduces with increasing temperature. This subsequently shifts reactions {10} to the right- and {13} to the left-hand side, respectively, thus largely facilitating Po transfer. Secondly, reaction {10} occurs more efficiently under high temperatures, as was confirmed in [133]. The fact that no significant difference was observed for extractions under stirring and stagnant conditions above 350 °C clearly indicates that the impurity uptake comes to a halt above this temperature. Since the oxygen solubility in molten hydroxides steadily rises with temperature [157], moisture has the most prominent effect at low temperature. Probably an uptake of oxygen in trace amounts immediately results in the formation of PbO, rather than in a back-extraction according to {13}. Only high concentrations of oxygen seem to have a significant influence on the Po equilibrium.

The confirmation of the proposed reaction equations remains to be studied in detailed investigations on the species present in the alkaline melt at each possible condition. However, the effect of oxidizing and reducing agents on the concentration of Po in the hydroxide phase is confirmed by the additional supporting experiments that were presented in Table 12.

High concentrations of oxygen, as found for experiments under air, are hindering the transfer process. The fact that only 3% of Po were transferred at 500 °C under air, clearly hints toward a shift of reaction {13} to the left-hand side. Similarly, large amounts of water also influence the equilibrium in such a way that more Po is found in the metallic phase. A preheating of the hydroxide prior to the extraction is thus important to reduce the inhibiting effect of moisture. Furthermore, the efficiency of Po transfer may not only be influenced by changing the cover gas passing over the melt as shown in [133], but also by the addition of different reagents. If added to the hydroxide melt under a nitrogen atmosphere, reductive agents such as NaH drastically increase the extraction efficiency if compared to extractions performed under nitrogen. This effect is explained by the ability of NaH to react with water and dissolved oxygen thus reducing their effect on the extraction efficiency according to



It is concluded that a complete transfer of Po may be achieved if the extraction system is held under reducing conditions (i.e. by adding NaH) and minimizing the ingress of moisture and oxygen. A temperature exceeding 350 °C is favourable in order to guarantee an efficient transfer disregarding whether both fluids stirred or not. It was furthermore shown that contact times as low as 1 minute are sufficient to yield near quantitative Po transfer under the given experimental conditions.

III.4.2 Extraction of spallation products

Much data was obtained for samples representing real spallation material. Generally, it was shown that a chemical separation of various nuclides present in a liquid metal is possible in practice for a

complex mixture of spallation products using the alkaline extraction method. Qualitative results have been obtained for more than 30 elements present in Pb, Bi or their eutectic mixture. The similarity of data obtained for Pb, Bi and LBE indicates that similar chemical processes are occurring in extraction systems containing these materials.

An overview on the obtained results is graphically summarized in Figure 34. All elements whose behaviour could be studied in the liquid metal – liquid hydroxide system are highlighted in colour. Green colouration indicates that under the studied conditions (inert atmosphere, 300 to 350 °C, 2:1 hydroxide to metal ratio, continuous agitation) the element readily transfers into the molten hydroxide, whereas elements with a red colour remain in the metallic phase. Most elements have been found to behave identically in Pb, Bi or their eutectic mixture. Easily extractable are alkali and alkaline earth elements, the 3d metals, the chalcogenes and lanthanides. Noble metals of the 5th and 6th period of the periodic table such as Ag, Ru, Rh, Ir, Pt, Au, Hg as well as Tl may not be separated by the alkaline extraction technique.

One important factor that influences the behaviour of an element in the investigated extraction is its oxidation potential in relation to that of Pb or Bi. Initially, all elements formed by nuclear reactions are present in an atomically dispersed form in the corresponding metallic solvent. Their further physico-chemical behaviour is very complex and depends on numerous factors (see [158] for further details). With the addition of NaOH or KOH and the presence of oxygen in the system, oxidation of these impurity elements may occur that results in separation of their oxides from the liquid metal and their transfer into the alkaline phase. At first, elements with a high affinity to oxygen will undergo oxidation and thus will be transferred. If their oxidation is complete and excess oxygen is present, elements with lower oxygen affinity will also be oxidized and extracted depending on their oxidation potential. Such a behaviour was indeed observed for the industrial purification of Pb involving the Harris process, see [136]. Assuming a similar behaviour for nuclear reaction products formed in a spallation target, their extraction should also occur in a step-wise manner depending on the oxidation potential of the different elements. The oxidation may either occur directly by the reaction with oxygen dissolved in the liquid metal or the hydroxide, or indirectly by the reduction of a less stable oxide [137]. This impurity oxidation and transfer process will occur until all elements with an oxygen affinity higher than that of the solvent are extracted. Then, the oxidation of the solvent becomes thermodynamically favoured.

A rough estimation on the oxidative extractability of an element in relation to Pb or Bi can be obtained from their standard redox potential. Elements with a lower standard potential than Pb or Bi will oxidize more readily and vice versa. If oxidized, elements will easily transfer into the alkaline phase; otherwise they may remain in the metallic solvent. Data on standard oxidation potentials for various metals is given in Table 14. According to the discussed relationship, the sequence of redox potentials already represents a good approximation on the behaviour of elements observed in the extraction experiments performed within this thesis, as shown in Figure 34. Elements with a lower oxidation potential than Pb/Pb²⁺ or Bi/Bi³⁺ will oxidize more readily and should thus be extractable. Certainly, the oxidation potential of metals in molten hydroxide melts at 350 °C will differ from data for aqueous systems presented here, however, only the relation of potentials to each other is of interest. Even if data on redox-systems in a non-aqueous solution differs from that given in Table 14, it may be assumed that overall the sequence of the oxidation potentials in relation to Pb or Bi would not change significantly. Nevertheless, this topic deserves more attention in the future in order to understand the processes occurring in the alkaline extraction reaction.

The data compiled in Table 14 indicate that chalcogenes do have a higher oxidation potential than Pb and Bi, and are thus not extractable by oxidation, in agreement to the thermodynamic calculation presented for values of K in Table 13. These elements are transferred by reduction according to the chemical pathway given by reaction {10}.

Based on data of the standard oxidation potentials given in Table 14 and on the chemical similarity of lanthanides, one would neither expect Hf nor Lu to be resistant towards oxidation under the studied conditions. In case of Rh isotopes in irradiated Pb, the effect was the opposite - 40% of Rh transferred into the hydroxide phase despite its higher oxidation potential compared to Pb [159]. No conclusive explanation could be given for the behaviour of these elements in the experiments with irradiated Bi and Pb, respectively.

Table 14: Standard potentials of various metals in alkaline aqueous solution (pH = 14) at 298 K; where data was available, the redox-system of the lowest oxidation state is given; based on data from [159].

redox-pair	potential [V]	redox-pair	potential [V]
Li / Li ⁺	-3.04	Ge / Ge ⁴⁺	-0.89
Ca / Ca ²⁺	-3.02	Cd / Cd ²⁺	-0.824
Sr / Sr ²⁺	-2.99	V / V ²⁺	-0.82
K / K ⁺	-2.925	Fe / Fe ²⁺	-0.877
Cs / Cs ⁺	-2.923	Co / Co ²⁺	-0.733
Be / Be ²⁺	-2.62	Ni / Ni ²⁺	-0.72
Sc / Sc ³⁺	-2.6	As / As ³⁺	-0.68
Ln ¹ / Ln ³⁺	> -2.5	Sb / Sb ³⁺	-0.639
Hf / Hf ⁴⁺	-2.5	Pb / Pb ²⁺	-0.5
Zr / Zr ⁴⁺	-2.36	Bi / Bi ³⁺	-0.452
Al / Al ³⁺	-2.31	Te / Te ⁴⁺	-0.42
Ba / Ba ²⁺	-2.166	Se / Se ⁴⁺	-0.366
Ti / Ti ²⁺	-2.13	Re / Re ³⁺	-0.333
Mn / Mn ²⁺	-1.55	Cu / Cu ⁺	-0.358
Cr / Cr ³⁺	-1.33	Hg / Hg ²⁺	0.0977
Zn / Zn ²⁺	-1.285	Pt / Pt ²⁺	0.15
Ga / Ga ³⁺	-1.22	Ag / Ag ⁺	0.342
W / W ⁴⁺	-0.982	Po / Po ²⁺	0.65
Mo / Mo ⁴⁺	-0.98	Au / Au ³⁺	0.7
Sn / Sn ²⁺	-0.909	Pd / Pd ²⁺	0.897

¹Lanthanides

However, it is important to note that the behaviour of different elements toward a pyrochemical extraction is also strongly dependent on their initial chemical state. Depending on the treatment history of the involved sample, various processes (e.g. oxidation) could influence the chemical nature and the distribution of the trace elements within the metallic sample. Oxidized species could be enriched at the surface and hence be more easily extracted.

It is concluded that tabulated thermodynamic data on the redox potential of many elements present as spallation products in irradiated Pb, Bi or LBE may be used to qualitatively predict their behaviour towards an extraction with hydroxide melts. The obtained data, which is summarized in Figure 34, should serve as a first indication on the potential of the described method. Taking the variation of extraction efficiency under different conditions, as observed for Po, as basis for chemical separation, the pyrochemical extraction method could be not only applied for the purification of irradiated liquid metals, but also for a targeted separation of certain valuable isotopes.

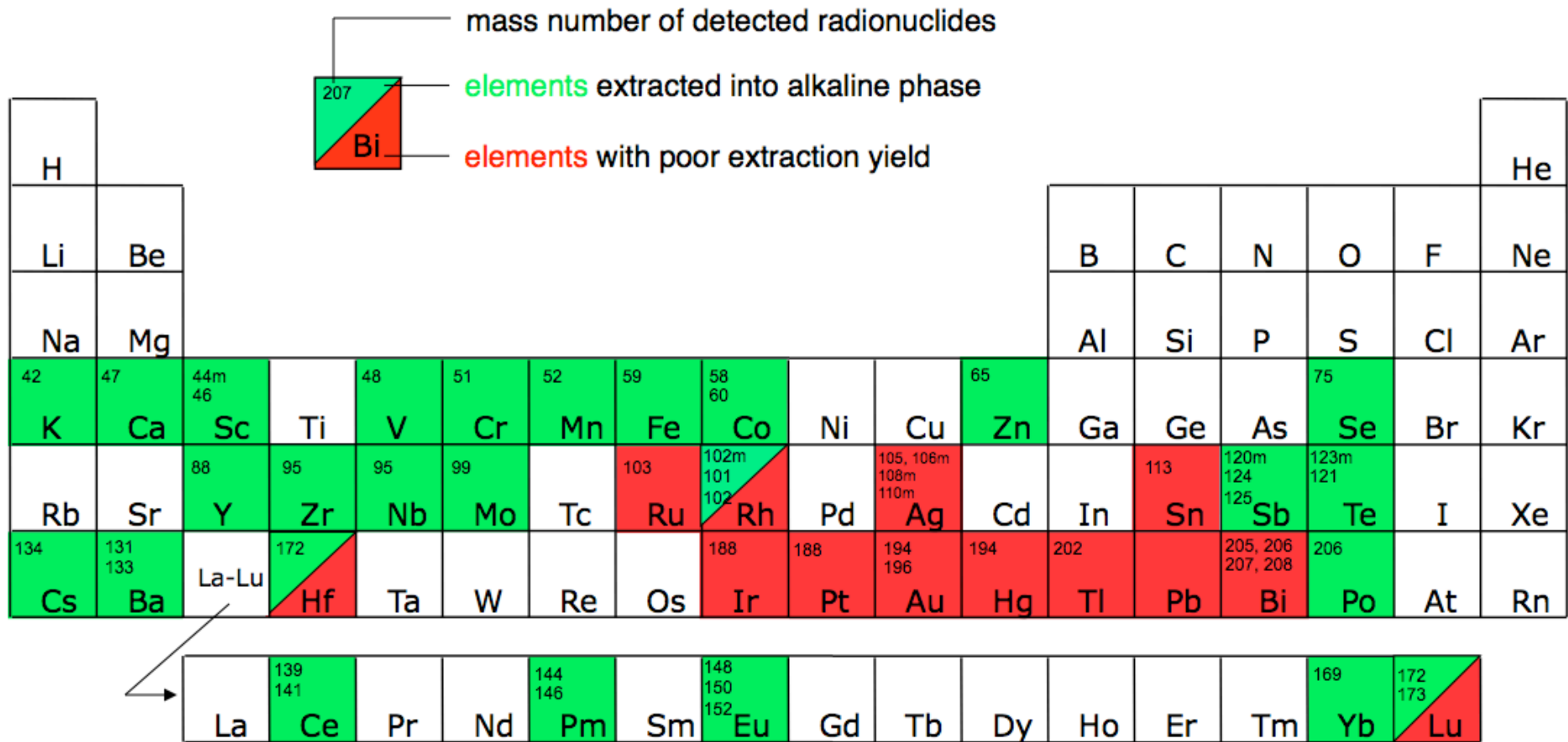


Figure 34: Chart of elements summarizing data on detected isotopes in irradiated Pb, Bi and LBE with their respective extraction efficiency by alkaline melts. For Rh, Lu and Hf the experiments did not give conclusive results; for details, please refer to the main text.

III.5 Summary

In the present study the Po extraction process was investigated under variation of experiment duration, temperature and stirring conditions. It was shown that ^{210}Po could be efficiently extracted from irradiated LBE material. The extraction was shown to work under inert and reducing conditions. Initially, the transfer process was observed to occur almost instantaneously and with high efficiency. However, after the initial almost complete transfer of Po to the molten hydroxide phase, a back-extraction to the liquid metal was observed. The extent of this back-extraction becomes smaller with increasing temperature, while its rate increases with increasing temperature and agitation.

From these observations, it was concluded that the processes involved in the alkaline extraction of Po from LBE are more complex than expected at the start of this work. The Po transfer, as observed under the studied experimental conditions, represents at least a two-step process. It was observed that due to uptake of impurities, the Po transfer efficiency is reduced, and consequently, a transfer of Po from alkaline melt back to the liquid metal can occur. This effect is attributed to traces of oxygen and moisture, most probably originating from the cover gas and from ingress through leaks in the vacuum apparatus. Therefore, it was not possible within this experimental study to achieve conditions clean enough to study the thermodynamics and kinetics of the underlying reactions. However, different chemical reactions that have a crucial influence on the Po distribution between LBE and the hydroxide melt have been discussed, and a consistent interpretation of the results obtained in this work and in preceding studies was given based on thermodynamic data. Thus, finally a plausible explanation was found for the behaviour of Po in the liquid metal-liquid alkali hydroxide system under different chemical environments.

The results of this work indicate that studying the thermodynamics and kinetics of the alkaline extraction of Po from LBE more precisely and in more detail, a considerable experimental effort will be necessary. To study the equilibrium distribution in the absence of oxygen and moisture, extreme care must be taken to achieve the required environmental conditions. Such experiments will have to be performed within a state-of-the-art inert gas glove box employing a sophisticated gas purification system that allows the removal of oxygen and moisture to the lowest possible values. Furthermore the preconditioning of the chemicals should be improved, including thorough outgassing of the LBE and the hydroxide prior to the experiments. Most probably, it will be even necessary to build a sophisticated reactor for preconditioning of the LBE – including electrochemical oxygen sensors - to prepare LBE samples with a defined oxygen content. Furthermore, since the rate of the initial Po transfer to the alkaline melt was observed to be unexpectedly fast, studies of the extraction kinetics may require the development of a special apparatus that allows quick heating and subsequent freezing of the extraction system to obtain data on the extraction rate.

Valuable information has been obtained from extraction experiments involving material originating from real spallation sources. Qualitative data on the extraction behaviour of more than 30 elements from Pb, Bi and LBE were obtained using γ -spectroscopy. As a general rule, elements that are more easily oxidized than Pb or Bi do transfer to the hydroxide phase. These comprise alkali and alkaline earth elements, Sc - Zn (except Cu), Y - Mo and lanthanides. Elements Ir - Tl, Ru, Rh and Ag may not be separated by this method. The obtained results are in agreement with the behaviour of impurities in the metallurgical processes used for the refining of crude Pb and Bi metal. The specific behaviour of different elements in the alkaline extraction can be nicely explained considering their oxidation potential.

As for the alkaline extraction process in general, it represents a powerful technique for the extraction of numerous radionuclides present in the irradiated liquid metal used as target and coolant material. As far as the extraction of Po isotopes is concerned, maintaining reducing conditions would guarantee their fast and reliable separation. In principle, this technique offers the possibility to render an online and offline liquid metal purification process avoiding very high temperatures. This would decrease radiological concerns during maintenance or shutdown of the facility.

Nevertheless, several crucial problems remain to be solved before such a separation method may be licensed on an industrial scale. First, the high corrosivity of hydroxides requires additional measures. Material investigations have to be performed in order to find suitable containment material that would withstand corrosion. Second, the hygroscopic property of hydroxides makes handling and storage rather complicated. Inert gas systems are mandatory for operations involving these chemicals. Problems arising from a reducing atmosphere are yet another peculiarity to be studied. Under reducing conditions, the hydroxide mixture would probably also continuously extract oxygen dissolved in the liquid metal. This is a non-favourable side effect, since the oxygen concentration in LBE has to be maintained at a certain level to minimize corrosion of construction materials. Taking this into account, a precise monitoring and control of the oxygen content inside the liquid metal should be accomplished before entering and after leaving the extraction apparatus. Systematic investigations on this topic are mandatory to assure a safe and reliable operation of a facility using a LBE purification system.

Finally, refinements and optimizations could possibly take this extraction method to an element-selective level, opening up new routes for the production of valuable radionuclides for medical, scientific or technical purposes that cannot be produced using reactors or cyclotrons. Thus, for the mid-term future, the method shows potential for improvement of today's spallation target technology if separation of radionuclides from the liquid metal is of concern.

IV Mobility of polonium in solid Pb, Bi and LBE

IV.1 Introduction

Knowledge on the mobility of Po in liquid and solid LBE is of importance for the safety of nuclear facilities that use this alloy as target material or coolant. If the eutectic alloy is in the liquid state, Po remains dissolved in it and is believed to be distributed homogeneously throughout the liquid metal volume if a thorough mixing of the metal is ensured [37]. For the description of the kinetics of transport phenomena such as evaporation of Po from the liquid metal, some data are available [69, 160]. Data on diffusivity of some elements in liquid LBE are summarized in [37]. The mobility of Po in solid metals and alloys, however, has so far not received much attention in safety related research. Since diffusion in solids is known to occur at a much slower rate than in gases or liquids [161], it could be assumed that the mass transport as well as the evaporation rate will be significantly reduced after solidification of the material.

In the last 20 years, there have been investigations on the behaviour of Po in solid Pb [79] and its eutectic with Bi [162] that have surprisingly shown that the diffusion of Po through these materials occurs much faster than expected. For example, the diffusion coefficient of Po in Pb at room temperature was found to be at least 10^4 higher than that for Bi or Pb in solid Pb [163], indicating that Po diffusion in this material occurs on pathways enabling a high mobility. Earlier investigations [164] already revealed that Po is enriched at grain boundaries of Sn, Sb, Pb and Bi. The Po concentration in these grain boundaries is several orders of magnitude higher than found within the grains [164]. Further investigations have shown that Po tends to accumulate at surfaces, resulting in much higher α -count rates than expected for samples showing homogeneous Po distribution [79, 165, 166].

All these observations have direct consequences for radiation safety in facilities operating with liquid metals containing large quantities of Po. In case of a spill, the α -activity at the surface of the solidified metal will be predominantly dependent on the Po concentration at the surface of the metal. If a fast diffusion of Po to the surface occurs, as indicated by [79, 162, 165], the α -activity on the surface will continuously increase with time. This may require special precautions in order to minimize radiation hazards. One of the important consequences of Po enrichment at surfaces is directly connected to the sputtering effect discussed in section I.6.3. Sputtering will result in the formation of airborne Po by the force of its own decay. Hence, this phenomenon will play a significant role for radiation safety when material containing large amounts of α -decaying isotopes have to be handled [167]. As a consequence, for safety assessments concerning future nuclear facilities using LBE as coolant and/or target material, it is important to accurately predict the behaviour of Po in the solidified coolant or spallation material. For this reason, Po diffusion in Pb, Bi and LBE as well as its segregation to the surface of the alloy was studied to obtain a better understanding of these phenomena.

IV.1.1 Diffusion theory

The motion of atoms within a crystal lattice may occur on different pathways [168]. If one assumes an ordered three-dimensional lattice of atoms A, where the material A represents the host of an impurity B, then the movement of B within such a lattice may occur by:

- a) simultaneous exchange between A and B.
- b) movement of B through interstitial sites
- c) position change of B by movement into a nearby vacancy

An overview on the possible diffusion mechanisms is given in Figure 35. Which of these mechanisms will dominate, depends on the size of B compared to A, the lattice structure and on the temperature [168]. Since the activation energy for atomic movement by the vacancy mechanism c) is lowest, self-diffusion in most metals and alloys and diffusion of foreign atoms occurs mainly by the vacancy

mechanism [169]. As a consequence, the migration of atoms in metals and alloys will strongly depend on the presence of vacancies. As their concentration increases with temperature, the movement of atoms will be enhanced at higher temperatures [161].

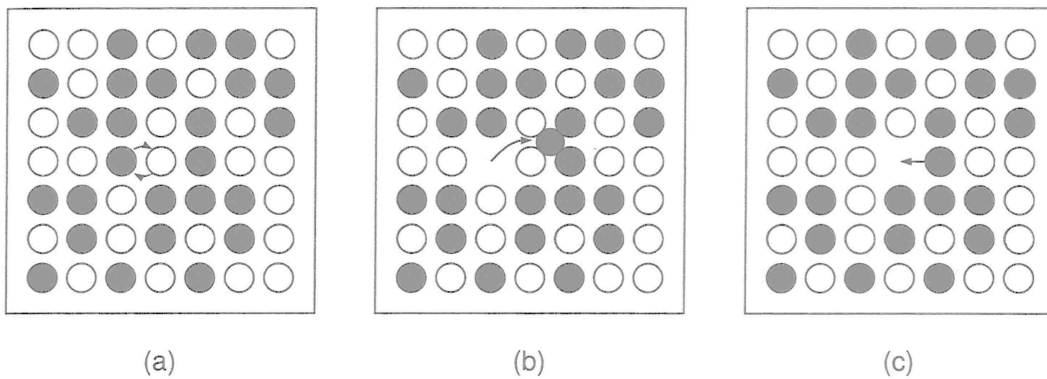


Figure 35: Three basic mechanisms of diffusion: a) Interchange, b) migration through interstitial positions and c) position exchange with a vacant lattice site; taken from [168]

All diffusion mechanisms shown in Figure 35 apply to a regular lattice structure, as it is usually present in single crystals. In such a crystal, the shown mechanisms describe the process of *bulk diffusion*. On a microscopic scale, however, ordinary metals consist of numerous of such single crystals – grains of different size and shape. Their crystallographic orientation relative to each other is random, and each grain thus will be separated from its neighbours by a grain boundary. In contrast to the adjoining crystal lattices, grain boundaries are highly disordered atomic structures [169]. With good approximation from grain boundary diffusion data, the grain boundary width may be assumed to be around 0.5 – 1 nm [170].

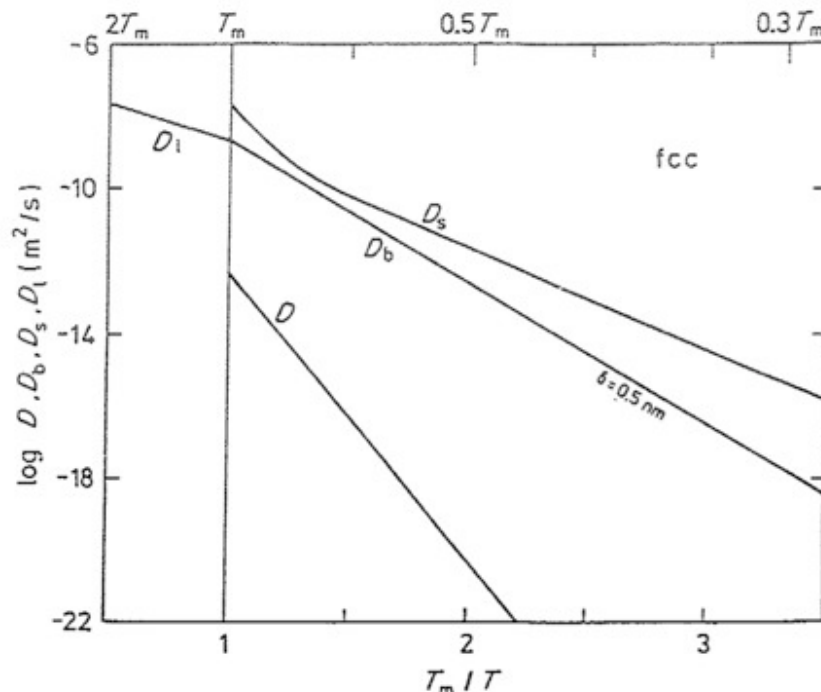


Figure 36: Different diffusion coefficients (D – bulk diffusion, D_b – grain boundary diffusion, D_s – surface diffusion, D_l – liquid diffusion) for fcc metals as function of temperature relative to the melting point T_m ; taken from [170].

The diffusion mechanisms described above only refer to the diffusion of impurity atoms inside the grains, but not in the space between them. It was found that diffusion may occur within such boundary

areas. This kind of diffusion is referred to as *grain boundary diffusion* [161]. In contrast to bulk diffusion, the motion of atoms along grain boundaries does not depend on the concentration of vacancies inside the lattice, as atoms now may move relatively freely inside the interstitial space between the grains [171]. As a direct consequence, the diffusion through a boundary will be much faster than through the bulk.

In addition to the diffusion through the lattice and grain boundaries, there is another type of diffusion occurring at the surface of a material. *Surface diffusion* was found to be the fastest diffusion process in solid-state [169]. A comparison of all three types of diffusion occurring in the solid state as function of temperature is given in Figure 36. As an example, the bulk diffusion coefficient in Pb, crystallizing in a face-centred cubic (fcc) structure, at room temperature (approximately $0.5T_m$) is by a factor 10^8 smaller than for grain boundary diffusion.

IV.1.2 The laws of Fick

For the mathematical description of the diffusion process, Fick's first and second law [172] on material transport have to be applied. The first law implies that the rate of transfer of the diffusing substance through a unit area of a section of the sample is proportional to the concentration gradient measured normal to this section [173]:

$$J = -D \frac{dc}{dx}. \quad (6)$$

Here, J represents the flow rate of a substance per unit area, and dc/dx the concentration gradient perpendicular to that area. The term J is also referred as the particle flux. The factor D is the diffusion coefficient and has the units of length²/time. The negative sign indicates that diffusion occurs from regions of high towards regions of low concentration. From Fick's first law, one can easily show that the concentration change with time, dc/dt , is dependant on the derivative of the concentration gradient:

$$\frac{dc}{dt} = D \frac{d^2c}{dx^2}. \quad (7)$$

This differential equation, constituting Fick's second law, is used to describe the change of the concentration profile with time for a specific diffusion problem. With boundary conditions that are defined by the diffusion experiment, the solution of (6) may have different mathematical forms. In [173], many general examples on the mathematical treatment of Fick's second law have been published and the solution for different boundary conditions are given.

Equation (7) holds true if the diffusion coefficient is independent from the concentration of the diffusing substance [170]. This condition, however, is not met in many media, for example, in the case of inter-diffusion in metals [169]. Nonetheless, if the concentration of the diffusing element is small enough, equation (7) describes the diffusion process with sufficient precision [170]. Thus, for Po, which is usually present in the matrix in sub-ppm quantities, one may apply equation (7) for describing diffusion in different host metals such as Pb, Bi and their mixtures.

The dependence of the diffusion coefficient on temperature is given by

$$D = D_0 \cdot e^{-\frac{E_A}{RT}}, \quad (8)$$

where D_0 is the standard diffusion coefficient, E_A the activation energy, T the absolute temperature and R the universal gas constant [171]. The higher the temperature, the faster atoms move, thus increasing the diffusion constant. An overview on values for D_0 and E_A determined for the diffusion of metals in polycrystalline Pb and values for diffusion coefficients at 300 and 500 K calculated according to equation (8) are given in Table 15. Especially for noble metals such as Ag, Au and Cu a high

mobility in solid Pb is observed even at room temperature, which is explained by the low melting temperature of Pb, see Figure 36. Another explanation is given by the fact that Pb is considered as an “open” metal where solvent atoms have a high atomic radius if compared to that of the solute [170].

Table 15: Overview on measured values for D_0 and E_A for different solutes in polycrystalline Pb. Additionally, values of the diffusion coefficient at 300 and 500 K calculated by equation (8) are given; data are taken from [169].

solvent	solute	D_0 [cm ² /s]	E_A [kJ/mol]	temperature range [K]	calculated diffusion coefficient [cm ² /s] at	
					300 K*	500 K
Pb	Co	0.009	46.4	383 - 573	7.5×10^{-11}	1.3×10^{-7}
	Ni	0.011	45.4	481 - 593	1.4×10^{-10}	2.0×10^{-7}
	Cu	0.0079	33.6	498 - 598	1.1×10^{-8}	2.4×10^{-6}
	Ag	0.046	60.8	423 - 573	1.2×10^{-12}	2.0×10^{-8}
	In	33	112.2	437 - 493	9.6×10^{-19}	$6.3 \times 10^{-11*}$
	Au	0.0028	37.3	334 - 563	9.0×10^{-10}	3.6×10^{-7}
	Tl	0.511	101.9	480 - 596	9.2×10^{-19}	1.2×10^{-11}
	Pb	0.281	101.4	470 - 573	6.2×10^{-19}	7.2×10^{-12}
	Bi	6.8	112.2	564, 596	2.0×10^{-19}	$1.3 \times 10^{-11*}$

* extrapolated

IV.1.3 Segregation effects in metals

The surface composition of compounds and alloys generally differs from their bulk composition [174]. It has been postulated and shown by many investigations that impurities migrate to surfaces and grain boundaries [175]. This leads to an enrichment of the migrating species at these surfaces, in contrast to the principles of diffusion, which state that mass flux occurs from high to low concentrations. An explanation for this effect was based on the assumption that small foreign atoms will fit with less strain into grain boundary regions than they do within the crystal lattice, thus lowering the free energy. As a direct consequence, the concentration of the impurity should be higher at the boundary interface than it is within the grains [176]. This effect is usually known as segregation. Although the thermodynamics of surface segregation was already described a century ago, it was only recently possible, thank to the progress in experimental and theoretical methods achieved during the past 30 years, to reveal the composition and structure of interfaces and to obtain more insights into segregation phenomena [174].

Segregation was observed for example for Sn [177] and Bi [178] in Cu, for various elements in iron and many different types of steels [179], in Al and Ni alloys etc. [180]. A review on the existing studies in segregation phenomena may be found in [181]. As a general rule, the overall enrichment factor of a solute, which is defined as the ratio of its surface to volume molar fraction, was found to depend upon the solid solubility of the solute atom in the corresponding solvent [182]. This dependence is shown in Figure 37.

All of the above relationships are valid for systems where the crystal lattice is in thermal equilibrium with the surrounding media. However, in the case studied here, α -radiation of the decaying Po influences this equilibrium by transferring additional energy to the crystal lattice. Numerous publications exist on diffusion phenomena under the influence of radiation [183-186], and several effects have been reported that are only occurring under conditions involving radiation. One of these effects is known as *radiation enhanced diffusion* [170]. By irradiation, point defects in excess of the thermodynamic equilibrium values are generated in the crystal lattice [187]. The atomic diffusion in the bulk will thus be enhanced, as it is proportional to the defect concentration. As consequence, the diffusion of atoms in a solid host material will also depend on the net energy transferred to its lattice by radioactive decay. Therefore, it may be expected that the mobility of Po and any other impurity atom in solid LBE will rise with increasing Po activity concentrations.

Another effect is referred to as *radiation-induced segregation* [187]. Here, a net flux of defects towards grain boundaries and the surface will occur. The coupling between impurity flux and the defect flow will

result in an increase of the surface concentration of the impurity [175]. This is strictly non-equilibrium segregation and the enrichment layer may also dissolve into the bulk after irradiation is stopped if the diffusion coefficient is high enough [175]. Summarizing, the magnitude of the effects involving radiation enhanced diffusion and radiation induced segregation depends upon various factors such as temperature, dose rate and kind of radiation [183, 185]. A detailed analysis of radiation-induced mechanisms occurring in metals containing Po is beyond the scope of this work. Therefore, a qualitative description of the observed effects involving Po will be given in the next section.

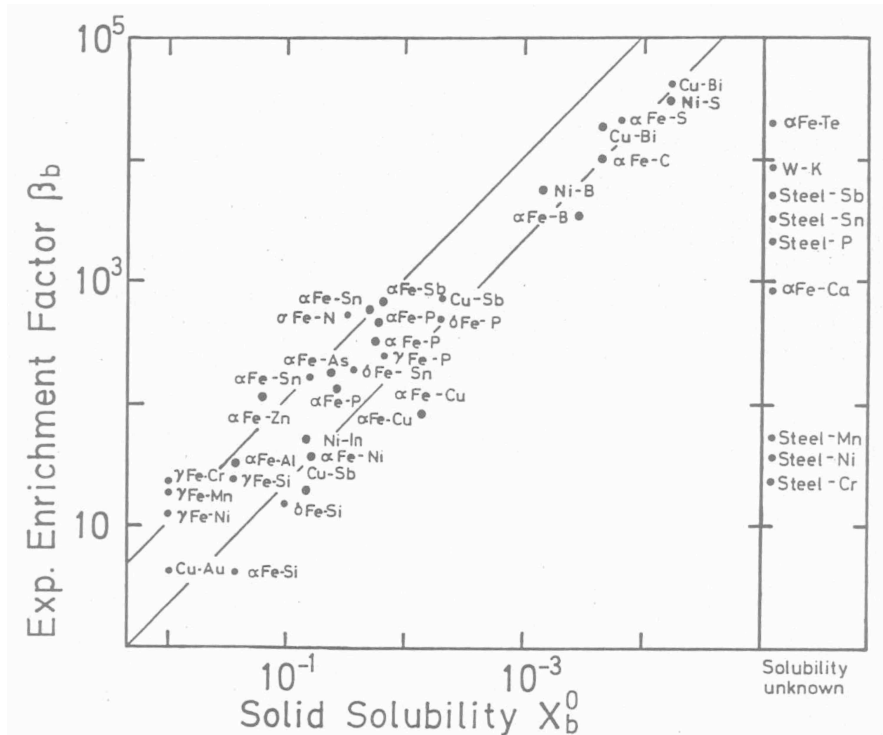


Figure 37: The correlation between the enrichment factor and the solid solubility of a solute in a corresponding solvent; reproduced from [174], original data from [182].

The following literature review should give an overview on studies performed in the past on the Po segregation phenomenon in LBE. The review has been extended to Po diffusion and segregation phenomena in pure Pb, Bi and other metals.

IV.1.3.1 The behaviour of polonium in various metals

Studies on Po mobility in various metals date back to the 30ies of the last century. As Po seemed to exhibit unusual diffusion behaviour which influenced measurements of its half-life [75], various reports qualitatively describing the behaviour of Po deposited on different host materials have been published, as for example for Au and Pt [188, 189], Ag [190], Pb [191] and various other materials [192].

First systematic investigations on the behaviour of Po in different solid metals were performed by [164]. In this study, Po was spontaneously deposited from a radium solution on various metals such as Ag, Sn, Sb, Pb, Bi etc. The samples obtained in this way were subsequently melted to homogenise the Po distribution. After cooling, autoradiograms of the polished metal surface were taken and compared with respect to the relative orientation and distribution of grain boundaries in each metal. For all investigated metals, the pattern on the exposed film emulsion, representing regions with high ^{210}Po accumulation, completely coincided with the orientation of the metal grain boundaries. This led to the conclusion, that the solubility of Po in each of the investigated solid metals is very low (mole fraction $< 10^{-10}$), while it is much higher in the liquid. During the metal solidification process, Po is transported with the crystallization front [164]. At the end of the crystallization process, Po is finally enriched at the crystal grain boundaries as seen in Figure 38.

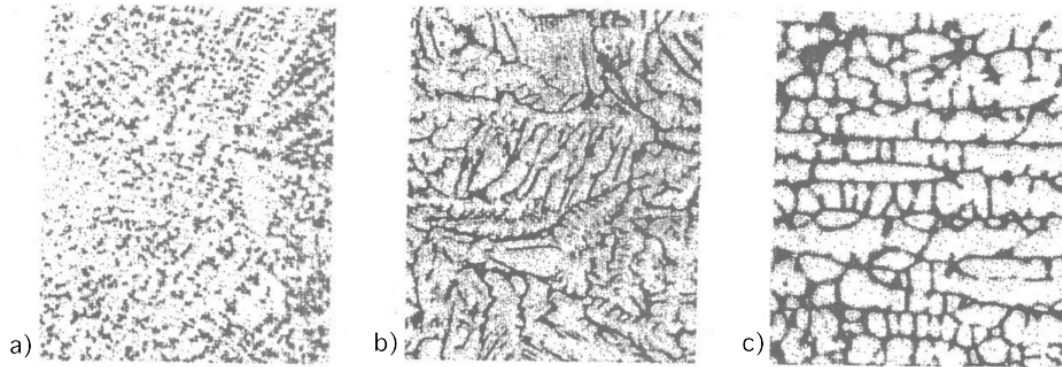


Figure 38: Autoradiographic images of the surfaces of metallic a) Pb, b) Bi, and c) Sn samples containing ^{210}Po after solidification, showing an inhomogeneous ^{210}Po distribution; pictures taken from [164].

This implies that for any metal investigated in [164], Po may be efficiently enriched by the process of zone refining. This was indeed tested in laboratory experiments with elemental Bi [193]. Bi (97% purity) containing ^{210}Po was filled into 20 cm long quartz ampoules and zone refined with a movable furnace operating at 370 °C. With increasing furnace velocity a decreasing enrichment of Po at the end of the Bi bar was observed. However, this process offers only poor separation yields of only a 2- to 5-fold Po enrichment compared to the starting concentration.

IV.1.3.2 Investigations on polonium in lead

The first measurement of the diffusion coefficient of Po in solid Pb has been reported by [194]. In Pb single crystals and polycrystalline Pb foils, the authors measure a diffusion coefficient of $1.5 \times 10^{-10} \text{ cm}^2/\text{s}$ at 310 °C. In a later study, the diffusion of Po in Pb foils was measured by using the method of radiography [195] and values of 5×10^{-14} , 10^{-13} and $10^{-12} \text{ cm}^2/\text{s}$ were deduced for temperatures of 100, 150 and 200 °C, respectively.

More recent investigations on the natural radioactivity in different construction materials showed that Pb had the highest surface activity if compared to Si, Au, Cu, steel or Teflon [196]. Most of the radioactivity arose from α -activity attributed to ^{210}Po , which is the daughter nuclide of the isotope ^{210}Pb present as a natural contamination in Pb samples.

Based on this study, a series of papers on the ^{210}Po activity in Pb samples was published by Zastawny et al [79, 163, 197-200]. These studies qualitatively describe the behaviour of Po in Pb samples under different experimental conditions. All experiments are based on measurements of the α -activity of Pb surfaces as function of storage time. Pb surfaces previously scraped by a knife showed lower α activity, which then was found to exponentially recover to the initial value observed before scraping [197]. The author concludes that by the mechanical treatment (scraping) of the Pb surface, lattice defects are introduced that enhance the diffusion of Po atoms to the sample surface. It was further found that samples stored under air exhibit lower ^{210}Po accumulation than samples stored at inert conditions [199].

Additional experiments were performed at different temperatures [79, 163, 200]. Higher temperatures yielded higher accumulation of ^{210}Po . A model was presented to explain the observed migration of Po to the sample surface and a Po thermal diffusion coefficient was measured to be in the order of 10^{-15} to $10^{-13} \text{ cm}^2/\text{s}$ at room temperature, 50 and 100 °C. These values are in good agreement with Po diffusion data reported earlier [195]. For the migration process towards surfaces, values in the order of $10^{-11} \text{ cm}^2/\text{s}$ at room temperature were deduced [79]. Up to now, studies published by Zastawny et al. represent the most extensive set of data for the migration of Po in solid Pb, although the presented results often lack explanation and are sometimes contradictory.

Investigations on the mobility of Po in solid Pb have also been performed in the context of the OPERA project [165]. In this experiment, which was performed to investigate neutrino oscillations, a large grid detector was installed and is currently operating at the Gran Sasso underground laboratory, Assergi, Italy. For the detection of particles produced by the interaction of neutrinos with matter, a series of 56 Pb plates is stacked with emulsion films in order to allow particle tracking. As the emulsion films are also sensitive towards α -radiation, series of tests were performed in order to reduce the known effect of Po migration towards Pb surfaces [165] by alloying Pb with small amounts of other metals. It was found that in Pb alloyed with 0.07 wt% Ca the background α -radiation originating from ^{210}Po decay is significantly reduced. The addition of 2.5 wt% of Sb, on the contrary, does not prevent the accumulation of Po at the Pb surface.

The effect of Po accumulation at the surface of Pb-Sn alloys, used as solder in microelectronics, is a well-known problem in the semiconductor industry. Here, radiation of ^{210}Po may induce soft errors in computer memory chips [201, 202]. Standard procedures for the monitoring of the Pb α -activity have been proposed in [203, 204]. Increase in background count rates detected by a high purity germanium gamma detector were also attributed to ^{210}Po accumulation in solder bumps of the measuring electronics [205].

All these effects were found to occur at Po activity concentrations as low as 10^{-3} Bq/g Pb, i.e. for Pb that is usually available on the market without any restrictions. As a consequence of these enrichment effects, in laboratories performing low-level activity measurements, very old Pb, where the ^{210}Pb isotope has significantly decayed, is used for shielding purposes. These materials are provided from old leaden roofing sheets and from Pb ingots recovered from ancient sunken ships. These materials show significantly lower α -background rates than Pb provided from metal refineries nowadays.

IV.1.3.3 Investigations on polonium in bismuth

Studies on the distribution of Po in Bi metal have been published in the early 1930ies. Bi containing 5% of Pb has been exposed to radium emanation salt to accumulate a certain amount of decay products, such as ^{210}Pb , ^{210}Bi and ^{210}Po [176]. Investigations on these samples using a nuclear tracking method (autoradiography) showed that Po tends to concentrate at the grain boundaries. At the grain boundary perpendicular to the direction of crystal growth, a pronounced blackening of the photographic film due to emission of α -particles was observed. It was further found that Po not only diffuses to grain boundaries and sample surfaces, but also shows an inhomogeneous distribution within the bulk of the sample. The concentration was found to vary periodically, where the periodicity was dependent on the crystal growth speed. Such effects were already observed earlier for Bi single crystals, where Po was found to segregate into small regions with nearly regular spacing [206].

Some small-scale experiments on the diffusion of ^{210}Po through Bi were performed at the Mound laboratory in 1950. A declassified report [207] describes the measurement of the Po diffusion coefficient in different materials, including Bi. At 150 and 200 °C, a value on the order of $10^{-11} - 10^{-10}$ cm²/s was found although the data is poorly reliable due to cracks and holes in the used Bi foils.

IV.1.3.4 Investigations on polonium in LBE

The behaviour of Po in LBE did not receive any attention in the past except in the last 10 years. A study on the distribution of Po in neutron irradiated LBE has been recently reported in [208]. Within this study, a computer-aided Monte-Carlo method was applied to analyse a α -spectrum recorded from a LBE sample to determine the distribution of Po as function of depth. The spectrum revealed one sharp peak appearing at 5.3 MeV and a broad one at 4.9 MeV. It was calculated that in the analysed LBE sample, Po is enriched at the surface and in a narrow region between 1 – 2 μm below the sample surface, whereas its concentration in the bulk was found to be rather uniform. The method presented in this paper nevertheless suffers from large uncertainty and poor resolution. No explanation is given for the appearance of two distinct enrichment regions of Po in the analysed sample.

A recent report on the segregation phenomenon of ^{210}Po in irradiated LBE has been published in [56, 162]. The kinetics of migration of Po to the surface of a solidified LBE sample was studied by means of α spectroscopy. One sample of LBE containing ^{210}Po was homogenized by melting at 600 °C in a H_2 stream and put into an α chamber directly after solidification. Spectra were recorded for 12 days using a batch routine. The result of this measurements revealed that for irradiated solid LBE, there is a pronounced increase in α activity with time. Similar to [208], the analysis was performed with data originating from one single sample and no repetition measurements have been performed. However, similar samples were successively etched with HNO_3 solution to measure the depth distribution of Po. Here, it was found that a 10-fold enrichment of ^{210}Po in a region of about 20 μm below the surface of the LBE sample occurs [166].

Summarizing, the Po segregation phenomenon in metals and alloys based on Pb and Bi has gained more scientific interest in the last 20 years, and the number of publications dealing with this effect is rising. Nevertheless, the amount of available scientific investigations that quantitatively describe the Po enrichment process or provide reliable data for diffusion coefficients is rather scarce. Up to now, still no investigation exists that would have carefully deduced physical functions describing the segregation of Po in solid Pb, Bi or their eutectic alloy. Although some quantitative data on Po diffusion in Pb and Bi was reported, their extrapolation to the eutectic binary mixture is not straightforwardly possible. However, the knowledge on the diffusion coefficient of Po in solid LBE is of importance to evaluate possible safety issues related to surface segregation and sputtering occurring in this material.

To overcome this lack of data, at first the diffusion coefficient of Po in LBE and polycrystalline Pb and Bi was measured at different temperatures within this work. With the obtained data, the temperature-dependant relationship according to equation (8) was deduced. As a second step, the kinetics of the Po segregation process occurring at the surface of LBE samples was studied by means of α -spectroscopy and by the sectioning technique. Here, the data obtained for the diffusion of Po in LBE served as reference for the deduction of parameters critical for the segregation phenomenon.

IV.2 Experimental

IV.2.1 Impurities in LBE

Two different LBE batches were used for the current investigation. LBE of batch number 03A124 was purchased in 2003 from Impag AG, Switzerland. Another batch of LBE was delivered by Compumet AG, Switzerland, in June 2005 and had the number 05B124. In Table 16 the concentration of impurity elements determined by ICP-OES are given. For comparison, data for another batch of LBE with the designation 05BI56PB44C1 is also given in the table. This LBE was used in the MEGAPIE experiment performed at PSI in 2006, the supplier being also Compumet AG. Further details on the analysis method can be found in section II.3.3.

Table 16: Impurity concentration in LBE of different batches; values denoted by “<” were below the quantification limit of the ICP-OE spectrometer.

impurity	impurity concentration [mass ppm] in LBE batch		
	03A124	05B124	05BI56PB44C1
Ag	5 ± 1	7 ± 1	24 ± 1
Al	4 ± 1	3 ± 1	<
Ca	<	<	22 ± 3
Cd	<	1 ± 1	1 ± 1
Cu	1 ± 1	2 ± 1	23 ± 1
In	<	29 ± 1	<
Na	5 ± 1	3 ± 1	3 ± 1
Ni	<	3 ± 1	<
Sn	82 ± 2	129 ± 3	15 ± 1

In Table 25 in the Appendix, an overview on the cylindrical LBE samples used for diffusion and segregation studies performed during this work is given. All samples had a diameter of 7 mm and were produced in the same procedure as described below. Their respective height was calculated from the masses given in Table 25.

IV.2.2 Sample preparation

IV.2.2.1 Preparation of cylindrical metallic samples

A glass tube ($L = 30$ cm, $r = 0.35$ cm), closed at one end, was placed in a vertical furnace heated to 500 °C. During the heating procedure, the glass tube was connected to a nitrogen-vacuum line. The tube was evacuated to 10^{-2} mbar and flushed with N_2 several times to remove any oxygen or moisture. A schematic layout of this experimental setup is shown in Figure 39.

Approximately 100 g of inactive Pb (Sigma-Aldrich, 6N purity), Bi (Fluka, 99,995% purity) or LBE (for the impurity content, see section IV.2.1), respectively, was heated in a stainless steel beaker under a N_2 atmosphere to 400 °C (for Pb or Bi) or 250 °C (for LBE). The liquid metal was then quickly poured into the glass tube. A small glass pipette, connected to the N_2 gas supply, was placed above the glass tube in such a way, that during the transfer procedure a continuous flow of N_2 minimized oxidation of the liquid metal. At the end of the pouring procedure, the pipette was removed and the open end of the glass tube was reconnected to the N_2 -vacuum manifold. By applying a vacuum of 10^{-2} mbar, the liquid metal was outgassed. During this process, gas bubbles penetrate the metal/gas interface. The degassing procedure was stopped when no gas bubble formation was observed anymore.

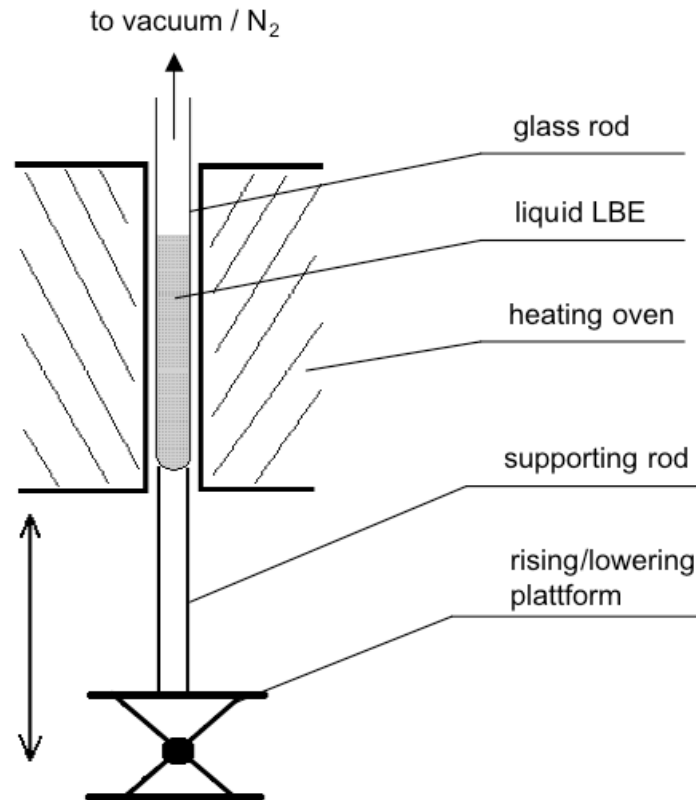


Figure 39: Experimental setup for the preparation of cylindrical metal samples

At the end of the degassing procedure, the glass tube with the liquid metal was slowly lowered out of the furnace with a velocity of 5 mm/min using a rising/lowering platform as shown in Figure 39. This ensures a homogeneous crystallization of the metal from bottom to top and prevents the formation of any voids. After cooling down, the glass tube was put into a vessel filled with liquid N₂ for a short time. Due to different thermal expansion coefficients of glass and the metals, it was possible to separate the metal from the glass by simply mechanically cracking the glass in its middle part after removing it from the liquid N₂ bath. After this, both ends of the glass tube were slipped over the metal rod without producing additional mechanical stresses within the solidified metal. In such a way, a homogeneous 25-30 cm long, shiny metallic rod with no visual signs of oxidation was produced.

All of the following procedures were performed under ambient air. The metallic rod was cut to 10 mm long cylinders using a saw. By this procedure, up to 25 cylinders are obtained from one rod. Both front sides of each cylinder were then cut by a microtome to give a flat surface with a mirror-like appearance. This procedure is described below in section IV.2.3.1. After flattening the top and bottom surfaces, the cylinders were weighted, placed in a plastic capsule and enumerated. Before the experiments, the samples were annealed in a resistance oven for at least 48 h at the temperature the following diffusion or segregation experiment was to be performed at. LBE samples were annealed at 50, 80 or 110°C, Pb and Bi samples at 50, 100, 150 and 200 °C.

All samples produced with the procedure described above have been used for one of two different types of experiments. For the measurement of the diffusion coefficient of Po in Pb, Bi and LBE, ²¹⁰Po has been deposited on the top surface of previously inactive samples. Subsequently, the decrease in surface activity was measured as function of time and temperature. For these experiments, samples of Pb (L14 and L16 – L22), Bi (B12 – B19) and LBE (z12 – z20) have been used. In Table 25 and Table 26 in the Appendix the mass, height and anneal temperature is given for every sample used.

Another set of experiments involved the measurement on the Po migration towards surfaces in solid

LBE samples. In order to provide an initial homogeneous Po distribution, previously inactive samples were irradiated with neutrons to provide a uniform Po build-up in the bulk. For these experiments, LBE samples z01-z09, z21 and z30 - z54 have been used. Their irradiation history and ^{210}Po activity concentration is given in Table 25 in the Appendix.

IV.2.2.2 Sample preparation for diffusion studies

Po was deposited on the top surface of the cylinders from a 1M HNO_3 stock solution containing 1.9 kBq/ml ^{210}Po . Using an Eppendorf pipette, a droplet with a volume of 100 μl of the solution was placed on the top surface of each cylinder. The time for the spontaneous deposition of Po on the metallic surfaces was 30 minutes. Subsequently, the solution was sucked from the sample and the daytime was noted. The top surface was then rinsed twice with distilled water and the surface activity deposited on each sample was measured via α spectrometry.

After the measurement, sets of two cylinders were positioned to each other in such a way that the radioactive top surfaces were oriented face to face. This pile, containing two samples, was subsequently wrapped in aluminium foil and placed inside 10 cm long steel tubes and closed by a Swagelok connection. A steel valve capable to sustain temperatures up to 400 °C was used to evacuate the steel tube and to fill it with N_2 in order to avoid any sample oxidation during anneal. All samples were then placed inside a resistance furnace set to the temperature desired for the thermal diffusion experiment. For LBE samples, temperatures used were 50, 80 and 110 °C, whereas for Pb and Bi, 50, 100, 150 and 200 °C were maintained. The relative uncertainty for the temperature measurement was in the order of 2% of absolute temperature.

The cylinders were taken out of the furnace after 24 ± 1 h and immediately measured via α spectroscopy to determine the residual surface activity. After measurement, each set of samples was again put into the steel tubes, which was filled with N_2 and placed into the furnace. For Pb, Bi and LBE samples, the Po diffusion experiment lasted for 8, 9 and 16 days, respectively.

IV.2.2.3 Sample preparation for segregation studies

Segregation of Po was only investigated for LBE samples. After annealing, a batch of samples was irradiated at the PSI NAA neutron activation facility for 0.5 and 1 h at a flux of $5 \times 10^{13} \text{ n*cm}^{-2}\text{s}^{-1}$. The samples were stored for at least one month to allow a proper decay of the intermediate neutron activation product ^{210}Bi . After irradiation, the samples were used without any further treatment.

Similar to the procedure described for diffusion studies, the segregation of Po was also investigated at different temperatures and for different LBE batches. For this purpose, cylindrical irradiated LBE samples of batch number 03A124 (samples z1- z9, see Table 25 in the Appendix) and 05B124 (z22 – z27) were placed in pairs inside 10 cm long steel tubes, which then were closed, evacuated and filled with N_2 using a vacuum manifold. The tubes were then placed inside three different resistance ovens kept at 50, 80 and 110 °C, respectively. Four samples were left under a N_2 atmosphere at room temperature. After 3, 5, 7 etc. days, the samples are taken out and their top and bottom surface activity was measured via α spectrometry as described below.

IV.2.3 Analysis techniques

In the course of this investigation, two measurement techniques were involved to study the mobility of Po. A non-destructive method involved the measurement of the surface activity via α spectrometry. Additionally, the distribution of Po inside the sample was determined by sectioning using a microtome. Statistical errors of the measurement equipment used in experiments involving diffusion and segregation are given in Table 17.

Table 17: Relative statistical errors of measurement for scientific equipment used in the experimental investigations

device	relative statistical error	note
microtome, Leica RM2235	20% 4%	1 μm slices 10 μm slices
balance, Mettler Toledo	10%	absolute error: ± 0.1 mg
liquid scintillation counter, PerkinElmer 3110TR	1%	measurement time ≥ 15 min for an α activity of ≥ 10 Bq
α spectrometer, Canberra	1% 2%	without sample position change with sample position change

IV.2.3.1 Microtome sectioning of the samples

To allow for a careful measurement of diffusion and segregation phenomena, precise depth profiling of the Po concentration had to be performed. A rotational microtome RM2235 delivered by Leica, Germany, allowed sample sectioning of varying thickness down to 1 μm .

Cylindrical Pb, Bi or LBE samples were mechanically fixed in a moving piston. By rotation of a handling wheel, the piston could be moved vertically above a non-movable cutting blade. Hardened steel or a tungsten carbide knife was used for sample sectioning. With each stroke of the handling wheel, the sample was forced to glide over the blade subsequently cutting a thin metallic slice. The driving mechanism of the microtome allows the piston to be moved forward by 1 – 50 μm after each cut. In such a way, a desired number of layers with defined thickness could be obtained and collected for further analysis.

Initially it was intended to analyse diffusion and segregation of Po in a sample first by a non-destructive method, i.e. by α spectroscopy, and at the end of the experiment by microtome cutting with subsequent scintillation counting. Despite substantial effort, it was not possible to solve the problem of sample orientation relative to the cutting blade during microtome sectioning. As it is of inherent importance to achieve equidistant slicing perpendicular to the sample surface, any slight deviation of the sample position would result in substantial error regarding slice thickness and shape. It was not possible within this work to ensure reliable sectioning of samples that were used for thermal diffusion experiments. As a result, the microtome cutting technique was only applied to LBE samples containing Po from neutron irradiation, since these samples remained fixed in the microtome during the whole experiment.

The evolution of Po in the surface region of a cylindrical LBE sample was measured according to the following procedure. A set of ten 1 μm thin slices is sectioned with a microtome from a neutron activated LBE sample after different storage times under ambient conditions. At the beginning of the experiment, the surface region is flattened to ensure a homogeneous initial Po distribution. Then, sets of ten 1- μm slices were cut after 2, 19, 53, 128 and 237 h from the last microtome sectioning. The sample remained in the piston of the microtome during the whole course of the experiment. The cut slices were then weighted and analysed by liquid scintillation counting.

IV.2.3.2 Liquid scintillation counting

Each sectioned slice of the neutron activated LBE cylinder was transferred in a single LSC vial and 100 μL of 7M HNO_3 were added. After the sample dissolved, 1 ml of distilled water and 14 ml of scintillation cocktail were subsequently added. The vial was then shaken for homogenization and measured via liquid scintillation counting. Details on the liquid scintillation counting method are given in section III.2.5.1.

IV.2.3.3 α spectrometry

α spectra were recorded by four silicon PIPS detectors provided by Canberra, USA. All detectors were connected to appropriate signal processing hardware and the Genie2000 software, Canberra, USA, was used for the analysis of recorded α -spectra. Energy calibration was performed by using a certificated reference source containing a mixture of ^{241}Am , ^{239}Pu and ^{244}Cm . The efficiency calibration was done with the aid of a computer program called SOLANG [209] developed for efficiency calculation purposes.

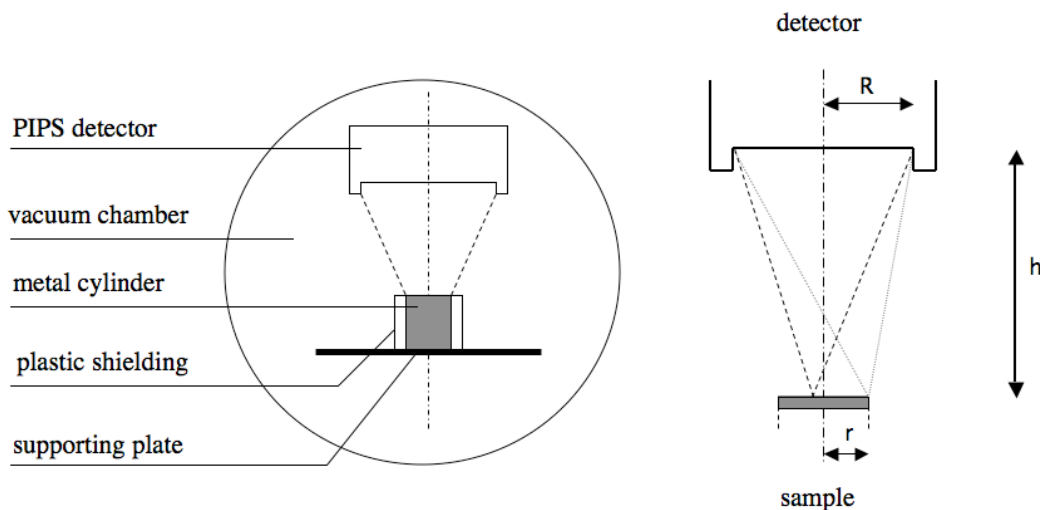


Figure 40: Measurement geometry used for α spectroscopy

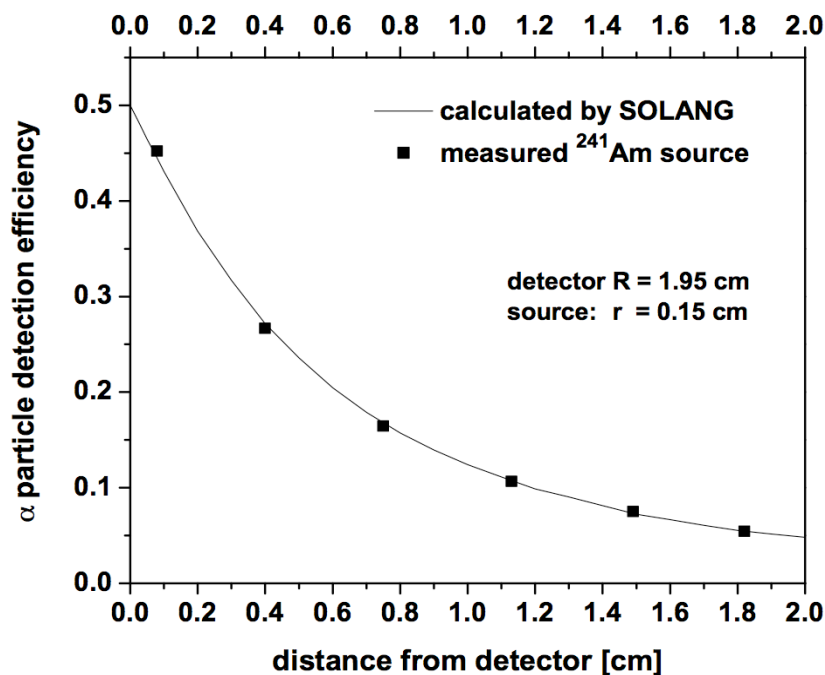


Figure 41: A comparison between calculated and measured α particle detection efficiency (4π geometry) for PIPS-detectors used in this study; calculations were done using the computer program SOLANG [209], a 255 Bq ^{241}Am source served for comparative measurements.

The detector area of each PIPS detector was 300 mm^2 , resulting in a diameter of 19.5 mm. In all experiments of this study, the samples had a diameter of 7.0 mm and a height corresponding to data

given in Table 25 in the Appendix. A graphical representation of the measurement geometry is shown in Figure 40. The resulting geometrical efficiency was calculated via SOLANG and verified experimentally by using a ^{241}Am standard α calibration source, which had a specific activity of 263 Bq on the 21.09.1993, and a diameter of the active spot of 3 mm. Measurement of this source at different distances to the silicon PIPS detectors gave decreasing count rates with increasing detector to source distance. The result is given in Figure 41. The experimentally determined efficiency coincides well with values predicted by theory.

With the described setup, the total rate of α particles emitted from the top sample surface could be measured. Since the ^{210}Po α -energy is 5.3 MeV (see Table 2 in section 1.6.3), counts appearing in the region below 5.3 MeV were summed up in order to obtain the total surface activity of the samples. Surface activity here refers to the count rate of α particles that are emitted on and below the sample surface and reach the α detector. The low energy part of the spectrum (0 – 1.5 MeV) was cut off because artefacts were observed in this region, probably caused by electronic noise and some β activity emitted by the measured sample. The measurement time was chosen to be sufficiently large to assure proper counting statistics in the mentioned counting region.

Background measurements were performed for every detector on a weekly basis to correct for signals originating from sputtered contamination present in the measurement chambers. Background spectra were recorded for 100h and the background for each detector was found to have sufficiently low count rate to have a significant influence on sample measurements.

Cylindrical samples of Pb, Bi and LBE, where Po was deposited at the surface, were measured with the following procedure. Directly after Po deposition or in any following measurement, a set of four samples was transferred into the α -measuring chambers and α spectra were recorded during 1 h for each sample under a pressure of 10^{-1} mbar. The sample position relative to the detector was maintained identical for every subsequent measurement to ensure the same geometrical detection efficiency for α particles emitted from the measured sample. Every sample was measured in the same α chamber used before.

Neutron activated LBE cylinders were measured by α spectroscopy to investigate the kinetics of Po segregation. After being pre-sectioned with the microtome, the cylinders with shielded lateral surfaces were directly transferred to the α -measuring chambers. Plastic tubes with an inner diameter of 7 mm ensured shielding of the lateral surfaces. Each chamber was evacuated to 10^{-1} mbar and spectra were recorded for 1 hour for each sample. The samples were left in the α -chambers and hourly spectra were recorded continuously during a desired period using a batch routine.

IV.2.4 Theoretical considerations

The amount of α particles, which leave the sample surface and can be detected by various detection methods, may be calculated by knowing the mean free path of α particles in a Pb-Bi matrix. This value, known also as penetration range, is calculated by the Bethe-Bloch equation describing the energy loss of a charged particle per travelled path length of a known material. In particle physics, the equation is used for describing the stopping power of different matrix materials for protons, electrons, α particles etc. At non-relativistic conditions, the formula is given by equation (9):

$$-\frac{dE}{dx} = \frac{4\pi n z^2}{m_e v^2} \left(\frac{e^2}{4\pi\epsilon_0} \right)^2 \left[\ln \left(\frac{2m_e v^2}{I} \right) \right], \quad (9)$$

where the parameters are:

- E – energy of the particle
- x – distance travelled by the particle
- v – velocity of the particle
- z - particle charge

- c – speed of light
- e – electron charge
- m_e – electron rest mass
- ϵ_0 – vacuum permittivity
- n – electron density of the target
- I – mean excitation potential of the target.

With $E = 5.3$ MeV and $z = 2$ for α particles emitted by the decay of ^{210}Po , and for LBE, where both metals have fairly similar properties, $I = 2$ eV and $n = 3.8 \times 10^{27}$ electrons/cm³, the maximum range R is calculated to be $14.6 \mu\text{m}$.

Another approach is the usage of computer programs for calculating the stopping range of particles in matter. A range of α particles in LBE of $16.1 \mu\text{m}$ was calculated with the SRIM program [210]. A literature review on the stopping range of α particles from ^{210}Po in LBE revealed that authors in [208] indicate the value to be $R = 12.6 \mu\text{m}$. In Pb, a value of $10.6 \mu\text{m}$ has been reported [79], which, however, seems to be too low. For the following calculations, the α particle range R will be assumed to be about $15 \mu\text{m}$, which represents an average value of the available data.

Let the activity of Po per unit volume be A_v and let the activity be homogeneously distributed throughout the whole sample. Then, the number of α particles leaving the sample surface may be calculated when the stopping range R is known. It is clear, that no α particles will penetrate from any region below the surface deeper than R . From a given surface layer, the number of α particles isotropically emitted to the surrounding will increase the nearer the decay occurs to the surface. At a distance R , the fraction of α particles leaving the sample is zero, while at the sample surface it is $\frac{1}{2}$. Figure 42 illustrates this circumstance.

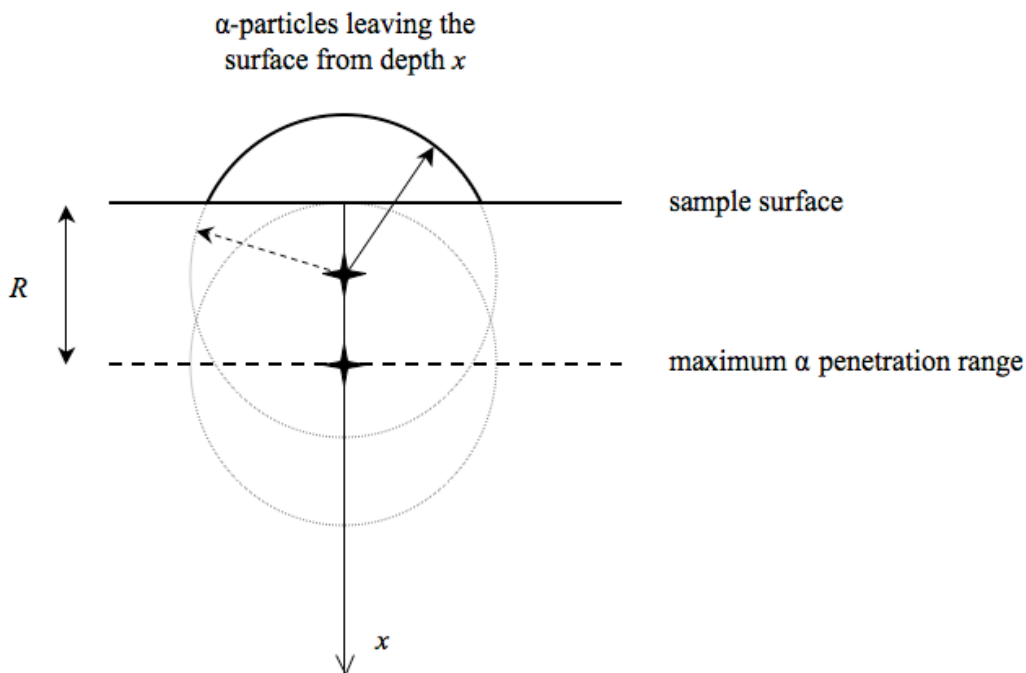


Figure 42: Schematic view on the penetration ranges of α particles emitted from different locations below the sample surface

The part of α particles leaving the sample is represented by a spherical cap, whose area is described by the solid angle of a circle with the radius R lying above the sample surface. The ratio between the area of the cap and $4\pi R^2$ is the fraction of α particles leaving the sample surface from a depth x . By integrating over the whole path $0 < x < R$ one obtains:

$$\int_0^R \frac{2\pi R(R-x)}{4\pi R^2} dx = \int_0^R \frac{R-x}{2R} dx = \frac{R}{4}. \quad (10)$$

The result of the above calculation indicates, that only a fraction of $\frac{1}{4}$ of all α decays occurring in the surface region with a depth $z < R$ will leave the sample surface and may be detected by physical means. Thus, knowing the total activity of the sample per unit volume, the surface activity A_s , i.e. the observable activity per unit area, may be described by

$$A_s = \frac{A_v R}{4}. \quad (11)$$

The surface activity or “visible” α activity of a given sample may be calculated by equation (11) if the activity concentration and the range of α particles in the host material are known. Thus, for a spherical LBE sample with a volume of 1 cm^3 , only a fraction of 1.8×10^{-3} of all ^{210}Po decays may be observed by particle detection methods. Equation (11), however, only applies when the activity is distributed homogeneously within the sample. Let us now consider two cases, where this condition is not given.

IV.2.5 Data analysis

IV.2.5.1 Diffusion of a thin substance film into a semi-infinite medium

A radioactive substance is deposited as an infinitesimal thin layer on a plane surface. If its resulting surface activity is A_s , then the volume activity A_v at a perpendicular depth x from the plane source as function of anneal time t is described by the following equation:

$$A_v = \frac{A_s}{\sqrt{\pi Dt}} e^{-\frac{x^2}{4Dt}}. \quad (12)$$

This equation represents a solution of Fick's second law for a plane source diffusing into a semi-infinite medium according to [173]. The boundary conditions are defined as follows: at $t = 0$, the surface activity of the substance is A_s at $x = 0$, and zero elsewhere. The diffusion coefficient D should be independent from solute concentration and the bulk should be an isotropic medium. Certainly, using equation (12) to describe Po diffusion into a cylinder would represent an approximation since the cylinder geometry is of finite dimensions. Nevertheless, equation (12) still may be used without introducing significant error if the cylinder height is greater than $4\sqrt{Dt}$ [171], which, as will be shown in the result section, is a condition that is met in every experiment performed.

In a diffusion experiment, let the count rate of resulting from Po decay at $t = 0$, i.e. at the beginning of the experiment, be $A_{s,0}$, and for time t it is $A_{s,t}$. The measured count rate $A_{s,t}$ would only depend upon the number of α particles that have diffused into the bulk not deeper than by R , which is their maximum penetration range. Then, the ratio between measured and initial count rate $A_{s,t}/A_{s,0}$ may be calculated according to [211]:

$$\frac{A_{s,t}}{A_{s,0}} = \int_0^R \frac{1}{\sqrt{\pi Dt}} e^{-\frac{x^2}{4Dt}} dx. \quad (13)$$

This equation holds true if one assumes that all α particles are emitted only perpendicular to the surface of the sample. As in reality α particles are emitted in all directions with equal probability as shown by Figure 42, the integrand of equation (13) should be multiplied with $(1-x/R)$ to correct for this effect. After integration, one obtains

$$\frac{A_{s,t}}{A_{s,0}} = \operatorname{erf}(\xi) - \frac{1}{\xi\sqrt{\pi}}(1 - e^{-\xi^2}), \quad (14)$$

where a substitution is made according to

$$\xi = \frac{R}{2\sqrt{Dt}} \quad (15)$$

and

$$\operatorname{erf}(\xi) = \frac{2}{\sqrt{\pi}} \int_0^{\xi} e^{-x^2} dx, \quad (16)$$

which represents the Gaussian error function [211]. For the determination of the diffusion coefficient at different temperatures, the measured count rate ratio $A_{s,t}/A_{s,0}$ is plotted against the time t . Then, the value of D , which is best fitting the plotted data, is determined iteratively by comparing with the predicted function calculated by equation (14).

IV.2.5.2 The simplified segregation model of Lea and Seah

Assuming no interaction between the individual segregating atoms, the transfer rate of an atom from a near surface layer to the surface will be independent of the surface concentration of these segregating atoms. In fact, it is possible to remove these atoms from the surface as soon as they arrive on the surface without having any influence on the rate of arrival of the subsequent atoms [175]. Mathematically speaking, the surface concentration is kept at a zero value for all time $t > 0$. The concentration of the segregating species should be constant at time $t = 0$ for all x [175], where x is the depth from the sample surface (see Figure 42). The solution of Fick's second law applying these boundary conditions will be:

$$C(x,t) = C_{bulk} \operatorname{erf}\left(\frac{x}{2\sqrt{Dt}}\right), \quad (17)$$

where C_{bulk} represents the bulk concentration of the segregating species for $t = 0$ and $x \rightarrow \infty$. To obtain a proper description for the surface accumulation of the segregating species at the surface, the total flux of atoms moving through $x = 0$ in a certain time t is of interest. The flux of atoms moving through $x = 0$ is given by

$$\left(D \frac{dC}{dx}\right)_{x=0} = \frac{DC_{bulk}}{\sqrt{\pi Dt}}. \quad (18)$$

To obtain the total amount of atoms M_t moving through an area F at $x = 0$ in time t , equation (18) is integrated and one may write

$$M_t = 2FC_{bulk} \sqrt{\frac{Dt}{\pi}}. \quad (19)$$

The surface concentration, i.e. the concentration of a segregated layer in a certain thickness d is given by

$$C_s = \frac{2FC_{bulk}\sqrt{\frac{Dt}{\pi}}}{Fd} \quad (20)$$

Since concentration and activity of a radioactive substance are directly proportional, it is possible to write $A_{s,t}$ and $A_{s,0}$ instead of C_s and C_{bulk} . Here $A_{s,t}$ is the surface activity of the sample at time t and $A_{s,0}$ represents its initial surface activity, derived from the bulk concentration as given by equation (11). Since the flux of atoms is independent from the surface concentration, we can add any starting value to the above expression. As the surface activity at $t=0$ is not zero, but $A_{s,0}$, one obtains

$$A_{s,t} = A_{s,0} \left[1 + \frac{2}{d} \sqrt{\frac{Dt}{\pi}} \right], \quad (21)$$

where D represents the diffusion coefficient as described by the first and second Fick's laws. The value d is a certain thickness below the surface in that $A_{s,t}$ is measured. It is defined by the boundary condition of the performed segregation experiment. For example, in experiments with microtome slicing, $A_{s,t}$ is determined by liquid scintillation counting of the Po activity present in the first sectioned layer of thickness d . For measurements with α spectrometry, the value of d is given by the maximum α penetration range that was already discussed in section IV.2.4. By plotting the increase in measured count rate $A_{s,t}/A_{s,0}$ against \sqrt{t} , one should obtain a straight line with the slope of $\frac{2}{d} \sqrt{\frac{D}{\pi}}$, from which the diffusion coefficient may be easily calculated.

As can be seen, the knowledge of the initial count rate $A_{s,0}$ is important for a careful deduction of the diffusion coefficient. The determination of $A_{s,0}$ may be performed by different ways. At first, the measurement of the count rate $A_{s,t}$ may be extrapolated to zero time, i.e. to the start of the segregation experiment. Another approach is the measurement of the bulk activity via liquid scintillation counting and, knowing the geometrical efficiency, subsequently applying equation (11) to determine the net counts registered by the detector in a certain time. Finally, an approximation may be made by extrapolating the counts recorded in the low-energy regions of the α -spectrum towards the high-energy region up to 5.3 MeV.

The segregation model presented above, however, does have a substantial drawback since it predicts the surface activity $A_{s,t}$ to become infinite at $t \rightarrow \infty$, which is physically not possible. Many segregation experiments have indicated that there is a certain maximum saturation concentration that is reached if the experiment time is long enough [175]. The mathematical description of segregation taking into account the surface saturation has been given by Lea and Seah [212]. For the description of the underlying process of Po segregation to LBE sample surfaces, the simplified model presented above, however, may also be applied with sufficient precision if the segregation time t is low. This condition is still met when linearity of the $A_{s,t}(\sqrt{t})$ - function is maintained. Thus, it has to be verified after each experiment if the model presented above is applicable for data analysis or more sophisticated models have to be used. A detailed description for the analytical treatment of segregation data may be found in [174, 187].

IV.3 Results and discussion

IV.3.1 Diffusion studies

In the following, the results on the diffusion experiments performed with ^{210}Po deposited on inactive cylinders of Pb, Bi and LBE are presented. The relative decrease of the Po surface activity for polycrystalline Pb with increasing anneal time at different temperatures measured by α spectrometry is given in Figure 43. For this and all the following graphs, all data points were corrected for the ^{210}Po decay during the experiment. Solid lines represent least-square fits according to equation (14). As can be seen in Figure 43, the model presented in section IV.2.5.1 represents a good fit for the measured data points. Longer anneal times result in a successive decrease in surface activity relative to the initial value due to diffusion of Po into the Pb matrix. As expected, higher temperatures accelerate the diffusion process, resulting in sharper activity decrease with higher temperatures. The deduced diffusion coefficients are presented in Table 18. In the temperature range between 50 and 200 °C, an increase of D by two orders of magnitude was measured for Pb.

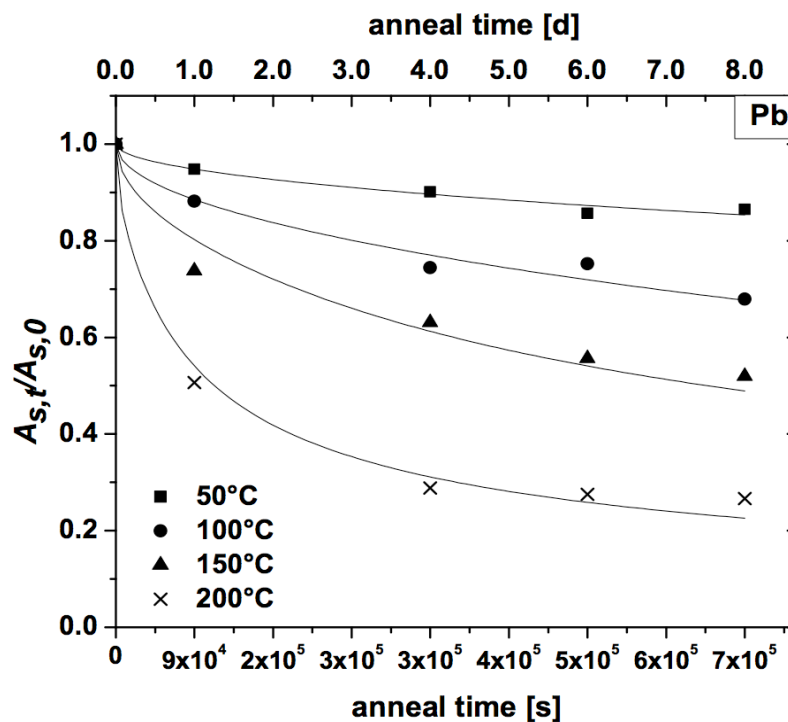


Figure 43: The decrease in surface activity by diffusion of deposited ^{210}Po into polycrystalline Pb as function of temperature and anneal time; solid lines represent least square fits according to equation (14).

Similarly, the diffusion coefficient in polycrystalline Bi was deduced for the same temperatures as for Pb. The results and calculated fitting functions are given in Figure 44. The calculated fit for data obtained at 100° C is given as a dotted line. It should denote that for the measurement at this temperature, the scattering of the data was very large due to unknown reasons. The Po diffusion coefficient in Bi at 50 °C is additionally subjected to a large uncertainty since the relative change in surface activity at this temperature was only 3 times higher than the statistical error of the measurement, which was determined to be 2%. The calculated lines still represent appreciable good fits although data is subjected to a larger scattering if compared to data obtained for Pb.

The measured decrease of surface activity with time at 50, 80 and 110 °C for LBE is shown in Figure 45. Compared to Pb and Bi, there is an increased mobility of Po observable. Consequently, higher diffusion coefficients are derived for Po in LBE compared to those in Pb and Bi. The model given in by equation (14) also represents a good fit for the measured values for the Po-LBE system, as indicated in Figure 45. It should be nevertheless stated that the model shows some systematic discrepancy for

all investigated systems at elevated temperatures. Here, it underestimates the decrease in activity for short diffusion times and vice versa. Such behaviour could be explained by Po losses due to evaporation at the start of each diffusion experiment.

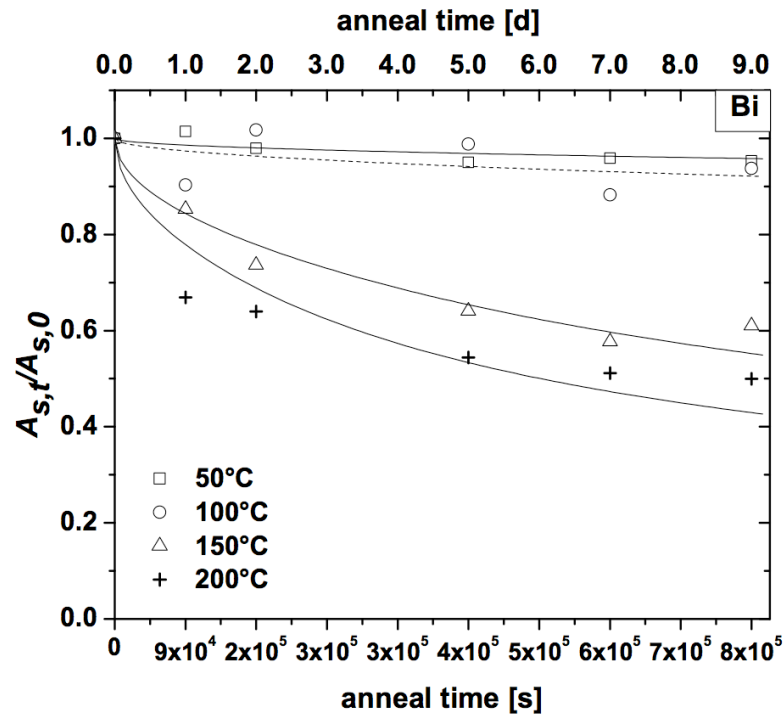


Figure 44: The decrease in surface activity by diffusion of deposited ^{210}Po into polycrystalline Bi as function of temperature and anneal time

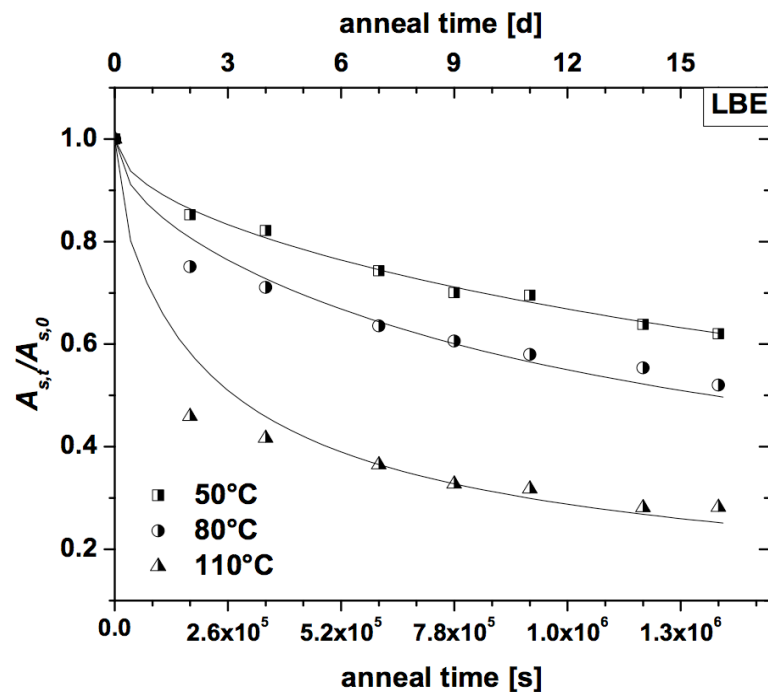


Figure 45: The decrease in surface activity by diffusion of deposited ^{210}Po into LBE as function of temperature and anneal time

As indicated in Table 18, the diffusion of Po in the temperature range between 50 and 100 °C is slowest in Bi. The calculated values for D indicate that Po diffuses 10 times faster in Pb, whereas in LBE there is again a 4-fold increase compared to solid Pb. The measured values of D are subjected to

uncertainties in the order of 50%. To deduce the activation energy E_A and the standard diffusion coefficient D_0 according to equation (8), an Arrhenius plot is given in Figure 46 that shows the dependence of $\log D$ with $1/T$ based on data given in Table 18. For comparison, data on the thermal diffusion coefficient of Po in polycrystalline Pb determined by [79] and [195] as well for Bi [207] is also given in the figure.

Table 18: Measured diffusion coefficients for Pb, Bi and LBE at different annealing temperatures.

temperature [K]	diffusion coefficient [cm ² /s] for		
	Pb	Bi	LBE
323	5.5×10^{-14}	5.0×10^{-15}	1.9×10^{-13}
353	/	/	3.8×10^{-13}
373	2.7×10^{-13}	1.4×10^{-14}	/
383	/	/	1.9×10^{-12}
423	8.0×10^{-13}	5.0×10^{-13}	/
473	4.8×10^{-12}	1×10^{-12}	/

As can be seen in Figure 46, there is a reasonably good agreement between data on Po diffusion in polycrystalline Pb deduced in this study and data reported both in [79] and [195]. For Po diffusion in polycrystalline Bi, however, the correlation with data reported in [207] is poor. In the temperature interval between 150 and 200 °C, a deviation of the diffusion coefficient of nearly three orders of magnitude is observed. This circumstance can certainly be explained by the poor reliability of the data reported in [207] and the large uncertainty of the measurements performed in the present investigation.

Additionally, data given in Table 18 indicate that for annealing times as high as 1.4×10^6 s (16 days), the mean penetration depth of Po atoms into the sample surface, \sqrt{Dt} , is in the order of 30 μm for Pb at 473 K. Thus, the required condition discussed in section IV.2.5.1 for the sample height to be larger than $4\sqrt{Dt}$ holds true for every performed measurement.

By comparing measured data for Pb, Bi and LBE, it may be seen that the dependence of the Po diffusion coefficient on temperature does not significantly alter between the investigated metals since the slopes of the lines representing least square fits are approximately similar. This indicates that the activation energy E_A for the diffusion process in these materials is comparable. Nevertheless, there is a difference by two orders of magnitude in the measured diffusion coefficients of Po when comparing the three matrices Pb, Bi and LBE. In the temperature range between 50 and 100 °C, the Po mobility in the host materials raises with the sequence $\text{Bi} < \text{Pb} < \text{LBE}$. The fact that diffusion in LBE is fastest may be explained by the low melting point of LBE. As may be seen in Figure 36, the diffusion coefficient linearly rises with the fraction T/T_m . Thus, the diffusion coefficient in metals with a low melting point should show a higher diffusion coefficient at a certain temperature if compared to higher melting metals. This is indeed the case for LBE if compared to Pb and Bi.

It should be nevertheless pointed out that neither Bi nor LBE are fcc metals. Bi is crystallizing in a rhombohedral structure, whereas the case for LBE is even more complicated. As already discussed in section I.6.1, LBE is an alloy consisting of two single phases, namely Bi and Pb_7Bi_3 , a compound with a hexagonal lattice. Thus, strictly speaking, the relationship given in Figure 36 does not apply to these materials and the nature of Po diffusion in Bi and LBE may significantly differ from that in Pb.

By consulting Figure 36 for the deduced value of the diffusion coefficient of Po in Pb, it is possible to derive which type of diffusion is present in this system. From the calculated value of approx. 10^{-18} m²/s (see Table 19 below) at room temperature ($T_m/T \approx 2$), it is concluded that bulk diffusion predominates. This is in agreement with literature data, where diffusion coefficients deduced for polycrystalline Pb are similar to those measured in Pb single crystals [181]. Due to similarities in physical properties between

Pb and Bi, it is reasonable to assume that the same diffusion type is present in Bi and LBE. Due to lack of literature data, however, this assumption may not be proven.

Comparing the values of the diffusion coefficient of Po in Pb at room temperature with data for other elements given in Table 15, it is evident that many solutes have a higher mobility in solid Pb than Po. For example, noble elements such as Au, Ag or Pt as well as Co or Ni show 10 to 1000 times higher room temperature diffusivity in Pb. For the mobility of Cu in Pb, the diffusion coefficient was reported to be even 5 orders of magnitude larger than that of Po. Still, the mobility of Po atoms is 10^5 times larger than that of Pb atoms itself as indicated by Table 15. Summarizing, the diffusion coefficient of Po in solid Pb is found to be enhanced if compared to the mobility of the solvent (self-diffusion), nevertheless there exist various other elements that were reported to be much more mobile in Pb than Po.

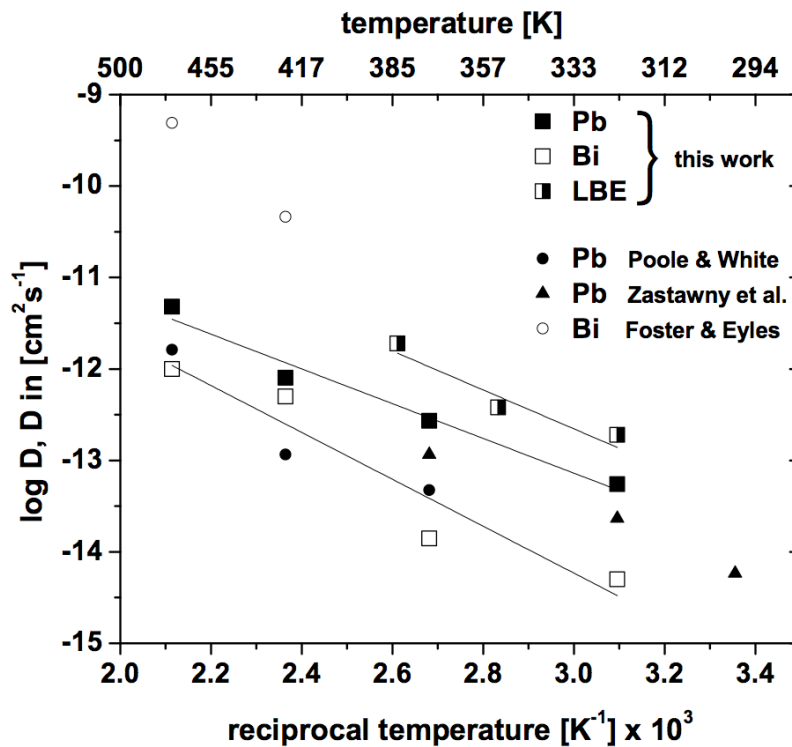


Figure 46: Arrhenius plots for measured Po diffusion coefficients in Pb, Bi and their eutectic as function of temperature; for comparison, Po thermal diffusion data in polycrystalline Pb reported by [79, 195] and Bi [207] is also given.

A summary on the calculated parameters fitting equation (8) is given in Table 19. As can be seen, the calculated values for $\log(D_0)$ and E_A are subjected to an uncertainty, which is in the order of $\pm 10\%$ for Pb and $\pm 25\%$ for Bi and LBE. Especially data for LBE lacks precision, as the number of measurements at different temperatures is too small. No further experiments to measure the diffusion coefficients were performed in the course of this thesis. Based on the underlying data it should be stressed that for the investigated materials, values of D may be considered as reliable only in the corresponding temperature ranges. If extrapolations are to be made, the calculated Po diffusion coefficient will represent only a rough order-of-magnitude approximation.

It should be mentioned that by deducing the diffusion coefficient, a simplification is made according to that D is independent on the solute concentration. This is indeed the case for tracer concentrations of the diffusing solute in chemically homogeneous systems. Nevertheless, solid LBE represents a system of at least two distinct phases of different crystal structures. It is to assume that the diffusion coefficient in both phases will vary and thus, a correct mathematical treatment for the deduction of D in an inhomogeneous binary alloy as LBE becomes complicated.

Table 19: Calculated thermodynamic parameters fitting equation (8) for the Po diffusion coefficient in different host materials; additionally, D is calculated for 298, 398 and 498 K.

matrix	$\log(D_0), D_0$ in [cm^2/s]	E_A [kJ/mol]	diffusion coefficient [cm^2/s] at		
			298 K	398 K	498 K
Pb	-7.44 ± 0.57	36.4 ± 4.2	1.5×10^{-14}	6.1×10^{-13}	5.6×10^{-12}
Bi	-6.54 ± 1.40	49.1 ± 10.4	7.2×10^{-16}	1.0×10^{-13}	2.1×10^{-12}
LBE	-6.50 ± 1.64	38.9 ± 11.0	4.8×10^{-14}	2.5×10^{-12}	/

In order to understand the influence of grain structure on the dynamics of Po diffusion in Pb and Bi, dedicated experiments using single crystal specimen and polycrystalline samples have to be performed. If polycrystalline materials are to be used, it is important to know the microstructure of the investigated metal. Proper metallographic analysis techniques such as imaging by transmission electron microscopy (TEM), radiography, and depth profiling in combination with chemical analysis of the specimens is mandatory. With the knowledge of the microstructure and the resulting behaviour of the Po diffusion process in the pure metals Pb and Bi, it should be possible to gain further insight into diffusion and segregation processes occurring in LBE.

IV.3.2 Segregation studies

IV.3.2.1 α spectrometry results

A typical α spectrum of an irradiated cylindrical LBE sample (z40, see Table 25 in Appendix) recorded by α spectrometry for 96 h is given in Figure 47. Decaying Po atoms present at the sample surface generate a pronounced peak at 5.3 MeV. The distribution of Po inside the bulk is approximately homogeneous, which is indicated by an inclined plateau in the α -spectrum below 4.5 MeV.

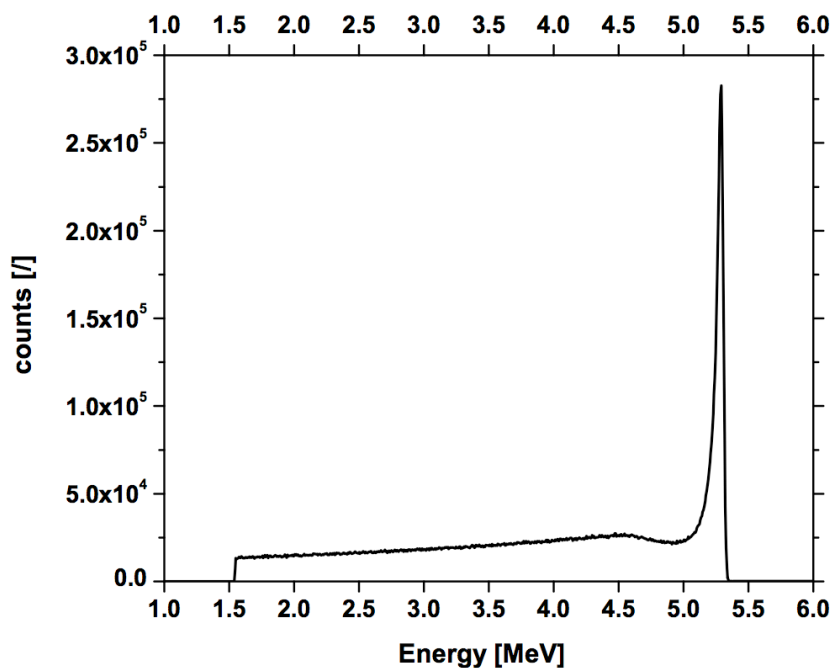


Figure 47: α spectrum of cylinder z40 after neutron irradiation; activity 9.17 kBq/g on the 01.02.2012; spectrum recorded for 96 h.

What can be seen further is a transient region between 4.5 and 5 MeV (corresponding to a depth of 1 – 2.5 μm), where even a decrease in count rate is observed if compared to that of the bulk. A similar observation was found in [208], where the 5.3 MeV peak of Po situated at the surface was accompanied by a broad one at 4.9 MeV. As will be shown later, this finding represents the real distribution of Po in the sub-surface region in LBE.

If the top or bottom surface of a cylindrical LBE sample is cut with a microtome, then the enriched layer of Po at the sample surface is removed. The Po segregation process then restarts and a subsequent measurement of the enrichment may be easily recorded by α spectrometry. A typical increase of the Po α peak at the top surface of the cylindrical sample z25 is given in Figure 48. It may be clearly seen that the Po Peak at 5.3 MeV steadily increases with time. Even 1 h after the flattening with the microtome, the peak clearly evolves in the region corresponding to the sample surface, indicating a fast ^{210}Po segregation process. In the region below approx. 5 MeV, the count rate does not change significantly for all recorded spectra. A very similar result has already been reported in [162].

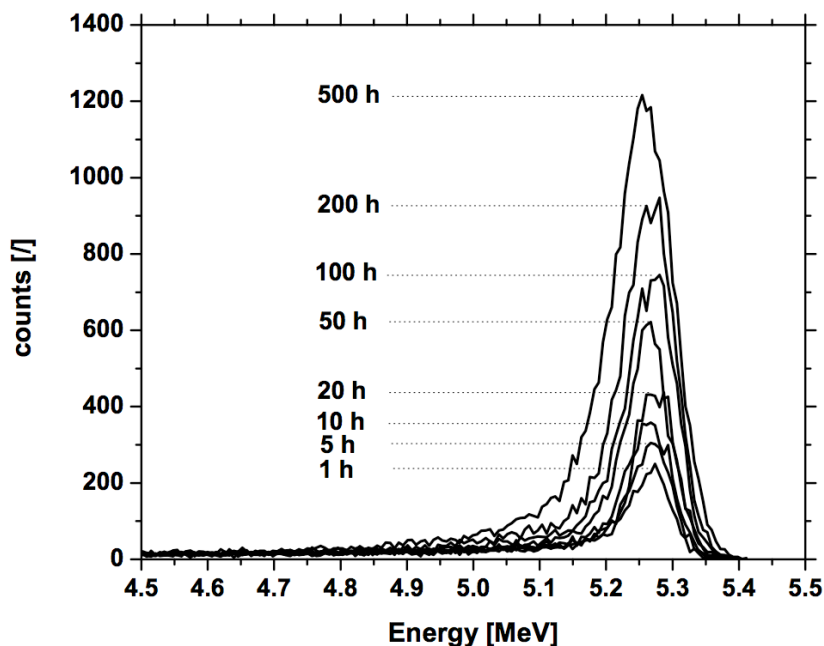


Figure 48: α spectra of sample z25 recorded for 1 h showing the continuous growth of the ^{210}Po peak indicating the accumulation of Po atoms at the sample surface at different times after the start of the experiment; activity of the sample 12.66 kBq/g (02.06.2010).

In order to quantitatively describe the Po enrichment process, all spectra of the measurement campaign partly shown in Figure 48 were integrated and the total half-life corrected count rate in the region between 1.5 and 5.3 MeV was plotted versus the square root of time to visualise the relationship given by equation (21). This dependence, obtained from 524 single α -spectra, is graphically shown in Figure 49. It may be clearly seen that the increase in surface activity linearly rises with \sqrt{t} as has been predicted by the model presented in section IV.2.5.2. Thus, for the analysis of data and the subsequent deduction of the diffusion coefficient, equation (21) represents a good approximation. For further data analysis, the relative increase of the surface activity relative to the initial value present at the start of the experiment was determined.

The deduction of the initial surface activity was performed by different ways. At first, the initial surface activity might be obtained from the intercept of the least square fit with the y-axis (at $t = 0$). However, as can be seen in Figure 49, there was a slight positive deviation from linearity for short experiment times. The reason for this discrepancy is not precisely known, possibly fluctuations in the measurement electronics may have caused the effect. A better approximation was made by the

following procedure: knowing the Po activity of sample z25 at the day of the experiment (12.66 kBq/g), the surface activity was calculated via equation (13), resulting in ca. 50 Bq/cm² of ²¹⁰Po. Thus, for this cylindrical sample with a diameter of 7 mm, the top surface had an “observable” activity of 19.2 Bq (2π geometry). Knowing the geometrical efficiency (8.3 % for a detector to source distance $h = 1.37$ cm), the α count rate registered by the α -detector corresponded to 3.26 counts per second, or 11740 counts in a 1 h measurement. This value was taken as $A_{s,0}$ and is indicated by an arrow in Figure 49.

To prove that this value is a reasonable approximation, another calculation was performed from data obtained in the α spectra. Since the count rate registered in the region below 4.5 MeV is nearly constant over time and energy, the total counts of the initial spectrum, i.e. without surface enrichment, might be found by extrapolating the “low-energy” part to 5.3 MeV. This procedure yielded a value of approx. 14 counts/channel, yielding 11500 counts in the region between 1.5 and 5.3 MeV, which is in good agreement with the value calculated above.

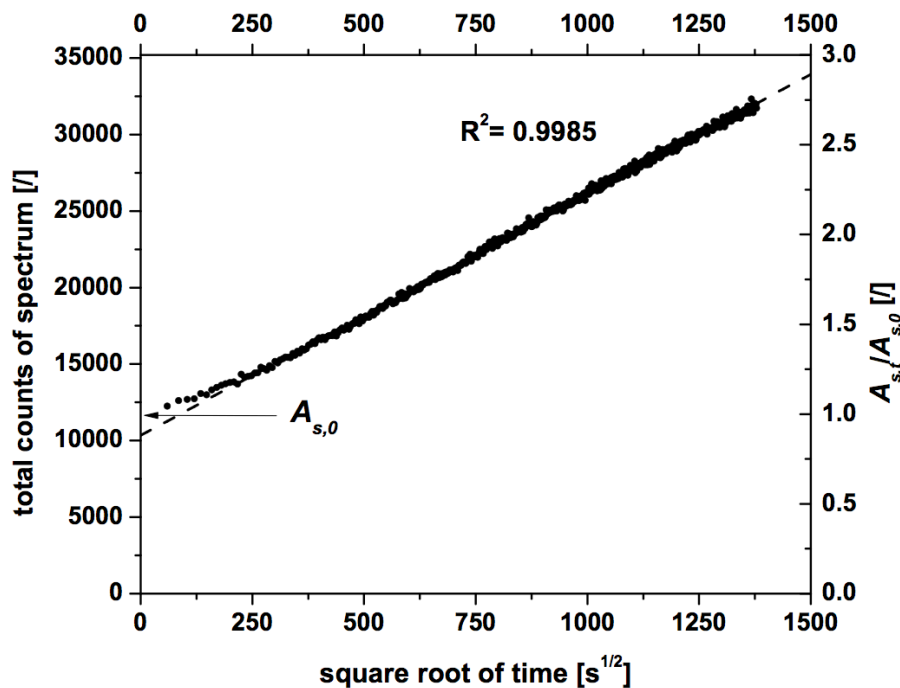


Figure 49: Increase of surface activity recorded by α spectroscopy of LBE sample z25 as function of square root of time since start of measurement (microtome sectioning); right ordinate indicates the increase relative to the initial value $A_{s,0}$.

The increase in total count rate relative to $A_{s,0}$ as function of \sqrt{t} is also presented in Figure 49. A least square fit, represented by the dotted line, yielded a slope of $1.34 \times 10^{-3} [\text{s}^{-1/2}]$. As has been explained earlier, the calculation of the diffusion coefficient requires the knowledge on the distance d , in which the Po enrichment is measured. In the underlying experiment, the surface activity was measured in the region between 5.3 and 1.5 MeV. Since the energy loss of α -particles linearly rises with the travelled distance in matter, this energy region corresponded to a layer thickness between 0 and $10.8 \mu\text{m}$ below the sample surface. Rearranging equation (21) and inserting the calculated slope and 1.08×10^{-3} cm for d yielded a value of $D = 1.6 \times 10^{-12} \text{ cm}^2/\text{s}$ for the diffusion coefficient of Po in LBE at room temperature. A critical discussion on the obtained value will be given after the next section.

IV.3.2.2 Results from microtome sectioning

The result obtained by microtome sectioning of sample z53 after different segregation times is given in Figure 50. The initial distribution of Po within the bulk of the LBE cylinder is given by black filled squares. As can be seen, the initial depth distribution may be considered to be homogeneous.

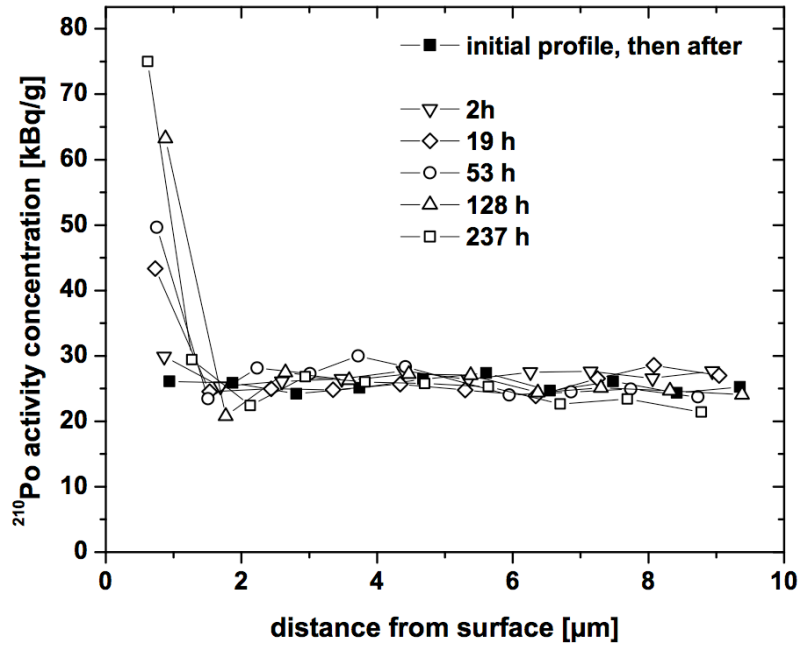


Figure 50: Depth profiles of the Po concentration in sample z53 after different segregation times; slices are taken by microtome sectioning with subsequent weighting and liquid scintillation counting; activity 26.08 kBq/g on the 17.04.2012.

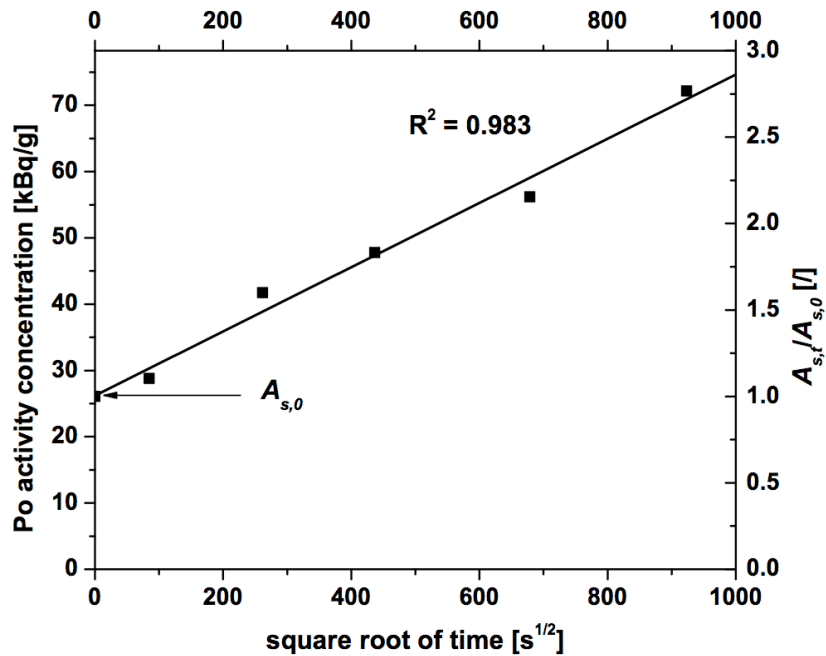


Figure 51: Increase of Po activity concentration in the first sectioned layer of sample z53 as function of square root of time; additionally, the increase relative to the initial value $A_{s,0}$ is shown by the right ordinate.

With increasing storage times, where Po segregation evolves, the count rate in the first cut layer steadily increases, while the concentration in deeper layers practically stays unchanged. Similar to the result obtained from α spectrometry, the bulk Po concentration below 2 μm is constant with a certain

statistical standard deviation. What also is seen in Figure 50 is a slight decrease in Po activity concentration in the second sectioned layer if compared to the average value. Such a decrease is comparable to the transient region observed in the α spectrum given in Figure 47, where a local minimum is observed between 4.9 and 5.3 MeV. Thus, for both samples z40 and z53, which consist of the same LBE batch but of different Po activities, the Po distribution in the bulk yields similar qualitative results.

It may be seen from Figure 50 that the average slice thickness is not 1 μm , but slightly lower, about 0.9 μm . Since the enrichment layer of Po is expected to be in the order of few nm, mechanical methods such as microtome sectioning fail in providing distribution data with acceptable resolution. Nevertheless, the use of the microtome in the underlying investigation proved useful as a complementary analysis technique and also for performing sample flattening, for the determination of the bulk concentration and for the cutting of thin LBE slices.

By plotting the ^{210}Po activity concentration in the first sectioned layer as function of \sqrt{t} , a linear dependence was expected similar to findings in the previous experiment. This dependence was indeed found as is shown by data points following a straight line as shown in Figure 51. The linearity again indicates that the model presented in section IV.2.5.2 is applicable for the underlying experimental results. Calculating the relative increase in Po activity concentration over time and applying a least square fit yielded a slope of $1.86 \times 10^{-3} [\text{s}^{-1/2}]$. With d being $9 \times 10^{-4} \text{ cm}$, the diffusion coefficient is calculated to be in the order of $D = 2.2 \times 10^{-12} \text{ cm}^2/\text{s}$, which is in good agreement with the value deduced above.

A summary on the available literature data for the segregation of Po in Pb [79] and LBE [162] with data obtained in this work is given in Table 20. For comparison, data reported in [79, 162] is recalculated using equation (21) to fit the model presented in this investigation. As can be seen, the overall agreement with data reported for LBE at room temperature [162] is reasonably good. Even recalculated data for Po in Pb show appreciable good agreement with data obtained for LBE. The fact that Po segregation in Pb is comparable to that in LBE again strengthens the assumption that similar processes occur during Po diffusion in these materials.

Table 20: Summary of room temperature diffusion coefficients for Po segregation reported in literature and those obtained in the present investigation.

determined diff. coefficient [cm^2/s]		method	reference
reported	recalculated		
	1.6×10^{-12} 2.2×10^{-12}	α spectrometry microtome sectioning	this work
2.3×10^{-11}	$5.1 \times 10^{-12} *$	scintillation counting	[79, 200]
$\approx 10^{-11}$	8.2×10^{-13}	α spectrometry	[162]

* data points taken from first stage of the reported experiments

As can be seen, both applied methods deliver room temperature diffusion coefficients that are at least two orders of magnitude higher than values deduced in the preceding section IV.3.1. Based on values given in Table 19, the calculated diffusion coefficient found in both segregation studies is comparable to “standard” bulk diffusion in LBE at 398 K. It thus becomes necessary to distinguish between normal diffusion and the enhanced diffusion during segregation.

The transient region just below the sample surface found by both, α spectrometry and microtome sectioning is an effect that might be explained by the observed discrepancy. The tendency of Po atoms to segregate to grain boundaries and free surfaces generates an atomic flux, which acts against the principles of Fick’s first and second law. During the enrichment process, a depletion of the segregating species occurs just below the surface. Principles of diffusion imply that this concentration gradient is “filled up” by atoms originating from deeper layers. The fact that a specific depletion zone just below the sample surface is encountered might indicate that the diffusion inside the bulk material occurs much slower than segregation to surfaces. Otherwise such concentration gradient would not be

possible, as it would contradict principles of mass flow. In other words, the deduced diffusion coefficient as described in section IV.3.1, which applies to atomic movement in bulk material, is physically not comparable to the diffusion coefficient found for segregation.

A model based on similar findings was already presented by authors working on Po segregation in solid Pb material [79]. They attribute diffusion phenomena to be driven by both, thermal diffusion and diffusion towards surfaces, where the latter is induced by lattice defects and is always the fastest. The authors attribute fast diffusion towards surfaces to a distortion of the surface layer by mechanical treatment (i.e. scraping with a knife), which is believed to induce a large number of lattice defects that enhances atomic movement. If the Pb surface is etched, no segregation is observed, which strengthens the presented hypothesis.

Whether the process of enhanced Po migration towards surfaces may be attributed to lattice defects or to grain boundary diffusion has to be verified in dedicated experiments with Pb and Bi single crystals containing Po. If in these specimen enrichment processes similar to polycrystalline materials occur, then grain boundary driven segregation has to be ruled out. Dedicated experiments with mechanical treatment and etching should give more insight into the underlying phenomena. Moreover, it would be advantageous to first analyse the segregation behaviour of Po in pure Pb and Bi metals under different conditions before performing experiments in more complicated systems such as LBE.

IV.3.2.3 Additional measurements and problems

During the course of this PhD thesis, segregation experiments presented in the section above were repeated in order to prove the reproducibility of the data. However, these repeated experiments failed to reproduce the obtained results. It is the intention of this section to give a short summary on additional experiments, which were performed in the course of this thesis and to show up problems and puzzling effects encountered during this work.

The result of the investigation on the migration behaviour of Po at different temperatures in samples of two distinct LBE batches is shown in Figure 52. Initially it was intended to use the data from this experiment for the calculation of the diffusion coefficient. However, the quality of measured data was poor and the graph shown in Figure 52 should only qualitatively show the observed effects.

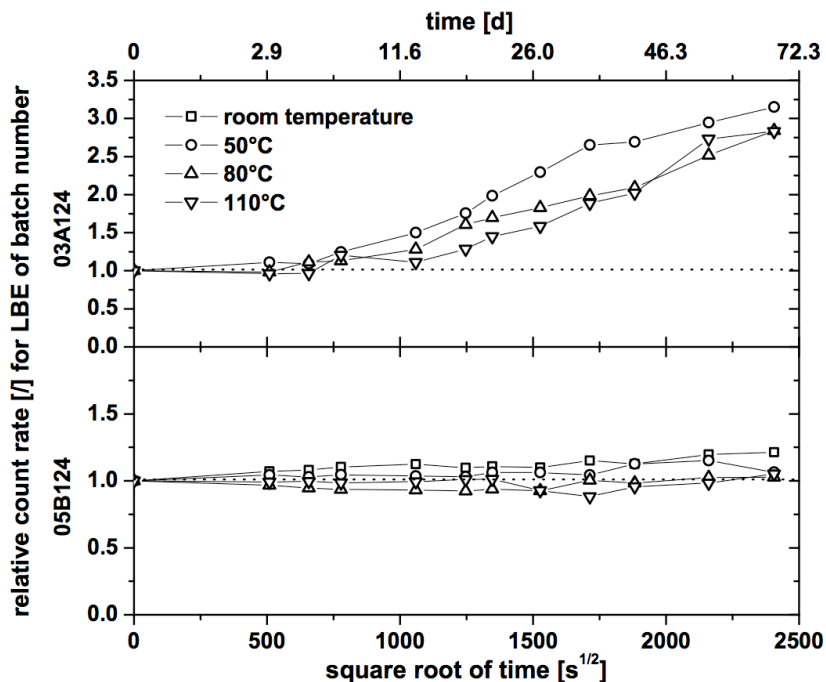


Figure 52: Graph showing the relative increase in Po surface activity for cylindrical samples of two different LBE batches 03A124 (samples z22 – z27) and 05B124 (z01 – z08) as function of time and temperature.

What may be seen first in Figure 52 is a significant difference in Po segregation behaviour between the LBE batches used for this experiment. While in LBE samples z22 – z27 of batch number 03A124 a steady increase in Po count rate is observed for every investigated temperature, no or only a very slight increase is observed for LBE samples z01 – z08 of batch number 05B124. Since both only differ by their age and the LBE impurity content, two distinct reasons might explain the observed discrepancy.

On one hand it is possible that various impurities in LBE might significantly change the segregation behaviour of Po in the material. It has been already shown in [165] that the addition of few per cent of Ca into Pb may significantly reduce the accumulation of Po at the sample surface, whereas the additions of Sb do not have any influence on the migration behaviour of Po. In LBE batches used during this thesis, impurities are present in only small concentrations. The impurity concentration of either Ca or Sb was even below the quantification limit (see Table 16 for details). As has been found, the composition of both LBE batches only differs by the amount of Sn, In and few other elements, as indicated in Table 16. Nevertheless, such differences might influence not only macroscopic properties of the material such as oxidation behaviour or resistance against acid attack [58], but also induce microscopic effects such as varying solute migration behaviour.

Another possible explanation are recrystallization processes that were reported to occur in LBE after solidification [213]. As has already been explained in section I.6.1, the ϵ -phase present in LBE continuously changes composition in the temperature range between 398 and 227 K. A precipitation of Bi from solid solution occurs, which leads to a rearrangement of the internal atomic structure of LBE cooled below the melting temperature. Such processes were reported to occur for at least 6 months at room temperature before reaching equilibrium conditions [214]. These recrystallization effects might certainly influence the mobility of solutes in fresh solidified LBE samples, as was shown in another experiment.

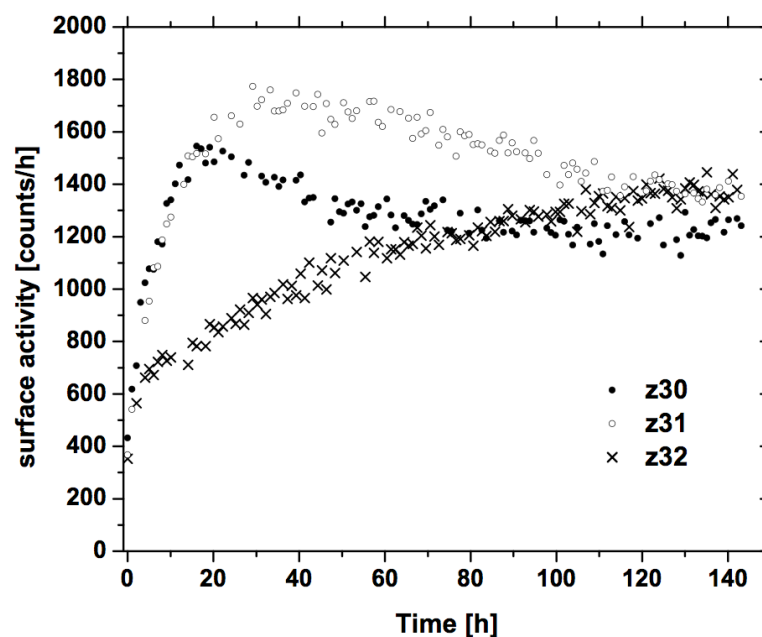


Figure 53: The increase of surface activity with time for three different LBE samples z30 – z32; activity concentration 0.9 kBq/g.

In Figure 53 the measurement of the surface activity by α spectrometry is shown for three identical cylindrical LBE samples z30, z31 and z32. As described in section IV.2.2.1, all samples originated from the same LBE rod, were freshly prepared and were treated identically until use. After the measurement by α spectrometry similar to the procedure described in IV.3.2.1, the increase in surface activity was found to substantially differ from sample to sample. While a typical Po segregation following the \sqrt{t} -law is observed for sample z32, samples z30 and z31 showed an activity maximum,

which also differs by the position appearing in the graph. Standard models behind segregation cannot explain such effects. Although the annealing temperature of all three samples was identical (room temperature), recrystallization processes are believed to cause such unusual behaviour Po segregation.

Finally, there are also processes that are attributed to oxidation of the sample surface during the investigation. Since all experiments reported here were performed without exclusion of atmospheric oxygen, oxidation of any free LBE surface has to be considered. As a direct consequence of this oxidation, the behaviour of impurities in the first atomic layers below the sample surface could also alter. For example, it has been found by auger electron spectroscopy (AES) that the segregation of Sn and Bi at the free surface of Pb depends upon the amount of adsorbed oxygen [215]. In absence of any impurity at the surface, Sn and Bi did not significantly segregate. When oxygen is adsorbed at the free surface of Pb, it causes strong segregation of Sn, whereas it induces surface depletion of Bi. Similar effects could be possible also for impurities present in a Pb-Bi alloy. The interaction with atmospheric oxygen thus should be considered for the interpretation of results in any experiment where a surface oxidation could have occurred.

All of the discussed effects – recrystallization, varying impurity concentration or the influence of oxygen upon segregation – have to be considered in future studies in the mobility of Po in solid metals and alloys. It is believed that if these phenomena are understood with sufficient precision, the surprising effects reported above may be mitigated in order to obtain reliable results.

IV.4 Summary

Within the underlying investigation, the bulk diffusion coefficient of Po in solid Pb, Bi and LBE has been deduced by the method of measuring the residual surface activity using α spectrometry. Data on the diffusion coefficient of Po between 50 and 200 °C in these materials has been determined. For Po in Pb, the deduced kinetic relationship shows good agreement with literature data reported in [79, 195], whereas data for Po in Bi significantly differs from numbers reported in [207]. For Po in LBE, the present investigation revealed Po diffusion to be highest if compared to Pb or Bi, and for this material, the obtained data represent the first reported in literature.

In a second stage of investigations, the segregation phenomenon of Po towards surfaces of LBE has been investigated. Based on a simplified segregation model, the diffusion coefficient for the surface migration process was measured by applying two different methods. α spectrometry turned out to be a reliable analysis technique for the Po enrichment process at LBE surfaces. Data obtained by microtome sectioning served as complementary data to the analysis performed by α spectrometry. Both experiments yielded comparable results on the room temperature surface diffusion coefficient of Po in LBE, which was measured to be in the order of $2 \times 10^{-12} \text{ cm}^2/\text{s}$.

From the difference of the measured Po diffusion data for bulk and near surface diffusion in LBE it was concluded that the mobility of Po inside bulk material is much lower than in the near surface region. A depletion zone just below the surface confirms the above statement. Although possible explanations have been given in literature [79], processes occurring on a microscopic scale inside such a complex system as Po in LBE are far away from being understood. Recrystallization issues, oxidation or impurities might significantly contribute to changes in Po mobility, making reliable and reproducible experimentation rather difficult.

Overall it has to be stated that the enrichment process of Po will be a significant effect in nuclear systems using LBE as coolant material. Since in such systems the Po activity concentration in LBE will be much higher than during this investigation, surface α activities exceeding the MBq/cm² range are to be expected in case of coolant spill and solidification. Such high activities will certainly contribute to volatilization of radionuclides involving the sputtering effect. Due to effects such as radiation enhanced diffusion and radiation induced segregation, it may be expected that the surface activity will rise even more than was observed here.

In order to verify and reproduce results presented here, several improvements have to be done to experimental procedures. One clear improvement at hand could be the exclusion of oxygen by transferring sample preparation and the experimental equipment into a glove box with controlled conditions. Metals used for the experimentation have to be preconditioned and the exact impurity concentrations must be known. The sample preparation should ensure reproducible cylindrical specimen, which should be checked for crystal structure if possible. This might be done with metallurgical investigations giving insight into crystallization phenomena and the underlying microstructure, grain size etc. Moreover, the diffusion and segregation experiments reported here could be repeated first with Pb and Bi single crystals, then with polycrystalline materials and, finally, with LBE.

V Final conclusions and outlook

During this thesis the intention was to show that many physical and chemical processes are important for the safe and reliable use of lead-based alloys in nuclear applications. Many interactions between different physical and chemical properties of these alloys make this field of science rather interdisciplinary.

For example, the literature review on diffusion in Pb has shown that Au shows a very high mobility in polycrystalline Pb at room temperature. This is certainly of importance for safety considerations if LGE is used as spallation target material. Since similar segregation phenomena are to be expected to occur in solid LGE as was found for LBE and Pb, the high diffusion coefficients found for Au in Pb could lead to high enrichment factors of radioactive impurities at the surface of solid LGE that would influence the radiation environment.

Before such investigations are undertaken, it has to be clearly elaborated whether LGE would serve as a suitable target material for future spallation sources. The author of this work doubts such a use in the near future, but LGE could certainly regain interest in the scientific community if other aspects except price and corrosion would become important.

Concerning investigations in solid materials that are to be used as spallation targets, a series of studies involving metallurgy and material science would be helpful. For the understanding of solid-state processes, some metallographic techniques have to be learned and applied. During experiments performed for this thesis, it was noted that parameters such as recrystallization, impurity concentration and possibly grain size and grain orientation in the samples turned out to be of importance for interpreting the results obtained. In order to gain knowledge on the effects of these parameters on various solid-state processes, it would be of value to perform an adequate grinding and polishing of the sample surfaces with subsequent microscopic investigations. All these operations should be performed in a suitable glove box to exclude any contact of the samples to atmospheric oxygen.

Additionally, a detailed analysis of segregation phenomena in the systems Pb-Po and Bi-Po, as well as Po in Pb_7Bi_3 have to be performed in future investigations. These could involve the use of α spectrometry, as it proved useful in the underlying study. The use of a microtome could lead to further improvements of the measurement precision by performing sample sectioning with subsequent analysis of the Po content in each sectioned layer.

Cylindrical samples as has been used in this investigation proved to give reliable results. It would thus be at hand to use this sample geometry for further investigations. Further segregation experiments of ^{210}Po in LBE and in Bi may easily be performed by neutron activation of the samples. For samples of Pb or LGE, it is difficult to introduce sufficient quantities of ^{210}Po without also introducing other long-lived Po isotopes that would disturb α spectrometry measurements. It would be advantageous to make use of the results obtained from Po extraction experiments. While extracting quantitatively a sufficient amount of Po from irradiated LBE or Bi under reducing conditions, it could be possible to perform a back-extraction of the Po into Pb or LGE by using oxidizing conditions. With this procedure, it is possible to obtain Pb or LGE samples of sufficient activity for further segregation or diffusion studies. Despite isotopes of Po, it would be also possible to use neutron-activated isotopes of Te or Se, directly added as oxides to the hydroxide melt.

Certainly, the knowledge on the impurity content within the material under investigation is of importance. Thus, it would be advantageous first to use materials of highest purity available and to precondition them under airtight conditions to obtain metallic samples with reproducible macro- and microscopic physical properties. Such properties also involve the concentration of dissolved oxygen, the concentration of other impurities, grain structure and overall shape. Later on samples with increasing concentration of certain impurity may be fabricated to study its influence on a number of important properties of the material.

For investigations on the extraction Po from irradiated liquid metals, it would be first necessary to transfer the experimental devices into a glove box in order to exclude any influence of atmospheric oxygen. Follow-up investigations could involve the use of neutron activated NaOH or KOH to reveal the nature of the extraction process. Such investigations could give insights into isotope exchange effects between the metallic and the hydroxide phase and the results could be used for a better understanding of the pyrochemical extraction process.

The method of cyclic voltamperometry proved useful for the determination of species, which occur in molten hydroxides such as the eutectic between NaOH and KOH. From the knowledge gained from investigations on Te and Se, it could be possible to adopt this measurement technique in a radioactive laboratory to investigate Po species present in a molten hydroxide melt. The concentration ranges, in which Po should be present, have to be determined in advance.

Finally, the investigations performed here on the extraction of spallation products formed within Pb, Bi and LBE have clearly shown the potential of the alkaline extraction technique for the purification of heavy liquid metals used in nuclear systems. Since dissolved oxygen in these metals and alloys proved to greatly influence corrosion towards steel structures, further experiments could be devoted towards monitoring the oxygen concentration in a liquid metal before and after contact to molten hydroxides. Despite that, experiments could be performed with irradiated materials containing an even more complex mixture of spallation products to fill the gaps in the table of elements presented in this thesis. With this knowledge, one could start performing studies similar to those done for the element Po to elucidate conditions for a selective extraction of valuable isotopes.

References

- [1] H. Becquerel: Émission de radiation nouvelles par l'uranium métallique, Comptes Rendus de l'Académie des sciences 122 (1896) 1086 - 1088.
- [2] O. Hahn, F. Strassmann: Über den Nachweis und das Verhalten der bei der Bestrahlung des Urans mittels Neutronen entstehenden Erdalkalimetalle, Naturwissenschaften 27 (1939) 11 - 15.
- [3] IAEA: Nuclear Power Reactors in the World, Reference Data Series 2 (2012)
- [4] M. R. Greenberg: Nuclear waste management, nuclear power and energy choices: public references, perceptions, and trust, Springer, London (2013).
- [5] J. Mahaffey: The future of nuclear power, Infobase Publishing, New York (2012).
- [6] R. J. M. Konings, J. L. Kloosterman: A view of strategies for transmutation of actinides, Progress in Nuclear Energy 38 (2001) 331.
- [7] E. Rutherford: Collisions of alpha particles with light atoms. IV. An anomalous effect in nitrogen, Philosophical magazine 37 (1919) 581 - 587.
- [8] C. Rubbia: Conceptual design of a fast neutron operated high power energy amplifier, CERN Report (1995).
- [9] G. S. Bauer: Physics and technology of spallation neutron sources, Nuclear Instruments & Methods in Physics Research Section a-Accelerators Spectrometers Detectors and Associated Equipment 463 (2001) 505-543.
- [10] D. Filges, F. Goldenbaum: Handbook of Spallation Research: Theory, Experiments and Applications, Wiley-VCH, Weinheim (2009).
- [11] K. H. Lieser: Einführung in die Kernchemie, 3rd edition, VCH, Weinheim (1991).
- [12] <http://asq.web.psi.ch>
- [13] <http://www.isis.rl.ac.uk>
- [14] <http://www.ornl.com>
- [15] <http://search.sckcen.be/>
- [16] <http://ess-scandinavia.eu/>
- [17] A. E. Waltar, D. R. Todd, P. V. Tsvetkov: Fast spectrum reactors, Springer, New York (2012).
- [18] C. D. Bowman: Accelerator-driven systems for nuclear waste transmutation, Annual Review of Nuclear and Particle Science 48 (1998) 505 - 556.
- [19] A. Abanades, et al.: Results from the TARC experiment: spallation neutron phenomenology in lead and neutron-driven nuclear transmutation by adiabatic resonance crossing, Nuclear Instruments & Methods in Physics Research Section a-Accelerators Spectrometers Detectors and Associated Equipment 478 (2002) 577-730.
- [20] A. Koning, et al.: HINDAS-a European nuclear data program for accelerator-driven systems, Journal of Nuclear Science and Technology 2 (2002) 1161-1166.
- [21] S. Andriamonje, et al.: Experimental-Determination of the Energy Generated in Nuclear Cascades by a High-Energy Beam, Physics Letters B 348 (1995) 697-709.
- [22] H. A. Abderrahim, P. Schuurmans, P. Kupschus, A. Verstrepen, J. Cools: VICE: R&D support for a windowless liquid metal spallation target in MYRRHA, SCK-CEN Report (2002).
- [23] A. Billebaud, et al.: The GUINEVERE Project for Accelerator Driven System Physics, GLOBAL 2009 - The Nuclear Fuel Cycle: Sustainable Options & Industrial Perspectives, Paris, France, 2009.
- [24] W. Uyttenhove, et al.: Experimental Results From the VENUS-F Critical Reference State for the GUINEVERE Accelerator Driven System Project, IEEE Transactions on Nuclear Science 59 (2012) 3194-3200.
- [25] H. Abderrahim, P. Baeten, D. De Bruyn, R. Fernandez: MYRRHA, A multi-purpose fast spectrum research reactor, Energy Conversion and Management 63 (2012) 4-10.
- [26] D. Maes: Mechanical design of the small-scale experimental ADS: MYRRHA, Energy Conversion and Management 47 (2006) 2710-2723.
- [27] J. M. Carpenter: Pulsed spallation neutron sources for slow neutron scattering, Nuclear Instruments and Methods 145 (1977) 91-113.
- [28] J. M. Miller, J. Hudis: High-Energy Nuclear Reactions, Annual Review of Nuclear Science 9 (1959) 159-202.
- [29] G. S. Bauer: Overview on spallation target design concepts and related materials issues, Journal of Nuclear Materials (2010) 19 - 27.

- [30] R. Lyon: Liquid Metals Handbook, 2 ed., Govt. Print. Office, Washington, D.C. (1954).
- [31] S. J. Stachura, G. Burnet: The lead-bismuth eutectic as a heat transfer medium, *Chemical Engineering Reviews* 60 (1964)
- [32] S. Z. Verhovodko, V. V. Zamukov: The experience of designing, using and utilizing the nuclear power installations with lead-bismuth liquid metal coolant for the "alpha" type nuclear submarines, HLMC98, Obninsk, Russia, 1998.
- [33] D. Gorse-Pomonti, V. Russier: Liquid metals for nuclear applications, *Journal of Non-Crystalline Solids* 353 (2007) 3600-3614.
- [34] H. U. Wider, J. Carlsson, E. Loewen: Renewed interest in lead cooled fast reactors, *Progress in Nuclear Energy* 47 (2005) 44 - 52.
- [35] A. Alemberti, J. Carlsson, E. Malambu, A. Orden, D. Struwe, P. Agostini, S. Monti: European lead fast reactor-ELSY, *Nuclear Engineering and Design* 241 (2011) 3470-3480.
- [36] D. A. McClintock, B. W. Riemer, P. D. Ferguson, A. J. Carroll, M. J. Dayton: Initial observations of cavitation-induced erosion of liquid metal spallation target vessels at the Spallation Neutron Source, *Journal of Nuclear Materials* 431 (2012) 147-159.
- [37] Handbook on Lead-bismuth Eutectic Alloy and Lead Properties, Materials Compatibility, Thermal-hydraulics and Technologies, OECD Nuclear Energy Agency, Issy-les-Moulineaux (2007).
- [38] J. A. Lane, H. G. MacPherson, F. Maslan: Fluid Fuel Reactors. Part III - Liquid metal fuel reactors, Addison-Wesley, Reading, USA (1958).
- [39] T. McManamy, J. Forester: SNS Target Systems initial operating experience, *Nuclear Instruments & Methods in Physics Research Section a-Accelerators Spectrometers Detectors and Associated Equipment* 600 (2009) 25-27.
- [40] M. Futakawa, K. Haga, T. Wakui, H. Kogawa, T. Naoe: Development of the Hg target in the J-PARC neutron source, *Nuclear Instruments & Methods in Physics Research Section a-Accelerators Spectrometers Detectors and Associated Equipment* 600 (2009) 18-21.
- [41] Selection of ESS Target Baseline, ESS TAC meeting, 2011.
- [42] S. Chiriki, J. Fachinger, R. Moormann, H. K. Hinssen, A. Bukaemskiy, R. Odoj: Decommissioning and safety issues of liquid-mercury waste generated from high-power spallation sources with particle accelerators, *Nuclear Technology* 168 (2009) 264-269.
- [43] A. R. Junghans, et al.: The nELBE neutron time-of-flight facility, *IEEE Nuclear Science Symposium and Medical Imaging Conference*, New York, 2008.
- [44] K. H. Roll: Lead and its alloys, *Chemical Engineering Reviews* 48 (1956) 1731 - 1734.
- [45] O. Landolt-Boernstein: Phase Equilibria, Crystallographic and Thermodynamic Data of Binary Alloys, Subvol. b, Macroscopic and Technical Properties of Matter, New Series by Springer-Verlag, vol. 5 (1991).
- [46] S. J. Stachura, G. Burnet: The Lead-Bismuth Eutectic, IS-316, Report (1961).
- [47] J. R. Weeks, A. J. Romano: Liquidus Curves and Corrosion of Fe Ti Zr and Cu in Liquid Bi-Pb Alloys, *Corrosion* 25 (1969) 131-136.
- [48] W. Wagner, F. Groschel, K. Thomsen, H. Heyck: MEGAPIE at SINQ - The first liquid metal target driven by a megawatt class proton beam, *Journal of Nuclear Materials* 377 (2008) 12-16.
- [49] <http://myrrha.sckcen.be/>
- [50] P. N. Martynov, R. S. Ashadullin, A. A. Simakov, A. Y. Chaban, M. E. Chernov, V. S. Lanskih: Development of the automatized system for monitoring, forecasting and controlling the condition of lead-bismuth (lead) coolant and circuit surfaces of nuclear power installations, Heavy liquid-metal coolants in nuclear technologies (HLMC), Obninsk, 2008.
- [51] P. Agostini, E. Baicchi, A. Zucchini, G. Benamati: The re-crystallization issue in lead-bismuth technology, *Journal of Nuclear Materials* 335 (2004) 275-279.
- [52] E. H. Pylchenkov: The issues of freezing-defreezing lead-bismuth liquid metal coolant in reactor facilities circuits, HLMC98, Obninsk, Russia, 1998.
- [53] L. Zanini, S. Lemaire: Update on Monte Carlo calculations of activation of the MEGAPIE target, PSI Report (2007).
- [54] J. Neuhausen, D. Schumann, R. Dressler, B. Eichler, S. Horn, T. Stora, M. Eller: Radiochemical aspects of liquid mercury spallation targets, *Journal of Nuclear Materials* 431 (2012) 224-234.
- [55] L. Zanini, S. Lemaire: Update on Monte Carlo calculations of activation of the MEGAPIE target, TM34-07-09, PSI Report (2007).

- [56] J. Neuhausen, et al.: Radiochemical aspects of liquid metal spallation targets, NUCAR, Visakhapatnam, 2011.
- [57] J. L. Courouau: Impurities and purification processes in lead-bismuth systems, NT DER LCEP 2003/001, CEA Report (2003).
- [58] J. S. Jacobi, B. H. Wadia: Betterments of the Quality of Refined Lead, Transactions of the Institute of Mining and Metallurgy 67 (1958) 141 - 161.
- [59] D. V. Pankratov, E. I. Yefimov, S. V. Ignatiev, V. I. Levanov: Radiological properties of heavy liquid metal targets of accelerator driven systems, Scientific Basis for Nuclear Waste Management Xxii 556 (1999) 1215-1221.
- [60] H. V. Moyer: Polonium, TID-5221, Mound Laboratory Report (1956).
- [61] K. W. Bagnall: Chemistry of the rare radioelements. Polonium - Actinium, Butterworths, London (1957).
- [62] Gmelin: Polonium, Springer Verlag, Berlin (1990).
- [63] P. E. Figgins: The radiochemistry of polonium, NAS-NS 3037, Mound Laboratory Report (1961).
- [64] E. Ansoborlo, P. Berard, C. Den Auwer, R. Leggett, F. Menetrier, A. Younes, G. Montavon, P. Moisy: Review of Chemical and Radiotoxicological Properties of Polonium for Internal Contamination Purposes, Chemical Research in Toxicology 25 (2012) 1551-1564.
- [65] D. J. Storm: Health impacts from acute radiation exposure, PNNL-14424, Pacific Northwest National Laboratory Report (2003).
- [66] A. B. W. K. F. Eckerman, A. C. B. Richardson: Limiting values of radionuclide intake and air concentration and dose conversion factors for inhalation, submersion and ingestion, Federal Guidance Report No. 11, Oak Ridge National Laboratory Report (1988).
- [67] B. Eichler: Die Flüchtigkeitseigenschaften des Poloniums, PSI Bericht 02-12, Paul Scherrer Institute Report (2002).
- [68] J. N. Bernd Eichler: Verflüchtigungspfade des Poloniums aus einem Pb-Bi-Spallationstarget, Paul Scherrer Institute Report (2004).
- [69] J. Neuhausen: Reassessment of the Rate of Evaporation of Polonium from Liquid Eutectic Lead Bismuth Alloy, TM-18-05-01, Paul Scherrer Institute Report (2005).
- [70] E. F. Joy: The vapor-liquid equilibrium of the dilute solutions of polonium in liquid bismuth, MLM-987, Mound Laboratory Report (1954).
- [71] R. F. Bradley, L. F. Landon, G. W. Gibson: Separation of ^{210}Po from bismuth by liquid metal distillation, DP-1222, Savannah River Laboratory Report (1970).
- [72] J. Neuhausen, U. Köster, B. Eichler: Investigation of evaporation characteristics of polonium and its lighter homologues selenium and tellurium from liquid Pb-Bi eutecticum, Radiochimica Acta 92 (2004) 917 - 923.
- [73] S. Ohno, Y. Kurata, S. Miyahara, R. Katsura, S. Yoshida: Equilibrium evaporation behavior of polonium and its homologue tellurium in liquid lead-bismuth eutectic, Journal of Nuclear Science and Technology 43 (2006) 1359-1369.
- [74] J. Buongiorno, C. Larson, K. R. Czerwinski: Speciation of polonium released from molten lead bismuth, Radiochimica Acta 91 (2003) 153 - 158.
- [75] T. J. Trenn: Phenomenon of Aggregate Recoil - Premature Acceptance of an Essentially Incorrect Theory, Annals of Science 37 (1980) 81 -100.
- [76] N. E. Whitehead: Recoil sputtering from sources of alpha emitters, 3rd SPERA Workshop, Canberra, 1994.
- [77] N. Riehl, R. Sizmann: Die abnorme Flüchtigkeit α -strahlender Substanzen, Radiochimica Acta 3 (1964) 44 - 47.
- [78] B. F. Gromov, et al.: Liquid lead-bismuth target as intense neutron source in accelerator-driven systems for actinides transmutation and plutonium utilization, International conference on future nuclear systems, Yokohama, Japan, 1997.
- [79] A. Zastawny, J. Bialon, T. Sosinski: Migration of Po-210 in Lead to the Surface, Applied Radiation and Isotopes 43 (1992) 1147-1150.
- [80] R. Moormann, M. Medarde, E. Platadis, K. Thomsen: Proceedings of the International Workshop of Technology and Components of Accelerator Driven Systems, Karlsruhe, Germany, 2010.
- [81] M. Medarde, et al.: Lead-gold eutectic: An alternative liquid target material candidate for high power spallation neutron sources, Journal of Nuclear Materials 411 (2011) 72-82.

- [82] R. Moormann, M. Medarde, E. Platacis, K. Thomsen: Proceedings of the International Workshop of Technology and Components of Accelerator Driven Systems, Karlsruhe, Germany, March 15-17 2010.
- [83] Y. Plevachuk, V. Sklyarchuk, A. Yakymovych, S. Eckert, G. Gerbeth: Thermophysical properties of the liquid $Pb_{84.1}Au_{15.9}$ eutectic alloy, *Journal of Nuclear Materials* 434 (2013) 291-295.
- [84] L. Zanini, F. Carinci, D. Kiselev, K. Thomsen: Neutronic and nuclear behaviour of lead-gold eutectic as target material for ESS, IWSMT - 10th International Workshop on Spallation Materials Technology, Beijing, China, 2010.
- [85] Y. Dai, W. Gao, T. Zhang, E. Platacis, S. Heinitz, K. Thomsen: A comparative study on the compatibility of liquid lead-gold eutectic and liquid lead-bismuth eutectic with T91 and SS 316LN steels, *Journal of Nuclear Materials* 431 (2012) 113-119. submitted for publication
- [86] B. Legendre, C. Souleau: Phase Equilibrium Diagram of Binary-System Gold-Lead, *Bulletin De La Societe Chimique De France Partie I-Physicochimie Des Systemes Liquides Electrochimie Catalyse Genie Chimique* (1973) 2202-2206.
- [87] B. Landolt: *Zahlenwerte und Funktionen aus Naturwissenschaft und Technik*, Springer Verlag,
- [88] R. Vogel: Gold-lead alloys, *Zeitschrift Fur Anorganische Chemie* 45 (1905) 11-23.
- [89] J. P. Bhattacharya, K. A. Reynolds: Modification of Gold-Lead Binary Equilibrium Diagram, *Journal of the Institute of Metals* 99 (1971) 350.
- [90] Y. Fujiki, R. Sukanuma, T. Yoshida: A New Compound in Au-Pb Alloy System, *Journal of the Physical Society of Japan* 13 (1958) 969-970.
- [91] J. Wang, H. S. Liu, Z. P. Jin: Thermodynamic assessment of the Au-Pb system, *Computer Coupling of Phase Diagrams and Thermochemistry* 28 (2004) 91-95.
- [92] A. Bouhajib, A. Nadiri, A. Yacoubi, H. Bros, R. Castanet: Calorimetric investigation of the solid compounds of the Pb-Au system, *Journal of Alloys and Compounds* 282 (1998) 149-152.
- [93] C. Cretu, E. van der Lingen: Coloured gold alloys, *Gold Bulletin* 32 (1999) 115-126.
- [94] J. R. Weeks: Compatibility of structural materials with liquid lead-bismuth and mercury, *Proceedings of the Symposium on Materials for Spallation Neutron Sources*, held in conjunction with the 1997 TMS Annual Meeting, Orlando, FL, (1998).
- [95] M. N. Arnoldov: Solubility and corrosion of structural materials in liquid metal coolants (lead, bismuth and their alloys), *Review FEI-0228*, Moscow (1999)
- [96] T. Alden, D. A. Stevenson, J. Wulff: Solubility of Nickel and Chromium in Molten Lead, *Transactions of the American Institute of Mining and Metallurgical Engineers* 212 (1958) 15-17.
- [97] J. R. Weeks: Liquidus Curves of 19 Dilute Binary Alloys of Bismuth, *Asm Transactions Quarterly* 58 (1965) 302-322.
- [98] L. Brewer, R. H. Lamoreaux: *Phase-Diagrams*, Atomic Energy Review (1980) 195-356.
- [99] E. Pelzel: Die Löslichkeit von Tellur, Selen und Mangan in flüssigem Blei, *Metall* 10 (1956) 717 - 719.
- [100] C. J. Klamut, D. G. Schweitzer, J. G. Y. Chow, R. A. Meyer, O. F. Kammerer, J. R. Weeks, D. H. Gurinsky: *Material and fuel technology for an LMFR*, Progress in Nuclear Energy Series IV - Technology Engineering and Safety by Pergamon Press, vol. 2 (1960).
- [101] G. Rosenblatt, J. R. Wilson: The solubilities of several transition metals in liquid lead-bismuth eutectic, Session IV in corrosion by liquid metals of the 1969 fall meeting, Philadelphia, 1969.
- [102] J.-L. Courouau: Electrochemical oxygen sensors for on-line monitoring in lead and bismuth alloys: status of development, *Journal of Nuclear Materials* 335 (2004) 254-259.
- [103] L. Martinelli, F. Vanneroy, J. C. D. Rosado, D. L'Hermite, M. Tabarant: Nickel solubility limit in liquid lead-bismuth eutectic, *Journal of Nuclear Materials* 400 (2010) 232-239.
- [104] P. N. Martinov, K. D. Ivanov: Proceedings of four technical meetings held between december 1995 and april 1998, 177 - 184, 1998.
- [105] IAEA-TECDOC-1289: Comparative assessment of thermophysical and thermohydraulic characteristics of lead, lead-bismuth and sodium coolants for fast reactors, IAEA, (2002).
- [106] R. Hultgren, P. D. Desai, D. T. Hawkins, M. Gleiser, K. K. Kelley: Selected values of the thermodynamic properties of binary alloys, American Society for Metals, Metals Park, Ohio, 1973.
- [107] J. Neuhausen, D. Schumann, R. Dressler, B. Eichler, S. Horn, T. Stora, M. Eller: Radiochemical aspects of liquid mercury spallation targets, *Journal of Nuclear Materials* (2011) in Press

- [108] T. Kai, M. Ooi, Y. Kasugai, T. Wakui, H. Kogawa, K. Haga, K. Hanano: Proceedings 19th Meeting on Collaboration of Advanced Neutron Sources, ICANS XIX, Grindelwald, Switzerland, March 8-12, 2010.
- [109] J. Neuhausen: personal communication
- [110] K. Kikuchi, S. Saito, D. Hamaguchi, M. Tezuka: Ni-rich precipitates in a lead bismuth eutectic loop, *Journal of Nuclear Materials* 398 (2010) 104-108.
- [111] J. S. Zhang, N. Li: Review of the studies on fundamental issues in LBE corrosion, *Journal of Nuclear Materials* 373 (2008) 351-377.
- [112] F. E. Luborsky: The Kinetics of Growth of Spherical Iron Crystallites in Mercury, *Journal of Physical Chemistry* 61 (1957) 1336-1340.
- [113] J. Buongiorno, E. Loewen, K. Czerwinsky, C. Larson: Studies of polonium removal from molten lead-bismuth for lead-alloy-cooled reactor applications, *Nuclear Technology* 147 (2004) 407 - 417.
- [114] L. A. Ortiz, J. Braet: Purification of Lead-Bismut Eutectic Used in Accelerator Driven Systems, WM2009 - Conference on Waste Management, Phoenix, USA, 2009.
- [115] R. W. Endebrock, P. M. Engle: The separation of polonium from bismuth by distillation, AECD-4146, Mound Laboratory Report (1953).
- [116] J. Neuhausen, U. Köster, B. Eichler: Investigation of the evaporation characteristics of polonium and its lighter homologues selenium and tellurium from liquid Pb-Bi-eutecticum, *Radiochimica Acta* 92 (2004) 917.
- [117] O. Schipakin, N. Borisov, S. Churkin: Experimental-Study of Po-210 Release from ¹⁷Li-⁸³Pb Eutectic, *Fusion Engineering and Design* 29 (1995) 164-169.
- [118] J. J. Burbage: Chemistry of some alpha emitters, *Record of chemical progress* 14 (1953) 156 - 175.
- [119] A. S. Abakumov: Thermal Reactions of Polonium, *Uspekhi Khimii* 51 (1982) 1091-1102.
- [120] B. Eichler, J. Neuhausen: Verflüchtigungspfade des Poloniums aus einem Pb-Bi-Spallationstarget, Bericht 04-06, Paul Scherrer Institute Report (2004).
- [121] E. Konovalov, S. Pejzulaev, W. Emelianov: Concentration of polonium with the zone melting method, *Radiokhimiya* 9 (1967) 215 - 221.
- [122] B. L. Zhuikov, V. M. Kokhanyuk, N. A. Konyakhin, J. Vincent: Target irradiation facility and targetry development at 160 MeV proton beam of Moscow linac, *Nuclear Instruments & Methods in Physics Research Section a-Accelerators Spectrometers Detectors and Associated Equipment* 438 (1999) 173 - 179.
- [123] W. W. Schulz, G. F. Schiefelbein, L. E. Bruns: Pyrochemical Extraction of Polonium from Irradiated Bismuth Metal, *Industrial & Engineering Chemistry Process Design and Development* 8 (1969) 508 - 515.
- [124] W. Flick, A. Lenz, US Patent No. 0000119 (1978).
- [125] N. A. Reshetnikov, Vilutis, N. I.: The ternary system formed by the hydroxides of lithium, sodium and potassium, *Russian journal of inorganic chemistry* 4 (1959) 49 - 53.
- [126] H. W. Otto, Seward, R. P.: Phase equilibria in the potassium hydroxide - sodium hydroxide system, *Journal of chemical and engineering data* 9 (1964) 507 - 508.
- [127] I. N. Sheiko, T. N. Grechina, T. A. Bandur, V. V. Smeshkov: Density and Molar Volume of Melt of NaOH-KOH System, *Ukrainskii Khimicheskii Zhurnal* 45 (1979) 1013-1014.
- [128] R. S. Young, K. G. A. Strachan: Behaviour of Titanium, Vanadium, and Zirconium Towards Fusion Reagents, *Chemistry & Industry* (1953) 154-155.
- [129] G. P. Smith: Corrosion of materials in fused hydroxides, ORNL-2048, Oak Ridge National Laboratory Report (1956).
- [130] E. J. Wheelwright, J. L. Swanson, T. R. Myers: Purification of Po-210 Using Pyrochemical Extraction, *Separation Science and Technology* 15 (1980) 987-997.
- [131] Y. E. Lebedev, N. J. Edison, W. C. Klein, US Patent No. 3,607,232 (1971).
- [132] L. E. Auman, E. P. Loewen, T. F. Gesell, S. Ohno: The chemical kinetics of alkaline extraction of tellurium from lead-bismuth eutectic, *Journal of Nuclear Science and Technology* 42 (2005) 618-625.
- [133] S. Heinitz, J. Neuhausen, D. Schumann: Alkaline extraction of polonium from liquid lead bismuth eutectic, *Journal of Nuclear Materials* 414 (2011) 221-225.
- [134] H. Harris, US Patent No. 142,398 (1919).
- [135] M. Behl, J. Gerlach, F. Pawlek, W. Wuth: Zur Kinetik des Harris-Verfahrens, *Erzmetall* 21 (1968) 411 - 415.

- [136] K. Emicke, G. Holzapfel, E. Kniprath: Bleiraffination an der Norddeutschen Affinerie, *Erzmetall* 24 (1971) 205 - 215.
- [137] P. Paschen, H. Winterhager: Die Raffination von Blei mit Ätznatron, *Erzmetall* 21 (1968) 14 - 20.
- [138] T. R. A. Davey: The physical chemistry of lead refining, Lead-zinc-tin '80: Proceedings of a world symposium on metallurgy and environmental control at the 109th AIME annual meeting, Las Vegas, USA, 1980.
- [139] W. Kroll: Fortschritte auf dem Gebiete der Metalltrennung, *Metall und Erz* 38 (1938) 252 - 286.
- [140] R. A. Barney: Extraction of polonium from molten bismuth with fused sodium hydroxide, NAA-SR-MEMO-746, North American Aviation Inc. Report (1953).
- [141] J. Oishi, H. Moriyama, K. Moritani, S. Maeda, M. Miyazaki, Y. Asaoka: Behavior of several lanthanide and actinide elements in a molten salt/liquid metal extraction system, *Journal of Nuclear Materials* 154 (1988) 163-168.
- [142] S. Yamagishi, Y. Kamemoto: *Nippon Genshiryoku Gakkaishi* 5 (1963) 210.
- [143] S. Yamagishi, Y. Kamemoto: *Nippon Genshiryoku Gakkaishi* 6 (1964) 158.
- [144] S. Yamagishi, Y. Kamemoto: *Nippon Genshiryoku Gakkaishi* 6 (1964) 500.
- [145] C. J. Raseman, H. Susskind, C. H. Waide: Pilot plant generation of fission products in uranium-bismuth reactor fuel, *Chemical Engineering Progress* 53 (1957) 86 - 92.
- [146] E. I. Yefimov, D. V. Pankratov, S. V. Ignatiev: Removal and containment of high-level radioactive polonium from liquid lead-bismuth coolant, *Materials Research Society Symposium Proceedings* 506 (1998) 679-686.
- [147] E. Loewen: Investigation of polonium removal systems for lead-bismuth cooled FBRs, *Progress in Nuclear Energy* 47 (2005) 586-595.
- [148] Y. Dai, et al.: The Second SINQ Target Irradiation Program, STIP-II, *Journal of Nuclear Materials* 343 (2005) 33 - 44.
- [149] D. Kiselev, Y. Dai, S. Lüthi, J. Neuhausen, D. Schumann, P. W. Kubik, H.-A. Synal, V. Alfimov: Nuclide inventory in proton irradiated lead - comparison of simulation and measurement, *Shielding Aspects of Accelerators, Targets and Irradiation Facilities, SATIF10*, 2010.
- [150] Y. Tall, et al.: Volatile elements production rates in a proton-irradiated molten lead-bismuth target, *International Conference on Nuclear Data for Science and Technology, Vol 2*, Proceedings by E D P Sciences, vol. (2008).
- [151] A. Serov, et al.: Adsorption interaction of astatine species with quartz and gold surfaces, *Radiochimica Acta* 99 (2011) 593-599.
- [152] <http://nucleardata.nuclear.lu.se/database/nudat/>
- [153] J. A. DeKeyser, W. E. Jaspers: The Harris Refinery of S.A. *Metallurgie Hoboken-Overpelt N.V.*, TMS Paper Selection by The Metallurgical Society of AIME, vol. A81-10 (1981).
- [154] W. G. Witteman, A. L. Giorgi, D. T. Vier: The Preparation and Identification of Some Intermetallic Compounds of Polonium, *Journal of Physical Chemistry* 64 (1960) 434-440.
- [155] I. Barin: *Thermochemical Data of Pure Substances*, 3rd edition, VCH, Weinheim (1995).
- [156] P. Claes, Y. Dewilde, J. Glibert: Chemical and electrochemical behaviour in molten alkali hydroxides - Part II: Electrochemistry of chalcogenide ions in molten NaOH+KOH (49 mol%) eutectic mixture, *Journal of Electroanalytical Chemistry* 250 (1988) 327 - 339.
- [157] O. G. Zarubitskii: The Electrochemistry of Hydroxide Melts, *Russian chemical reviews* 49 (1980) 536 - 548.
- [158] J. Neuhausen, S. Horn, B. Eichler, D. Schumann, T. Stora, M. Eller: Mercury Purification in the Megawatt Liquid Metal Spallation Target of EURISOL-DS, *AccApp'07*, Pocatello, Idaho, USA, 2007.
- [159] Hollemann, Wiberg: *Lehrbuch der Anorganischen Chemie*, 102th edition, Walter de Gruyter, Berlin, New York (2006).
- [160] R. B. Tupper, B. Minuskin, F. E. Peters, Z. L. Kardos: Polonium hazards associated with lead-bismuth used as reactor coolant, *International Conference on Fast Reactors and Related Fuel Cycles - Current Status and Innovations Leading to Promising Plants*, Kyoto, Japan, 1991.
- [161] W. Seith: *Diffusion in Metallen (Platzwechselreaktionen)*, Springer, Berlin (1939).
- [162] F. von Rohr, J. Neuhausen, D. Schumann, S. Horn, S. Chiriki: Surface enrichment of polonium in solidified lead bismuth alloy: first kinetic studies, *LCH Annual Report*, Paul Scherrer Institute Report (2008).

- [163] A. Zastawny, J. Bialon, T. Sosinski: Changes in the Surface Radioactivity of Lead - the Effect of the Diffusion of Bismuth and Polonium Radioisotopes, *Applied Radiation and Isotopes* 40 (1989) 19-25.
- [164] G. Tammann, A. Löwis von Menar: Über das Verhalten von Polonium bei der Kristallisation von Metallen, *Zeitschrift Fur Anorganische Und Allgemeine Chemie* 205 (1932) 145-162.
- [165] L. Patrizii, et al.: Study of the effects induced by lead on the emulsion films of the OPERA experiment, *Journal of Instrumentation* 3 (2008)
- [166] J. Neuhausen, F. von Rohr, D. Schumann: Segregation of ^{210}Po in eutectic lead-bismuth alloy. Analytics and sample homogenisation, LCH Annual Report, Paul Scherrer Institute Report (2006).
- [167] A. S. Icenhour: Transport of Radioactive Material by Alpha Recoil, TM-2005/22, Oak Ridge National Laboratory Report (2005).
- [168] C. Kittel: Einführung in die Festkörperphysik, Oldenbourg Verlag, Munich (2006).
- [169] Landolt-Börnstein: Numerical Data and Function Relationships in Science and Technology, New Series, Group III, Volume 26 - Diffusion in Solid Metals and Alloys, Springer-Verlag, Berlin (1990).
- [170] J. Kärger, P. Heitjans, R. Haberlandt: Diffusion in Condensed Matter, Vieweg, Wiesbaden (1998).
- [171] P. G. Shewmon: Diffusion in solids, McGraw-Hill, New York (1963).
- [172] A. Fick: Über die Diffusion in festen Körpern, *Poggendorffsche Annalen der Physik* 94 (1855) 59.
- [173] J. Crank: The Mathematics of Diffusion, Clarendon press, Oxford (1975).
- [174] P. A. Dowben, A. Miller: Surface segregation phenomena, CRC Press, Boca Raton (1990).
- [175] J. du Plessis: Diffusion and defect data. Part B - Solid state phenomena. Vol. 11 - Surface segregation, Sci-TechPublications, Vaduz (1990).
- [176] W. R. Thomas, B. Chalmers: The Segregation of Impurities to Grain Boundaries, *Acta Metallurgica* 3 (1955) 17-21.
- [177] S. Hofmann, J. Erlewein: A model of the kinetics and equilibria of surface segregation in the monolayer regime, *Surface Science* 77 (1978) 591 - 602.
- [178] B. D. Powell, H. Mykura: Segregation of bismuth to grain boundaries in copper-bismuth alloys, *Acta Metallurgica* 21 (1973) 1151 - 1156.
- [179] H. J. Grabke: Surface and grain boundary segregation on and in iron and steels, *ISIJ International* 29 (1989) 529 - 538.
- [180] S. Hofmann, P. Lejcek: Solute segregation at grain boundaries, *Interface Science* 3 (1996) 241-267.
- [181] Landolt-Börnstein: Numerical Data and Function Relationships in Science and Technology, New Series, Group III, Volume 42 - Surface segregation and adsorption on surfaces, Springer-Verlag, Berlin (1990).
- [182] E. D. Hondros, M. P. Seah: Grain-boundary segregation, *Proceedings of the royal society of London, Series A - mathematical, physical and engineering sciences* 335 (1973) 191 - 212.
- [183] P. R. Okamoto, L. E. Rehn: Radiation-Induced Segregation in Binary and Ternary Alloys, *Journal of Nuclear Materials* 83 (1979) 2-23.
- [184] C. A. English, S. M. Murphy, J. M. Perks: Radiation-Induced Segregation in Metals, *Journal of the Chemical Society-Faraday Transactions* 86 (1990) 1263-1271.
- [185] G. J. Dienes, A. C. Damask: Radiation Enhanced Diffusion in Solids, *Journal of Applied Physics* 29 (1958) 1713-1721.
- [186] V. Naundorf: Diffusion in Metals and Alloys under Irradiation, *International Journal of Modern Physics B* 6 (1992) 2925-2986.
- [187] P. Lejček: Grain boundary segregation in metals, Springer, Heidelberg (2010).
- [188] L. Wertenstein, H. Dobrowolska: Diffusion des éléments radioactifs dans des métaux, *Journal de Physique et le Radium* 4 (1923) 324 - 332.
- [189] H. Jędrzejowski: Sur un exemple de la mobilité des atomes radioactifs sur les surfaces des corps solides, *Comptes Rendus de l'Académie des Sciences* 194 (1932) 1340 - 1343.
- [190] K. Schwarz: Über die Beweglichkeit des Poloniums in und auf Silber, *Zeitschrift für physikalische Chemie* 168 (1934) 241 - 247.
- [191] E. Montel: Sur la pénétration du polonium dans le plomb, *Journal de Physique et le Radium* 10 (1929) 78 - 80.

- [192] E. Rona, E. A. W. Schmidt: Untersuchungen über das Eindringen des Poloniums in Metalle, Sitzungsberichte der Akademie der Wissenschaften in Wien, Abteilung IIa 136 (1927) 67 - 73.
- [193] A. N. Kirgintsev, V. I. Koslyakov, L. A. Prokhorov, A. S. Aloj, I. M. Selivanov: Investigation of the purification of black bismuth from polonium, Soviet Radiochemistry 14 (1972) 307-312.
- [194] G. Hevesy, Obrusheva: Self-diffusion in solid metals, Nature 115 (1925) 674 - 675.
- [195] J. H. J. Poole, J. N. T. White: The use of nuclear plates for the measurement of the diffusivity of an alpha ray active element into a solid, The scientific proceedings of the Royal Dublin Society 27 (1955) 1 - 15.
- [196] M. Wojcik: Measurement of Natural Radioactivity in Construction Materials with Silicon Detectors, Nuclear Instruments & Methods in Physics Research 189 (1981) 645-648.
- [197] A. Zastawny, B. Rabsztyn: A Needle Gas Counter for Measurements of Low Beta-Radioactivity Solid Emitters, 1st Measurements, Isotopenpraxis 22 (1986) 193-197.
- [198] A. Zastawny, B. Rabsztyn: A Double Needle Gas Counter Arrangement for Measurements of Low Beta Radioactivity Solid Emitters, Nuclear Instruments & Methods in Physics Research Section B-Beam Interactions with Materials and Atoms 17 (1986) 506-508.
- [199] A. Zastawny: Investigation of Lead Radioactivity, Applied Radiation and Isotopes 39 (1988) 447-449.
- [200] A. Zastawny, J. Bialon, T. Sosinski: Investigation of the Surface Alpha Radioactivity of Lead, Rare Nuclear Processes (1992) 291-299.
- [201] D. P. Bouldin: The Measurement of Alpha-Particle Emissions from Semiconductor Memory Materials, Journal of Electronic Materials 10 (1981) 747-795.
- [202] M. S. Gordon, K. P. Rodbell, D. F. Heidel, C. E. Murray, H. H. K. Tang, B. Dwyer-McNally, W. K. Warburton: Alpha-Particle Emission Energy Spectra From Materials Used for Solder Bumps, IEEE Transactions on Nuclear Science 57 (2010) 3251-3256.
- [203] B. Momčilović, G. I. Lykken, C. Nitsche: Micron slices of lead for assessment of alpha particle emission in computer chip manufacturing, 129th Annual Meeting of the Minerals, Metals, and Materials Society, Nashville, USA, 07-12.05.2000.
- [204] G. I. Lykken, B. Momčilović, US Patent No. US6674072 (2004).
- [205] R. Brodzinski: The "discovery" of alpha activity in lead and solder, Journal of Electronic Materials 29 (2000) 1294-1298.
- [206] A. B. Focke: Segregation of polonium in bismuth crystals, Physical Review 46 (1934) 0623-0628.
- [207] K. W. Foster, T. E. Eyles: Diffusion of polonium through aluminium, stainless steel and bismuth, MLM-569, Mound Laboratory Report (1951).
- [208] T. Miura, T. Obara, H. Sekimoto: Unfolding of polonium distribution in depth of irradiated lead-bismuth eutectic from [alpha]-particle pulse-height distribution, Applied Radiation and Isotopes 61 (2004) 1307-1311.
- [209] N. A. C. Diaz, A. M. Sanchez, J. D. Perez: SOLANG: A user-friendly code to calculate the geometry factor using Monte Carlo simulations. Application to alpha-particle spectrometry, Applied Radiation and Isotopes 69 (2011) 822-824.
- [210] J. F. Ziegler, J. P. Biersack: SRIM: Stopping Range of Ions in Matter, IBM Research, Yorktown (2008).
- [211] F. Auerbach, W. Hort: Handbuch der physikalischen und technischen Mechanik, Band VII - Grenzgebiete der technischen und physikalischen Mechanik, Johann Ambrosius Barth Verlag, Leipzig (1931).
- [212] C. Lea, M. P. Seah: Philosophical magazine 35 (1977) 213.
- [213] P. Agostini, E. Baicchi, A. Zucchini, G. Benamati: The re-crystallization issue in lead-bismuth technology, Journal of Nuclear Materials 335 (2004) 275 - 279.
- [214] R. A. Khairulin, K. M. Lyapunov, A. G. Mozgovoï, S. V. Stankus, P. V. Ulyusov: Crystallization and relaxation phenomena in the bismuth-lead eutectic, Journal of Alloys and Compounds 387 (2005) 183 - 186.
- [215] P. Dumoulin, J. L. Caillerie, M. Guttmann: An AES study of the segregation of tin and bismuth at the surface of lead - influence of adsorped oxygen, Surface Science 104 (1981) 559 - 568.

Appendix

Table 21: Chronological overview on ^{210}Po extraction experiments performed during this investigation.

Date of experiment	Temperature [°C]	Cover gas	Time [min]	Agitation mode	Po extracted	Remarks
8.9.2011	250	N ₂	30	stirring	22%	
8.9.2011	250	N ₂	30	stirring	14%	
8.9.2011	250	N ₂	30	stirring	20%	
9.9.2011	250	N ₂	60	stirring	22%	
9.9.2011	250	N ₂	120	stirring	2%	
9.9.2011	250	N ₂	180	stirring	19%	
12.9.2011	250	N ₂	15	stirring	36%	
12.9.2011	250	N ₂	30	stirring	9%	
12.9.2011	250	N ₂	30	stirring	16%	
12.9.2011	250	N ₂	30	stirring	15%	
12.9.2011	250	N ₂	30	stirring	22%	
12.9.2011	250	N ₂	45	stirring	9%	
13.9.2011	250	N ₂	240	stirring	18%	
13.9.2011	250	N ₂	330	stirring	2%	
14.9.2011	250	N ₂	90	stirring	18%	
14.9.2011	250	N ₂	90	stirring	9%	
14.9.2011	250	N ₂	90	stirring	20%	
14.9.2011	250	N ₂	420	stirring	7%	
10.10.2011	250	N ₂	30	stirring	14%	
10.10.2011	250	N ₂	30	stirring	10%	
10.10.2011	250	N ₂	30	stirring	11%	
10.10.2011	250	N ₂	180	stirring	8%	
10.10.2011	250	N ₂	180	stirring	6%	
10.10.2011	250	N ₂	180	stirring	7%	
11.10.2011	300	N ₂	120	stirring	13%	
11.10.2011	300	N ₂	120	stirring	6%	
11.10.2011	300	N ₂	120	stirring	33%	
11.10.2011	200	N ₂	180	stirring	5%	
11.10.2011	200	N ₂	180	stirring	8%	
11.10.2011	200	N ₂	180	stirring	10%	
12.10.2011	275	N ₂	30	stirring	30%	
12.10.2011	275	N ₂	30	stirring	24%	
13.10.2011	275	N ₂	30	stirring	31%	
13.10.2011	275	N ₂	30	stirring	47%	
13.10.2011	300	N ₂	120	stagnant	56%	
13.10.2011	300	N ₂	120	stagnant	38%	
13.10.2011	300	N ₂	120	stagnant	56%	
14.10.2011	300	N ₂	30	stagnant	73%	
14.10.2011	300	N ₂	30	stagnant	65%	
14.10.2011	300	N ₂	30	stagnant	88%	
14.10.2011	300	N ₂	120	stagnant	55%	
14.10.2011	300	N ₂	120	stagnant	29%	
14.10.2011	300	N ₂	120	stagnant	62%	
7.11.2011	300	N ₂	30	stagnant	64%	

7.11.2011	300	N ₂	30	stagnant	52%
8.11.2011	325	N ₂	30	stagnant	89%
8.11.2011	325	N ₂	30	stagnant	87%
8.11.2011	325	N ₂	30	stagnant	91%
9.11.2011	350	N ₂	30	stagnant	92%
9.11.2011	350	N ₂	30	stagnant	89%
9.11.2011	350	N ₂	30	stagnant	94%
9.11.2011	500	N ₂	30	stagnant	71%
9.11.2011	500	N ₂	30	stagnant	75%
9.11.2011	500	N ₂	30	stagnant	80%
10.11.2011	250	N ₂	30	stagnant	78%
10.11.2011	250	N ₂	30	stagnant	67%
10.11.2011	250	N ₂	30	stagnant	79%
14.11.2011	200	N ₂	30	stagnant	100%
14.11.2011	200	N ₂	30	stagnant	96%
14.11.2011	200	N ₂	30	stagnant	100%
14.11.2011	250	N ₂	120	stagnant	65%
14.11.2011	250	N ₂	120	stagnant	38%
14.11.2011	250	N ₂	120	stagnant	30%
16.11.2011	200	N ₂	5	stagnant	99%
16.11.2011	500	N ₂	5	stagnant	85%
16.11.2011	200	N ₂	10	stagnant	99%
16.11.2011	500	N ₂	10	stagnant	84%
16.11.2011	200	N ₂	20	stagnant	98%
16.11.2011	500	N ₂	20	stagnant	87%
18.11.2011	200	N ₂	240	stagnant	59%
18.11.2011	350	N ₂	240	stagnant	93%
18.11.2011	500	N ₂	240	stagnant	85%
21.11.2011	350	N ₂	5	stagnant	97%
21.11.2011	350	N ₂	10	stagnant	94%
21.11.2011	350	N ₂	20	stagnant	91%
22.11.2011	200	N ₂	180	stagnant	70%
22.11.2011	350	N ₂	180	stagnant	91%
22.11.2011	500	N ₂	180	stagnant	88%
24.11.2011	350	N ₂	360	stagnant	94%
24.11.2011	500	N ₂	360	stagnant	86%
24.11.2011	200	N ₂	480	stagnant	33%
24.11.2011	350	N ₂	480	stagnant	89%
24.11.2011	500	N ₂	480	stagnant	87%
28.11.2011	200	N ₂	60	stagnant	75%
28.11.2011	350	N ₂	60	stagnant	94%
28.11.2011	500	N ₂	60	stagnant	93%
28.11.2011	200	N ₂	120	stagnant	52%
28.11.2011	350	N ₂	120	stagnant	94%
28.11.2011	500	N ₂	120	stagnant	81%
30.11.2011	500	N ₂	30	stagnant	90%
30.11.2011	200	N ₂	120	stagnant	70%
1.12.2011	200	N ₂	10	stagnant	78%
1.12.2011	250	N ₂	30	stagnant	63%
1.12.2011	300	N ₂	30	stagnant	85%
1.12.2011	400	N ₂	30	stagnant	94%
1.12.2011	450	N ₂	30	stagnant	99%
1.12.2011	200	N ₂	360	stagnant	43%

15.12.2011	200	Vacuum	30	stagnant	99%	
15.12.2011	200	Vacuum	30	stagnant	81%	
15.12.2011	200	Vacuum	120	stagnant	72%	
15.12.2011	200	Vacuum	180	stagnant	76%	
15.12.2011	350	Vacuum	180	stagnant	92%	
15.12.2011	500	Vacuum	180	stagnant	88%	
16.12.2011	200	Vacuum	30	stagnant	98%	
16.12.2011	200	Vacuum	30	stagnant	71%	
16.12.2011	200	Vacuum	30	stagnant	99%	
19.12.2011	200	Vacuum	60	stagnant	100%	
19.12.2011	200	Vacuum	60	stagnant	90%	
19.12.2011	200	Vacuum	60	stagnant	92%	
19.12.2011	200	Vacuum	60	stirring	38%	
19.12.2011	200	Vacuum	60	stirring	16%	
19.12.2011	200	Vacuum	60	stirring	29%	
20.12.2011	200	Vacuum	360	stagnant	44%	
20.12.2011	200	Vacuum	360	stagnant	53%	
20.12.2011	200	Vacuum	360	stagnant	77%	
21.12.2011	200	Vacuum	5	stagnant	96%	
21.12.2011	350	Vacuum	7	stagnant	87%	
21.12.2011	500	Vacuum	9	stagnant	90%	
5.1.2012	200	Vacuum	30	stagnant	99%	1
5.1.2012	350	Vacuum	30	stagnant	78%	1
5.1.2012	500	Vacuum	30	stagnant	82%	1
5.1.2012	500	Vacuum	360	stagnant	98%	
5.1.2012	350	Vacuum	360	stagnant	90%	
5.1.2012	500	Vacuum	360	stagnant	75%	
16.1.2012	200	Vacuum	30	stagnant	98%	
16.1.2012	350	Vacuum	30	stagnant	96%	
16.1.2012	500	Vacuum	30	stagnant	76%	
18.1.2012	500	Vacuum	30	stagnant	3%	3
20.1.2012	500	Glove box	30	stagnant	99%	
24.1.2012	500	N ₂	30	stagnant	98%	
26.1.2012	200	N ₂	30	stirring	17%	
26.1.2012	200	N ₂	30	stirring	16%	
26.1.2012	350	N ₂	30	stirring	95%	
26.1.2012	350	N ₂	30	stirring	85%	
27.1.2012	200	Glove box	30	stirring	12%	
27.1.2012	200	Glove box	30	stirring	1%	4
27.1.2012	200	Glove box	30	stagnant	46%	4
27.1.2012	200	Glove box	30	stagnant	87%	
2.2.2012	350	Glove box	30	stagnant	99%	
2.2.2012	350	Glove box	30	stagnant	88%	
3.2.2012	200	Glove box	30	stagnant	98%	5
3.2.2012	200	Vacuum	30	stirring	33%	
6.2.2012	200	Glove box	5	stirring	46%	
6.2.2012	200	N ₂	5	stirring	91%	
6.2.2012	200	Glove box	10	stirring	23%	
6.2.2012	200	Glove box	20	stirring	13%	
7.2.2012	200	Glove box	5	stirring	68%	
7.2.2012	200	Glove box	1	stirring	99%	
8.2.2012	200	N ₂	15	stirring	48%	
8.2.2012	200	Vacuum	120	stirring	25%	

10.2.2012	200	N ₂	360	stirring	10%	
10.2.2012	200	N ₂	360	stagnant	47%	
10.2.2012	200	Vacuum	360	stirring	27%	
10.2.2012	200	Vacuum	360	stagnant	69%	
16.2.2012	200	N ₂	30	stirring	92%	
16.2.2012	200	N ₂	30	stagnant	77%	1
16.2.2012	350	N ₂	30	stirring	96%	1
16.2.2012	350	N ₂	30	stagnant	97%	1
21.2.2012	200	N ₂	30	stirring	49%	2
21.2.2012	350	N ₂	30	stirring	87%	2
23.2.2012	350	N ₂	5	stirring	92%	
23.2.2012	350	N ₂	240	stirring	96%	
1.3.2012	350	N ₂	120	stirring	96%	
1.3.2012	200	N ₂	480	stirring	23%	
1.3.2012	350	N ₂	480	stirring	98%	
1.3.2012	200	Vacuum	5	stirring	97%	
1.3.2012	200	Vacuum	240	stirring	12%	

1 – with addition of 0.1 wt% NaH

2 – with addition of 0.01 % NaH

3 – the reaction vessel was opened and reactants left at air for 15 min before separation

4 – no preheating for H₂O removal

5 – stagnant experiment with PTFE stirrer bar

Table 22: List of nuclides detected by γ spectroscopy in Bi irradiated with ^{40}Ar ; date of measurements: 08.06.2010, 23.06.2010 and 17.11.2010.

Nuclide	Half-life [d]
Ca47	4.5
Sc44m	2.4
Sc46	83.8
V48	16.0
Cr51	27.7
Mn52	5.6
Fe59	44.5
Co58	70.9
Co60	1925
Se75	120
Y88	107
Zr95	64.0
Nb95	35.0
Mo99	2.7
Ru103	39.3
Rh101	1205
Rh102m	1059
Rh102	207
Ag105	41.3
Ag106m	8.3
Ag110m	250
Sn113	115
Sb120m	5.8
Sb124	60.2
Sb125	1007
Te121	16.8
Te123m	120
Ba131	11.5
Ce139	137.6
Ce141	32.5
Pm144	363.0
Eu148	54.5
Eu152	4944
Yb169	32.0
Lu172	6.7
Lu173	500.4
Hf172	683.0
Ir188	1.7
Pt188	10.2
Au196	6.2
Tl202	12.2
Bi205	15.3
Bi206	6.2
Bi207	11523.6
Po206	8.8

Table 23: List of nuclides with corresponding half-lives and activities detected by γ spectroscopy for proton irradiated LBE from the CERN-ISOLDE facility

Nuclide	Half-life [y]	Activity [Bq] on the 19.10.2010
Co60	5.3	2.2E+02
Rh101	3.3	2.7E+02
Rh102m	2.9	7.7E+02
Ag108m	418.0	4.3E+01
Ag110m	0.7	1.2E+02
Ba133	10.5	3.2E+02
Hf172	1.9	7.8E+03
Lu173	1.4	5.8E+03
Bi207	31.6	1.3E+04

Table 24: List of radionuclides with corresponding half-lives and activities detected by γ spectroscopy for proton irradiated Pb from the PSI-SINQ facility

Nuclide	Half-life [y]	Activity [Bq] on the 20.02.2012
K42	1.4E-03	7.4E+03
Co60	5.3	9.0E+04
Zn65	0.7	1.0E+03
Rh101	3.3	2.8E+04
Rh102m	2.9	8.1E+04
Ag108m	418.0	1.7E+04
Sb125	2.8	1.9E+04
Ba133	10.5	6.1E+04
Cs134	2.1	7.0E+04
Pm146	5.5	2.2E+03
Eu150	36.9	8.7E+02
Eu152	13.5	2.0E+03
Hf172	1.9	1.8E+05
Lu173	1.4	5.1E+04
Hg194	444.0	5.8E+05
Bi207	31.6	1.1E+06
Bi208	3.7E+05	2.9E+02

Table 25: Overview on all produced LBE cylinders with their respective mass, height, production and irradiation date, batch number and activity.

sample	mass [g]	height [mm]	anneal at [°C]	description		LBE batch	activity [kBq/g]	at date	
z01	3.6932	9.1	110	produced on 06.08.2010	irradiated on 12.08.2010	05B124	6.45	6.6.2011	
z02	3.4323	8.4	110						
z03	3.2913	8.1	80						
z04	3.3524	8.2	80						
z05	3.5990	8.8	50						
z06	3.5467	8.7	50						
z07	3.6444	8.9	none						
z08	3.5669	8.7	none						
z09	3.4574	8.5	none						
z10	3.4847	8.6	none		used for TEM tests				
z11	3.2299	8.0	none						
z12	3.6186	9.0	50		²¹⁰ Po solution deposited on 6.12.2010				
z13	3.5409	8.8	50						
z14	3.4589	8.6	50						
z15	3.6200	9.0	80						
z16	3.6125	8.9	80						
z17	3.8632	9.6	80						
z18	3.4083	8.4	110						
z19	3.8489	9.5	110						
z20	3.7002	9.2	110						
z21	3.8407	9.5	none	as z01-z09			6.2	7.6.2011	
z22	2.5444	6.3	110	produced on 5.11.2009	irradiated on 13.11.2009	03A124	n.d. ¹	/	
z23	3.1397	7.8	110						
z24	2.5888	6.4	80						
z25	2.9253	7.2	80						
z26	3.8328	9.5	50						
z27	3.1346	7.8	50						
z28									
z30	3.5433	8.8	none	produced on 25.11.2010	irradiated on 15.12.2010	03A124	11.61	7.6.2011	
z31	3.2186	8.0	none						
z32	3.3614	8.3	none						
z33	3.2133	8.0	none						
z34	3.2615	8.1	none						
z35	3.2615	8.1	none						
z36	3.0813	7.6	50		irradiated on 15.12.2010			11.61	7.6.2011
z37	3.3461	8.3	50						
z38	3.2450	8.0	50		irradiated on 11.11.2011			9.17	1.2.2012
z39	3.6884	9.1	50						
z40	3.4902	8.6	50		irradiated on 15.12.2010		11.42	7.6.2011	
z41	3.2286	8.0	50						
z42	3.4915	8.6	80		irradiated on 11.11.2011		n.d. ¹	/	
z43	3.4913	8.6	80						
z44	3.3904	8.4	80						
z45	3.6061	8.9	80		irradiated on 11.11.2011		11.42	7.6.2011	
z46	3.0061	7.4	80						
z47	3.7614	9.3	80						
z48	3.5811	8.9	80						
z49	3.0882	7.6	110	irradiated		11.42	7.6.2011		

z50	3.8591	9.6	110		on			
z51	3.6243	9.0	110		15.12.2010			
z52	3.3044	8.2	110		irradiated		35.61	16.2.2012
z53	3.3490	8.3	110		on		26.08	17.4.2012
z54	3.3579	8.3	110		11.11.2011		n.d. ¹	/

¹ not determined

Table 26: Overview on produced cylindrical Pb and Bi samples used for the measurement on the ²¹⁰Po diffusion coefficient

Bi samples				Pb samples			
label	mass [g]	height [mm]	anneal at [°C]	label	mass [g]	height [mm]	anneal at [°C]
B1	3.6388	9.7	none	L1	3.1450	7.2	none
B2	3.5198	9.4	none	L2	2.6960	6.2	none
B3	3.2929	8.8	none	L3	2.8115	6.4	none
B4	3.4565	9.2	none	L4	2.7588	6.3	none
B5	3.5500	9.5	none	L5	2.6840	6.1	none
B6	3.1268	8.3	none	L6	3.1222	7.1	none
B7	3.9485	10.5	none	L7	2.8141	6.4	none
B8	3.5319	9.4	none	L8	2.8914	6.6	none
B9	3.3593	9.0	none	L9	2.8823	6.6	none
B10	3.4837	9.3	none	L10	2.7352	6.3	none
B11	3.3259	8.9	none	L11	2.7249	6.2	none
B12	3.2499	8.7	200	L12	2.7949	6.4	none
B13	3.6170	9.6	50	L13	2.9935	6.9	none
B14	3.3899	9.0	50	L14	2.7776	6.4	50
B15	3.4050	9.1	100	L15	3.2185	7.4	none
B16	3.4063	9.1	100	L16	3.1399	7.2	150
B17	3.4973	9.3	150	L17	3.0239	6.9	150
B18	3.4628	9.2	150	L18	3.2697	7.5	50
B19	2.9820	7.9	200	L19	2.9059	6.7	200
				L20	2.8125	6.4	200
				L21	2.7688	6.3	100
				L22	3.0402	7.0	100

Acknowledgements

First of all I would like to thank Dr. Dorothea Schumann for providing me the ability to come to PSI and to join the RadWaste Analytics group. This unique opportunity gave me the possibility not only to work in an exotic and very interesting field of science, but also to attend various meetings, training courses and conferences in Switzerland, Germany, Belgium, Sweden, Italy, Russia and Japan. My special gratitude to her emerges from the ease and professionalism she met with while being our boss and for just simply being a fantastic person.

I am deeply indebted to Dr. Jörg Neuhausen, a great scientist who tried to teach me scientific thinking, arguing and writing. After gallons of red ink, myriads of cigarette breaks and with a lot of patience, he always encouraged me to rethink or redo my work. We had lot of helpful and sometimes irrational ideas to master problems appearing during this PhD. With his profound scientific knowledge and an adorable sense of humor, Jörg helped to create a great atmosphere in our group. I am very thankful for his criticism and I will make use of the gained knowledge in my future career.

My sincere thanks goes to Prof. Dr. Andreas Türlér at the University of Bern, also head of the Laboratory of Radiochemistry and Environmental Chemistry at PSI, who kindly agreed to supervise my PhD thesis. He was always willing to help and to discuss questions concerning scientific or general problems around the PhD. I am also thankful to Prof. Dr. Christian Latgé, professor at the Institut national des sciences et techniques nucléaires, CEA, France, who kindly agreed to serve as co-referee for this PhD thesis.

It is a duty for me to mention the invaluable help I received from Mrs. Sabrina Lüthi during the last year of my thesis. She assisted me in prolonged experiments and accomplished all tasks without any constraints. Sorely, she decided to leave science. I wish you the best on your further way of life, Sabrina! I also want to express my gratitude to all other persons working at the RadWaste group. It was a real pleasure to meet you guys not only as colleges but also as friends and to have some time together outside the PSI fence. Go-Kart races, Paintball games, chocolate degustation or the Fondue Tram is what gave our group a note of coherence and levity. Without doubt I might say the time with this group was unforgettable.

Silvia Köchli, Eugenia Minikus and Julijana Krbanjevic were of great help in providing scientific data or technical assistance in ICP-OES measurements, TEM and SEM imaging, radiography and the involved sample preparation. I would like to thank them for their great help. Dave Piguet taught me that there is no science without a technician. He is a truly expert in mastering every kind of small or big technical problems. I would like to deeply thank him for his time and help.

The Paul Scherrer Institute is acknowledged for the overall use of the facilities – the calm and inspiring rooms of the library, the mysterious underground tunnel system, the cooling Aare river at hot summer days, the beer vending machine near the SLS building, and certainly, the restaurant OASE. This institution truly offers a pleasant atmosphere for scientific working.

Apart from work, I certainly would like to mention people joining me in numerous games of badminton. Isn't it amazing how easily sport heals from a zombie-like mind-numbed coexistence after a wasted day in the lab? With Andreas Lagotzki, Urs Beyerle, and members of the sport club including Marco Felder, I had the possibility to forget the PhD once in a while. They also helped me to get known to the Swiss way of life and to explain the meaning of Swiss words I am even not able to spell.

Of course it is a pleasure for me to mention Jens Löbus and Thomas Siegfried, good friends of mine in sharing winged enthusiasm and desperate resignation during the PhD time. We have spent a lot of free time together discovering Switzerland's beauty, going for skiing and finding the best place to have a beer in Zurich.

Finally, I own great gratitude for all members of my family without whose help, patience, and assistance this work wouldn't exist. I am deeply indebted to my girlfriend Nicole, who took the load of organization, babysitting and homework off me, thus enabling me to finish this work in time. A special thanks goes to my son Raphael, born 21.08.2012, who constantly woke me up early, being the best motivation to seize the day. If some day you'll read those letters, then, dude, я хочу, чтобы ты знал, что ты самое светлое что у нас есть на свете!

Erklärung

gemäss Art. 28 Abs. 2 RSL 05

Name, Vorname: **Heinitz, Stephan**

Matrikelnummer: **09-120-569**

Studiengang: **Radiochemie**

Titel der Arbeit: **Investigations on physico-chemical aspects of lead-based alloys for nuclear applications**

Leiter der Arbeit: **Prof. Dr. Andreas Türler**

Ich erkläre hiermit, dass ich diese Arbeit selbstständig verfasst und keine anderen als die angegebenen Quellen benutzt habe. Alle Stellen, die wörtlich oder sinngemäss aus Quellen entnommen wurden, habe ich als solche gekennzeichnet. Mir ist bekannt, dass andernfalls der Senat gemäss Artikel 36 Absatz 1 Buchstabe o des Gesetzes vom 5. September 1996 über die Universität zum Entzug des auf Grund dieser Arbeit verliehenen Titels berechtigt ist.

Bern, den 04.06.2013

Stephan Heinitz

Curriculum vitae

Name: **Heinitz Stephan**

Date of birth: **23.07.1982**

Place of birth: **Pinsk, Belarus**

School education: 1989 - 1993 primary school № 9 in Dubna, Russia
1993 - 1997 Lyceum № 6 in Dubna, Russia
1997 - 1998 Ernst-Haeckel-Gymnasium in Jena, Germany
1998 - 2001 Carl-Zeiss-Gymnasium in Jena, Germany

Abitur certificate obtained in June 2001

Higher Education: 2001 - 2005 Bachelor of Science in Chemistry at the University of Jena, Germany

2003 – 2004 Year abroad at the University of Salamanca, Spain

2005 - 2008 Master of Science in Chemistry at the University of Leipzig, Germany

Master of Chemistry degree obtained in December 2008

2009 – 2012 PhD at the Paul Scherrer Institute, Switzerland

Erfurt, May 2013